

**WAVES AND INSTABILITIES IN  
INHOMOGENEOUS  
STRONGLY COUPLED DUSTY PLASMA**

*By*

**DEBABRATA BANERJEE**

(Enrolment No.-PHYS05200704016)

**Saha Institute of Nuclear Physics, Kolkata.**

*A thesis submitted to the*

*Board of Studies in Physical Sciences*

*In partial fulfillment of requirements*

*For the Degree of*

**Doctor of Philosophy**

**Homi Bhabha National Institute**



November 2013

# Homi Bhabha National Institute

## Recommendations of the Viva Voce Board

As members of the Viva Voce Board, we certify that we have read the dissertation prepared by Debabrata Banerjee entitled "Waves and Instabilities in Inhomogeneous Strongly Coupled Dusty Plasma" and recommend that it may be accepted as fulfilling the dissertation requirement for the Degree of Doctor of Philosophy.

P. Mitra

(Chairman- Prof. Parthasarathi Mitra )

Date: 18.11.13

M. S. Janaki

(Guide/Convener - Prof. M. S. Janaki )

Date: 18.11.2013

N. Chakrabarti

(Guide - Prof. Nikhil Chakrabarti)

Date: 18<sup>th</sup> Nov. 2013

A. N. Sekar Iyengar

(Member1- Prof. A. N. Sekar Iyengar)

Date: 18/11/13

Abhik Basu

(Member2- Prof. Abhik Basu)

Date: 18/11/13

Vinod Krishan

(External Examiner: Prof. Vinod Krishan )

Date: 18/11/2013

Final approval and acceptance of this dissertation is contingent upon the candidate's submission of the final copies of the dissertation to HBNI.

We hereby certify that we have read this dissertation prepared under our direction and recommend that it may be accepted as fulfilling the dissertation requirement.

M. S. Janaki

Guide: Prof. M. S. Janaki

Place: SINP, KOLKATA

Date: 18<sup>th</sup> Nov, 2013.

N. Chakrabarti

Guide: Prof. Nikhil Chakrabarti

Place: SINP, Kolkata.

Date: 18<sup>th</sup> Nov. 2013.

## STATEMENT BY AUTHOR

This dissertation has been submitted in partial fulfillment of requirements for an advanced degree at Homi Bhabha National Institute (HBNI) and is deposited in the Library to be made available to borrowers under rules of the HBNI.

Brief quotations from this dissertation are allowable without special permission, provided that accurate acknowledgement of source is made. Requests for permission for extended quotation from or reproduction of this manuscript in whole or in part may be granted by the Competent Authority of HBNI when in his or her judgment the proposed use of the material is in the interests of scholarship. In all other instances, however, permission must be obtained from the author.

*Debabrata Banerjee*

---

Debabrata Banerjee

## DECLARATION

I, hereby declare that the investigation presented in the thesis has been carried out by me. The work is original and has not been submitted earlier as a whole or in part for a degree/deploma at this or any other Institution/University.

*Debabrata Banerjee*

---

Debabrata Banerjee

*To our teacher*  
*Sri Subhash Chandra Kundu*

# Acknowledgements

My heart convey this cordial message of thanks and gratitude to the persons who have given me academic and mental support in the duration of successful completion of my thesis.

Specially, I am grateful to my supervisors Prof. M. S. Janaki and Prof. Nikhil Chakrabarti for their teaching and careful guidance in pursuing of this doctoral research. I can't forget those memorable days when we used to meet together to discuss results and argued in searching reasonable answers to various physics issues. They have guided me in all the way as writing manuscripts, preparing seminar talks, making justified reply to referee's comments.

I would like to thank my doctoral committee members in making yearly evaluation of my progress report and giving valuable suggestions.

I express my heartiest thanks to Prof. Parvez Guzdar of Maryland in guiding me to solve numerical problems.

I express my thanks to Prof. R. Pal, Prof. A. N. S. Iyenger, Prof. S. Saha and Prof S. Raychaudhury for their presence with fruitful comments in my renewal talks. I am thankful to Dr. Nirmal Bisai of IPR for his help in studying spectral analysis with his pseudo-spectral code and Dr. Samiran Ghosh of CU for valuable suggestions.

It's my great pleasure to have joyful company with research fellows and friends Anirban Da, Subir Da, Debu Da, Jaman Da, Chandan, Sudip, Anwasha, Michael, Sourav, Abhijit, Avik. I recall the happy moments with Subhasish Da, Monobir Da, Santanu Da, Partha Da, Dipankar Da and many other colleagues in SINP.

I should also acknowledge the encourage and support of my parents, my teachers, family members, dear friends and well wishers.

SINP, Kolkata

November 18, 2013

Debabrata Banerjee

**Publication in journals:**

1. “*Viscoelastic modes in a strongly coupled, cold, magnetized dusty plasma*”  
D. Banerjee, M. S. Janaki and N. Chakrabarti, Physics of Plasma, **17**, 113708 (2010).
2. “*Viscosity gradient-driven instability of ‘shear mode’ in a strongly coupled plasma*”  
D. Banerjee, M. S. Janaki, N. Chakrabarti and M. Chaudhuri , New Journal of Physics, **12**, 123031 (2010).
3. “*Shear waves in an inhomogeneous strongly coupled dusty plasma*”  
M. S. Janaki, D. Banerjee and N. Chakrabarti, Physics of Plasmas, **18**, 092114 (2011).
4. “*Jeans instability in a viscoelastic fluid*”  
M. S. Janaki, N. Chakrabarti and D. Banerjee, Physics of Plasmas, **18**, 012901 (2011).
5. “*Nonlinear shear wave in a non Newtonian visco-elastic medium*”  
D. Banerjee, M. S. Janaki, N. Chakrabarti and and M. Chaudhuri, Physics of Plasma, **19**, 062301 (2012).
6. “*Shear flow instability in a strongly coupled dusty plasma*”  
D. Banerjee, M. S. Janaki and N. Chakrabarti, Physical Review E, **85**, 066408 (2012).
7. “*Kelvin-Helmholtz instability in non-Newtonian complex plasma*”  
D. Banerjee, S. Garai, M. S. Janaki and N. Chakrabarti, Physics of Plasmas,

**20**, 073702 (2013).

8. “*Velocity shear effect on the longitudinal wave in a strongly coupled dusty plasma*”

S. Garai, D. Banerjee, M. S. Janaki and N. Chakrabarti, *Accepted in Astrophysics and space science.*

# Contents

synopsis	1
List of Figures	9
List of Tables	12
<b>1 Strongly Coupled Dusty Plasma: complex media for fundamental studies</b>	<b>15</b>
1.1 Introduction . . . . .	15
1.2 Visco-elastic and non-Newtonian properties . . . . .	18
1.3 Motivation . . . . .	20
1.4 Organization of this thesis . . . . .	21
<b>2 Shear wave and its characteristics in dusty plasma</b>	<b>25</b>
2.1 Introduction . . . . .	25
2.2 Generalized hydrodynamic model equations . . . . .	27
2.3 Existence of shear wave in dusty plasma . . . . .	31
2.4 Effect of inhomogeneity on shear wave in dusty plasma . . . . .	33
2.5 Effect of inhomogeneity on shear wave vortex in visco-elastic fluid . . . . .	34
2.6 Shear wave in magnetized dusty plasma . . . . .	39
2.7 Summary . . . . .	45
<b>3 Instability of ‘shear mode’ in presence of velocity shear</b>	<b>47</b>
3.1 Introduction . . . . .	47
3.2 Model of non-Newtonian viscous stress . . . . .	49
3.3 Basic equations and equilibrium . . . . .	50
3.4 Linear equations and eigenvalue analysis . . . . .	51
3.5 Summary . . . . .	58
<b>4 Kelvin-Helmholtz instability of dust shear flow in strong coupling</b>	<b>59</b>
4.1 Introduction . . . . .	59
4.2 Basic equations with linearized form . . . . .	61

4.3	Local approximation . . . . .	63
4.4	Non-local Eigenvalue Analysis . . . . .	64
4.4.1	Using step profile . . . . .	64
4.4.2	Shear layer of finite width . . . . .	68
4.5	Summary . . . . .	78
<b>5</b>	<b>Stabilization of Kelvin-Helmholtz instability in non-Newtonian dusty plasma</b>	<b>81</b>
5.1	Introduction . . . . .	81
5.2	Physical system and basic equations . . . . .	82
5.3	Steady state and bounded flow profile . . . . .	83
5.4	Linearized form of basic equations . . . . .	86
5.5	Eigenvalue analysis . . . . .	87
5.6	Summary . . . . .	92
<b>6</b>	<b>Nonlinear shear wave and recurrence</b>	<b>93</b>
6.1	Introduction . . . . .	93
6.2	Nonlinear shear wave equation . . . . .	94
6.3	Numerical solution . . . . .	97
6.4	Analytical approach . . . . .	101
6.5	Summary . . . . .	104
<b>7</b>	<b>Conclusion of results and future scope</b>	<b>105</b>
7.1	Summary . . . . .	105
7.2	Future directions . . . . .	109
	<b>Bibliography</b>	<b>111</b>

# Synopsis

The contents of this thesis provides a detailed analytical and numerical study of low frequency waves and instabilities in a strongly coupled dusty plasma considering the effect of viscoelastic and non-Newtonian properties in presence of inhomogeneous dust shear flow. The transverse mechanical shear mode coming from solid-like property in dusty plasma liquid was first proposed by Kaw and Sen[1] in their famous theoretical work in 1998. Two years later, Nunomura et. al, in their experiment with 2D dusty plasma crystal showed excitation of such shear wave[2]. In the year 2002, Pramanik et al., with levitating dust cloud in glow discharge plasma experiment in strongly coupled fluid regime[3], reported the existence of this transverse wave coupled with the longitudinal dust acoustic wave. The understanding of linear and nonlinear properties of such shear wave in inhomogeneous dusty plasma forms a motivation for this thesis. The main objectives of this doctoral research are: (i) The role of visco-elastic effect and non-Newtonian property on the Kelvin-Helmholtz (KH) instability of dust plasma flow. (ii) instability of transverse shear wave triggered by viscosity gradient of shear rate in plane Couette flow. (iii) the recurrence properties of nonlinear shear wave due to the nonlinear effect coming from velocity shear rate dependent viscosity.

Dusty plasma is greatly affectionate to the plasma physics community due to their natural occurrence in different places in our universe i.e. planetary rings, cometary tails, white dwarf matter[4], interplanetary and interstellar clouds[5, 6]. It also has existence in human made systems like plasma processing and plasma

etching equipments in industry, magnetic fusion plasmas[7], space stations[8] etc. and for such wide occurrence it is important to characterize the different features of this system. It is formed by the presence of the micron sized polymer or colloidal particles (dust particles) in normal electron-ion plasma. Since the thermal electron velocity is much larger than the thermal ion velocity, a grain embedded in plasma will very soon be charged negatively by thermal electron flux, then start to reflect the electrons and attract the ions until the ion and electron flux become equal. At low dust thermal temperature, potential energy of Coulomb interaction between neighboring dust particles becomes larger than the average kinetic energy of random thermal motion of dust grains and thus the particles remain strongly coupled with their neighbor. This is characterized by the coupling parameter  $\Gamma = q_d^2/(ak_B T_d)$  where  $q_d$ ,  $a(\simeq n_d^{-1/3})$ ,  $k_B T_d$  and  $n_d$  represent charge on a single dust particle, average inter particle distance, the average thermal energy of each particle and dust number density respectively. In the regime  $1 \leq \Gamma \leq \Gamma_c$  (a critical value beyond which system becomes solid) both viscosity and elasticity are equally important and therefore such a plasma exhibits visco-elastic behavior [9, 10].

The newly discovered transverse shear wave with phase velocity  $c_{sh} = \sqrt{\eta/\tau_m \rho}$ , where  $\eta$  and  $\rho$  denote shear viscosity and density respectively, is analogous to the transverse elastic wave propagating in a solid medium. Here,  $\tau_m = \eta/G$  represents Maxwell's relaxation time where  $G$  is the rigidity modulus. An ideal plasma (electron-ion) does not support solid like transverse wave but magnetic

field with the twisting nature of field lines generates transverse shear Alfvén wave of phase velocity  $c_A = B/\sqrt{4\pi\rho}$ , where  $B$  stands for magnetic field. In a strongly coupled dusty plasma, we introduce a magneto-elastic mode of phase velocity  $v_p = \sqrt{(v_A^2 + v_{sh}^2)}$  similar to magnetosonic mode which couples acoustic and Alfvén modes [11]. In an inhomogeneous dusty plasma, our analysis [12] with  $\text{sech}^2(\alpha x)$  type density profile shows that propagating shear mode is localized into different eigenstates with a discrete set of allowed frequencies  $\omega = \sqrt{n(n+1)}\alpha c_{sh}$ . In a cylindrical geometry with parabolic density profile along radial direction, periodic eigenfunctions are found to exist along poloidal direction and localized radial modes are described by Kummer hypergeometric function.

An unbounded parallel flow separated by a laminar shear layer could be unstable to small wavy disturbance depending on the presence of inflection point (where second derivative of velocity vanishes) in the velocity shear profile (Rayleigh 1880). This is a class of Kelvin-Helmholtz instability that arises in parallel shear flows, where small scale perturbations draw kinetic energy from the mean flow. In 1908, Orr and Sommerfeld derived a famous equation which analyzes the KH instability in viscous incompressible fluid. Being a dissipative agent, viscosity decreases the growth rate of instability. In a strongly coupled dusty plasma, the presence of elasticity and viscosity together enriches the analysis of the KH instability. In the present work, visco-elastic operator [13] is included in the famous Orr-Sommerfeld equation to obtain the generalized hydrodynamic Orr-Sommerfeld equation including  $\tau_m$ . Considering proper Galilean invariant form of the equation, KH instability

is studied numerically for hyperbolic tangent type dust shear profile. Before that a step profile has been chosen as simple mathematically solvable form of tanh type profile to treat the problem analytically (without involving numerical analysis). In weakly coupled limit, the stability of this type of piecewise continuous velocity profile in a viscous incompressible fluid was analytically studied and an instability [14] was predicted. In strongly coupled limit, increase of coupling parameter  $\Gamma$  effectively increases relaxation time  $\tau_m$  which manifests the increase of elastic property as well[15]. Having energy storing property, elasticity enhances the instability which is the effect of long range correlation (solid like behaviour) in dusty plasma fluid. Functional dependence of growth rate with wavenumber ( $k$ ) also changes with  $\tau_m$ . For small  $\tau_m$ , it shows parabolic dispersion but for  $\tau_m > 2$ , dispersion becomes linear. Linear stability analysis with realistic tanh type profile is done numerically using MATLAB. Here, matrix eigen value analysis of Generalized Hydrodynamic Orr-Sommerfeld equation is performed using standard eigenvalue subroutine(eig) after proper discretization of the equation with central difference scheme. These results show similarity with the analysis of step profile but the finite width of shear layer of tanh profile introduces different dispersive nature. Elastic property also increases the range of  $k$ -space which responds to instability [16].

Ivlev et al., in their recent experiment[17] with dusty plasma in PK-4 set up discovered the existence of non-Newtonian behaviour of dusty plasma. This important transport property is incorporated in this thesis to investigate KH instability

in a parabolic type bounded dust flow using linear stability analysis. The flow profile is evaluated from unperturbed steady force balance equation of dust fluid with the experimentally verified model of velocity shear rate dependent viscosity. Like the stabilizing effect of compressibility on the KH instability, the non-Newtonian effect in shear thickening regime suppresses the instability but on the contrary, shear thinning property enhances it. Depending on the variable parameter  $\epsilon$  (ratio of equilibrium plasma temperature to dust crystal melting temperature) the non-Newtonian property changes from shear thinning to shear thickening regime. We have shown that the shear thinning property is more favorable for instability [18]. Inclusion of compressibility (finite density fluctuation) lowers the growth rate as a part of energy available for the instability is exhausted for the longitudinal fluctuation in the system and thus instability weakens by some fraction.

An interesting property of non-Newtonian effect is that velocity shear rate dependent viscosity triggers the instability of shear mode for a Couette flow of dust fluid. The shear viscosity is modulated with velocity variation in space which provides feedback to the velocity through the momentum equation and positive feedback drives the instability. For a linear velocity shear profile with power law dependence of viscosity coefficient on shear rate, both local and nonlocal analysis are carried out and it addresses the instability of shear mode[19].

Convective nonlinearity in fluid momentum balance equation plays an important role to generate different structure like soliton and vortex formation [20].

Besides this nonlinearity, non-Newtonian property drives another type of nonlinearity coming from shear rate dependence of viscosity coefficient. In our studies,  $\eta$  is modeled as function of scalar invariant quantity of strain tensor[21] and a nonlinear shear wave equation is formed incorporating the nonlinearity arising from the non-Newtonian property. The numerical solution of this equation shows the famous Fermi-Pasta-Ulam (FPU) recurrence of initial periodic wave[22]. The wave energy of fundamental mode is distributed into different harmonic and after a recurrence time the total energy gets back to initial mode and the higher harmonics vanish.

In summary, the results and conclusion on the analysis of the KH instability in this thesis, would enrich the understanding of dust dynamics in different type of shear flow in strongly coupled regime. Also, our studies on the nonlinear shear wave arising from non-Newtonian behaviour could initiate experimental studies in the growing field of complex (dusty) plasma.

- 
- [1] P. K. Kaw and A. Sen, Phys. Plasmas **5**, 3552 (1998).
  - [2] S. Nunomura, D. Samsonov and J. Goree, Phys. Rev. Lett. **84**, 5141 (2000).
  - [3] J. Pramanik, G. Prasad, A. Sen and P.K. Kaw, Phys. Rev. Lett. **88**, 17500 (2002).
  - [4] F. Verheest, *Waves in Dusty Space Plasmas* (Kluwer Academic Publishers, Dordrecht, 2000)

- [5] C. K. Goertz, Rev. Geophys, **27**, 271 (1989).
- [6] T. G. Northrop, Phys. Scripta **45**, 475 (1992).
- [7] G. Federicia, C.H. Skinner, J.N. Brooksc, J.P. Coadd, C. Grisoliae, A.A. Haaszf, A. Hassaneing, V. Philipphsh, C.S. Pitcheri, J. Rothj, W.R. Wamplerk and D.G. Whytel, Nucl. Fusion **41**,1967 (2001).
- [8] E.C. Whipple, Rep. Prog. Phys. **44**, 1197 (1981).
- [9] H. Ikeji, Phys. Fluids **29**, 1764, 1986.
- [10] S. Ichimaru, Rev. Mod. Phys., **54**, 1017 (1982).
- [11] D. Banerjee, M. S. Janaki and N. Chakrabarti, Phys. Plasmas **17**, 113708 (2010).
- [12] D. Banerjee, M. S. Janaki and N. Chakrabarti, Phys. Plasmas **18**, 092114 (2011).
- [13] J. Frenkel, *Kinetic Theory of liquids*, (Dover Publications, INC., New York, 1955).
- [14] P. G. Drazin, J. Fluid Mech.**10**, 571(1961).
- [15] Y. Feng, J. Goree and B. Liu, Phys. Rev. E **82**, 036403 (2010).
- [16] D. Banerjee, M. S. Janaki and N. Chakrabarti, Phys. Rev. E **85**, 066408 (2012).
- [17] A. V. Ivlev, V. Steinberg, R. Kompaneets, H. Höfner, I. Sidorenko and G. E. Morfill, Phys. Rev. Lett **98**, 145003 (2007).

- [18] D. Banerjee, S. Garai, M. S. Janaki and N. Chakrabarti, communicated.
- [19] D. Banerjee, M.S. Janaki and N. Chakrabarti, *New J. Phys.***12**, 123031, 2010.
- [20] M. S. Janaki and N. Chakrabarti, *Phys. Plasmas* **17**, 053704 (2010).
- [21] R. B. Bird, R. C. Armstrong, and O. Hassager, *Dynamics of Polymeric Liquids, vol. 1* (John Wiley & Sons, Inc., New York, 1987).
- [22] D. Banerjee, M. S. Janaki, N. Chakrabarti and M. Chaudhuri, *Phys. Plasmas* **19**, 062301 (2012).

# List of Figures

2.1	In first three graphs, monopole, dipole and tripole structures of contours of magnitude of velocity of dust fluid are plotted respectively in $x - y$ plane as derived in the example-I. In the fourth graph, localized solutions (radial part) of $\bar{\psi}$ are shown for different values of $m$ as derived in example-II. . . . .	37
3.1	Normalized growth rate $\gamma/\omega_s$ as a function of $\alpha =  \eta'_0 v'_0/\eta_0 $ , shows the growth rate of shear mode for different velocity shear rate $v'_0$ . . .	54
3.2	The red line curve represents sinusoidal shear wave and the blue line curve represents amplified shear wave in presence of velocity shear rate $v'_0 = 1.2$ , $\alpha = 1.0$ . The velocity of dust fluid is normalized by $v'_0 L$ where $L$ is the length of plasma system. The amplitude increases monotonically with time. . . . .	57
4.1	Graphical representation of step profile (left figure) and tanh profile (right figure) is shown. Both of these are vortex sheet with step profile of zero thickness and tanh profile of finite thickness. . . . .	65

4.2	Growth rate (positive imaginary part of eigenvalue) is plotted against wavenumber ( $k_y$ ) for step profile with Reynolds Number $R = 1$ and different values of $\tau_m$ enlisted in the legend. Increase of relaxation time enhances the growth rate and also changes the dispersion. . . .	68
4.3	Discretization of x-space where white dots are inner and filled dots represent boundary points . . . . .	69
4.4	The similarity of two figures provides the validity of eigenvalue analysis code developed in this thesis. The left figure represents the result from this code and the right figure is taken from the Ref.[85]. Growth rate( $k_y c$ ) is calculated in unit of $V_0/L$ and wavenumber( $k_y$ ) in unit of $1/L$ . Viscous stabilization is clearly seen for small R and large growth rate proceeds towards inviscid limit ( $R \rightarrow \infty$ ). . . . .	74
4.5	Eigenvalues are shown in complex plane in the left two figures - the upper figure for $\tau_m = 1$ and $R = 10$ and the lower one for $\tau_m = 1$ and $R = 1$ . Red (big) dot represents the only unstable mode which is purely imaginary. Corresponding eigenfunctions of the unstable mode are shown in the right two figures. Blue line represents the real part of eigenfunction and the red one represents the imaginary part. . . . .	75
4.6	Growth rate vs. wavenumber curves are shown for different values $\tau_m$ and $R = 1$ for two different cases – left one with taking $\tau_m (\mathbf{v} \cdot \nabla)$ term in GH model and right one without that term. . . . .	75

4.7	In left figure, growth rate vs. $k_y$ is plotted for $R = 40$ and different $\tau_m$ . Right figure shows growth rate variation with $k_y$ for $\tau_m = 5$ but different Reynolds numbers. . . . .	77
4.8	Growth rate of KH instability is plotted in 2D plane of $k_y$ and $R$ for both $\tau_m = 0$ and $\tau_m = 1$ which shows rapid increase of unstable region in presence of strong coupling. Colorbar indicates the values of growth rate in different color regions. . . . .	78
5.1	In the left figure, equilibrium flow profiles of dust grains are plotted for different $\epsilon$ . The solid red line curve shows the same for the Newtonian limit( $\epsilon, \gamma \rightarrow 0$ ). In the right figure, non-Newtonian viscosity is plotted against unperturbed velocity shear rate. For $\epsilon = 0.1$ , shear thinning property exists then as $\epsilon$ increases, the property changes from shear thinning to shear thickening and for $\epsilon = 0.8$ , shear thinning property almost ceases. . . . .	85
5.2	Growth rate of instability is plotted against wave number for different values of parameter $\epsilon$ in incompressible limit. The solid red line curve shows that for Newtonian limit. For $\epsilon = 0.2$ , the growth rate is close to that of Newtonian limit. . . . .	88

5.3	In the left figure, two sets of curves are shown for two different Mach number ( $M$ ) including and excluding dispersion term in Poisson's equation for $\epsilon = 0.1$ . In each set of curves, dotted line represents the curve without dispersion effect and the solid line with dispersion term. In the right one, compressibility is introduced by increasing the Mach number and it indicates that the growth rate diminishes as compressibility strengthens in the medium for $\epsilon = 0.3$ . Here, $M = 0$ curves shows incompressible limit for comparison. . . . .	90
5.4	The left figure shows contour plot of growth rate in the plane of mach number ( $M$ ) and wave number for $\epsilon = 0.1$ . In the right figure surface plot of growth rate is drawn on the parametric space of $\epsilon$ and $k_y$ for mach no. $M = 2.4$ . . . . .	91
6.1	Time evolution of the shear wave structure for $\alpha = 0.1$ for different time(time increasing column wise) with initial and final state almost identical. X-axis represents space and y-axis represents time slots .	98
6.2	Energy of different harmonics is plotted against normalized time for different values of nonlinearity $\alpha$ . Blue line shows energy of fundamental harmonic and other red, brown, yellow etc show for different higher harmonics. Hence, energy sharing to higher harmonics is greater for $\alpha = 0.3$ than that of 0.1 and 0.2. Also recurrence is faster for larger values of $\alpha$ . Fourth graph is for shear thinning medium. . . . .	99

# List of Tables

4.1	Comparison of growth rates for Galilean invariant and non-invariant	
	GH model for $R = 1$ . . . . .	76



# Chapter 1

## Strongly Coupled Dusty Plasma: complex media for fundamental studies

### 1.1 Introduction

With rapid progress in the theoretical and experimental exploration of strongly coupled dusty plasma systems, it is reasonable to anticipate that study of such system returns many realistic and interesting facts of natural science. This strong coupling effect is seen in dusty plasma at low temperature when potential energy of the long range Coulomb interaction exceeds average thermal energy of dust grains. Dusty plasma contains microscopic solid particles immersed in the usual electron-ion plasma. These grains are negative or positive in charge depending on different charging mechanisms. For negatively charged dust particles, ions shield the large electrostatic potential of each dust particle and hence dusty plasma is formed satisfying the basic properties of being a plasma like collective behaviour and quasineutrality[1]. The charged particles interact through the long range Coulomb

interaction which is proportional to the square of charge on each dust particle. The large amount of charge enables dust grains to make strong coupling with the neighbours which makes dusty plasma a complex media for fundamental research. The concept of different types of coupling (basic forces) between the constituent elements (atoms and molecules) explains different states of matter in our nature. In solid state, the coupling (bonding) is so strong that the molecules can only vibrate around their respective positions. In liquid state, bonding between molecules are weaker than solid so that it can flow in an organized way. In gaseous phase, coupling is very weak and the gas molecules perform random motion having no definite shape or volume. In plasma, oppositely charged electrons and ions shield out their long range Coulomb potential and the charged particles interact weakly but perform collective motion. The role of coupling is more interesting in dusty plasma due to the large amount of charge on each micron size dust grain. The different charging mechanisms are charge collection[2], photoelectric emission, secondary emission [3, 4] etc. Dusty plasma can exist in liquid phase having prominent viscous nature[5]. At low temperature, the coupling would be more efficient so that the plasma system can transform into crystalline state called dust crystal [6]. The great advantage of studying dusty plasma lies in the laboratory experiment where a single system can be easily transformed into different states such as gaseous plasma, liquid plasma and plasma crystal with varying density, charge, temperature and size of the dust particles.

The study of dusty plasma has been started after first realization in space plasma[7, 8]. For a long period, active research has been done on the effect of dust

particle in astrophysical plasma[9] like as interstellar clouds[10], solar wind[11], formation of Saturn's ring[12], dust particle in the magnetosphere of earth [13] and jupiter[14], in the vicinity of artificial satellites and space stations[15, 16] etc. In 1989, first levitation of dust cloud in the laboratory was noticed in a laser induced plasma processing device[17]. Then the theoretical and experimental research on laboratory dusty plasma has been accelerated in studying its various properties. The generation of dust particles in plasma based industrial devices also becomes a problem now-a-days. For example, in plasma vapour deposition technique, dust particles are produced in plasma reactors which need to be removed[18]. In fusion also, the research on accurate designing is under progress to get rid of the production of radioactive and toxic dust particles in plasma wall interactions[19, 20].

The presence of strong coupling in dusty plasma was first predicted by Ikeji[21]. With the discovery of dust crystal in the laboratory, a new field of research namely strongly coupled dusty plasma (complex plasma) starts its golden days[22, 23, 24, 25]. The dust particles are the main constituent elements in dusty plasma like that of atoms and molecules in solids, liquids or gases. The motion of atoms or molecules is impossible to track individually however the dynamics of each dust particle can be tracked with video imaging in simple laboratory experiment because of longer time scale and large spatial scale of dust particle dynamics. Overall dynamical time scales associated with the dust components are in the range of 1 – 100 Hz. Typical dust particles are of few micrometer( $\mu m$ ) in size and the mean inter particle separation is nearly 100  $\mu m$ . So, this system can be considered as a model to study molecular transport phenomena, phase transition at the most fundamental kinetic level[26]. Dusty plasma is also known as Complex plasma in analogy with

complex fluid which defines the class of soft matter systems like colloidal suspension where the charged polymer particles are immersed in an aqueous solution[27]. However, different properties of colloids depend on the solvent but dust particles with shielded Coulomb potential form an independent fluid in dusty plasma system like ion or electron fluid. Unlike the colloidal grains, the rate of momentum or energy exchange between micro particles can substantially exceeds the damping rate due to neutral gas friction and thus virtually undamped dust particle motion can be studied. Complex plasma is also known as non Hamiltonian system where energy of particles is not constant due to charge variation. Some review articles are cited here for the better knowledge of recent developments in complex plasma[28, 29, 30].

## 1.2 Visco-elastic and non-Newtonian properties

To form dusty plasma in the laboratory, micron size colloidal or polymer particles are usually inserted in a dc discharge or rf discharge plasma having electrons, ions and few neutrals. Since the thermal electron velocity is much larger than the thermal ion velocity, a grain embedded in plasma will very soon be charged negatively by electron flux which will then start to reflect the electrons and attract the ions until the ion and electron flux become equal. Hence, the grain will have a floating potential equal to the electron temperature  $Ze^2/d \approx T_e$  and, for a fixed electron temperature  $T_e$ , the grain charge is proportional to its size  $d$  and attains high negative charge. In plasma, the potential on each particle is shielded out by a factor  $\exp(-r/\lambda_D)$  due to the Debye shielding[31]. So, any pair of dust particles separated by a distance  $r$  interact through screened Coulomb potential

$\phi(r) = q_d^2 \exp(-\kappa r)/r$ , where  $q_d$  is the charge on each dust grain and the screening parameter  $\kappa$  (inverse of the Debye length  $\lambda_D$ ) is determined by the density and temperature of electrons and ions. This type of potential is well known as the Yukawa potential and is a good approximation for all the cases without streaming electrons or ions.

The strength of the Coulomb coupling is characterized by the coupling parameter  $\Gamma = q_d^2/(k_B T_d a)$  where  $a(\simeq n_d^{-1/3})$  is the average distance between dust grains with density  $n_d$ ,  $T_d$  is the average temperature of the dust particle and  $k_B$  is the Boltzmann constant. At high temperature, with the parameter  $\Gamma \ll 1$ , the medium belongs to weakly coupled state showing purely viscous property. But, as the coupling parameter goes to the regime  $1 \leq \Gamma \leq \Gamma_c$  (a critical value beyond which the system becomes crystalline) the coupling becomes stronger and the system shows elastic property as well. Hence, the dusty plasma can be classified as a visco-elastic medium[21, 32]. When  $\Gamma > \Gamma_c$ , viscosity disappears and only elasticity reigns over the system leading to crystal formation.

Complex plasma exhibits non-Newtonian behaviour that is the variation of viscosity with velocity shear rate. Recent experiments[33, 34] have demonstrated this property. For low shear rate, viscosity remains constant obeying the Newtonian linear stress strain relation. As the shear rate increases, it goes through both shear thinning and shear thickening phases. For shear thinning regime, viscosity decreases with the increase of velocity shear rate. But for shear thickening regime, viscosity increases with increasing shear rate. Comparable examples of viscoelastic, non Newtonian behavior are also found in the other branches of physics such as polymeric liquids[35], colloidal suspensions[36], human blood[37] etc.

### 1.3 Motivation

The motivation of this research work is to explore the interesting physical phenomena related to some new features in dusty plasma in general and viscoelastic non-Newtonian properties in particular. These properties are recently discovered in different experiments in the laboratory. In the strong coupling limit, dusty plasma liquid could sustain transverse shear wave identical to the transverse wave in elastic rod or s-wave during earthquake. Theoretically, this wave was first predicted [38] in 1998 and subsequently experimentally verified in the laboratory [39, 40]. The study of shear wave in presence of inhomogeneous dust particle density and velocity is one of the aim of this thesis. The effect of strong coupling and viscosity gradient on the Kelvin-Helmholtz instability of dust shear flow has been thoroughly analyzed. The main ingredients in this doctoral research are summarized as:

- The density inhomogeneity results in discrete eigenstates of shear wave with localized eigen function.
- The energy storing property of elasticity enhances the growth rate of Kelvin-Helmholtz instability. The domain of instability in wavenumber is widened in presence of strong coupling so that even shorter wavelengths respond to grow.
- In a non-Newtonian dusty plasma, shear thinning property enhances the growth rate of the Kelvin-Helmholtz instability. But, shear thickening property stabilizes instability. Hence measuring the growth rate of the instability, non-Newtonian property can be predicted.

- In strongly coupled non-Newtonian dusty plasma, shear wave becomes unstable in presence of the dust Couette flow due to the shear rate dependence of viscosity. In our analysis, non-Newtonian property drives the instability with essential energy from the equilibrium shear flow.
- Non-Newtonian property introduces nonlinearity in the system which causes shear wave to exhibit recurrence behaviour with soliton formation similar to the famous Fermi-Pasta-Ulam (FPU) recurrence in vibrating string.

## 1.4 Organization of this thesis

In this thesis, detailed analytical and numerical studies of different characteristics of low frequency transverse shear wave and the effect of visco-elastic and non-Newtonian properties of complex plasma on velocity shear driven low frequency instabilities are investigated.

**In chapter-II**, short history of the discovery of shear wave is reviewed and the effect of inhomogeneity on shear wave is introduced analytically. Spatially varying dust particle density is considered through different type of physically acceptable profiles which lead to inhomogeneous partial differential equations identical to the Schrodinger's equation. At first, we consider wave propagation along  $y$ -direction with variation in  $x$  where density varies as  $\text{sech}^2(\alpha x)$ . The role of inhomogeneity is shown to give rise to a discrete set of allowed frequencies corresponding to different localized eigen states. Finally a density profile  $f(r) = (1 - \alpha^2 r^2)$  in cylindrical plasma is also analyzed and results are shown in details.

**In chapter-III**, instability of shear wave is reported under the effect of linear velocity shear (Couette flow) in presence of shear thinning effect of dusty plasma.

Viscosity gradient drives this instability with drawing free energy from velocity shear and then by supplying it to the linear wave. The linearized generalized hydrodynamic equation is used with non-Newtonian stress. Proper power law dependence of viscosity on velocity shear rate is addressed to represent shear thinning region only. The second order differential equation is reduced to the form of Weber equation which has been solved for well behaved localized eigen function. The positive imaginary part of the eigen value serves the growth rate of instability. The growth rate is shown to be increasing with the increase in velocity shear rate.

**In chapter-IV**, the effect of strong coupling on the Kelvin-Helmholtz instability of dust shear flow is shown. The strong coupling introduces elastic property in dusty plasma which manifests in our calculation through the Maxwell relaxation time. Relaxation time increases with increase of coupling parameter  $\Gamma$ . Linear stability analysis is carried out for unbounded laminar dust shear layer having an inflection point in equilibrium velocity profile. The results are shown for two types of velocity profile. First one is a step profile which is a discontinuous one and hence physically unrealistic but we consider since it is easy to tackle mathematically. So we can get primary knowledge about the effect of more complicated realistic velocity profile. The results of strongly coupled limit are compared with that of weakly coupled one in a recent article where the result of step profile has been reported using non-invariant momentum equation. In our analysis, the generalized hydrodynamic equation of dust fluid is used with proper invariant form. A comparative study is tabulated with data of growth rate which shows the growth rate to be much higher for invariant model equation than the existing result of non-invariant model. The graphical comparison in Fig(4.6), clearly shows distinct

variation in dispersion. For non invariant model, a bunching of curves for different  $\tau_m$  can be seen at large shear rate. But this is missing in the results from proper invariant model. Next a physically realistic tangent hyperbolic profile is used and the equation is solved numerically in standard software Matlab. The growth rate (positive imaginary values of eigen frequency  $\omega$ ) is plotted in parameter space of wave number  $k_y$  and Reynolds number  $R$  and the corresponding localized eigenfunctions in  $x$  (inhomogeneity direction) are also shown. In the complex plane of eigen frequency(Fig-4.5), only one such positive imaginary eigen frequency is found that has no real part which proves non propagating nature of the disturbance. The values of growth rate increases with the increase of solid type strong coupling (representing through  $\tau_m$ ) and the range of  $k$ -space responding to instability also widens. The externally driven shear flow acts as an energy source to the KH instability and the strong coupling between the particles helps to draw more energy so that instability could be enhanced easily. However, viscosity in shear layer dissipates energy into heat which lowers the growth rate.

**In chapter-V**, the role of non-Newtonian property on the stability of dust shear flow is concerned. This property is modeled following the functional dependence of  $\eta$  and  $\gamma$  given in the recent experimental paper[33]. The equilibrium dust flow is considered as bounded and the consistent profile is generated by solving proper equilibrium equation with the experimentally verified model. Different values of  $\epsilon$  (ratio of equilibrium plasma temperature and melting temperature) generate different types of velocity and corresponding viscosity profile with shear rate. With numerical eigenvalue analysis, it is shown that shear thinning property enhances the KH instability but shear thickening property stabilizes it. In

Fig.(5.3), the effect of compressibility is shown with different parameter value of Mach no. ( $M$ ). The growth rate decreases with the increase in  $M$ . The dispersion effect from Poisson's equation is also reported.

**In chapter-VI**, it is shown that the dependence of viscosity on shear rate leads to nonlinear effect in dusty plasma. This is invoked in the dust particle momentum equation with popular Carreau-Bird non-Newtonian model with propagation of shear wave in one spatial dimension. This leads to a wave equation with cubic nonlinearity. The time evolution of this equation with a simple sine wave as initial is numerically solved using a software 'CAPOW'[41]. In this chapter, the recurrence property of shear wave that shows re occurrence of the initial simple sine wave passing through intermediate different localized structures are reported. The energy of initial harmonic is distributed among different higher harmonics but after a recurrence time total energy gets back to the initial mode again. This results find similarity with the famous FPU recurrence in lattice[42]. This recurrence behaviour consolidates about the soliton formation in the system[43]. Proper mathematical approach leads to the formation of modified KdV equation which leads to solitary wave solution[44].

**In chapter-VII**, a summary of the results and discussions made in this doctoral research work is presented. The problems remain unsolved are also discussed point wise which could be interesting to pursue further.

# Chapter 2

## Shear wave and its characteristics in dusty plasma

### 2.1 Introduction

In plasmas, waves are broadly classified as ‘shear wave’ and ‘compressional wave’. Compressional wave (also known as longitudinal wave) propagates through the process of compression and rarefaction in the medium similar to the propagation of sound wave in fluid. The well known compressional waves are ion-acoustic wave in electron-ion plasma, dust acoustic wave in dusty plasma etc. Shear wave usually comes as elastic deformation of particles perpendicular to the direction of wave motion and hence also called as transverse wave. The well known example of shear wave is the transverse wave in elastic rod, the secondary wave (s-wave) in the interior of earth originating from earthquake. An ideal plasma (electron-ion) does not support such transverse wave in absence of any elastic property but magnetic field with the twisting nature of field lines generates another kind of transverse wave called shear Alfvén wave. In dusty plasma, strong coupling between particles provides a long range correlation which causes birth of elastic property. This strong coupling enables the system to support transverse shear wave. This is a

low frequency wave (few Hz) compare to dust acoustic wave ( $\sim$  KHz). This shear wave in dusty plasma was first introduced by Kaw and Sen[38] in 1998 and later experimentally verified. Since then it has been a new direction in dusty plasma research in studying different properties of shear wave. At high temperature, dust particles remain in weak coupling state. So, the system no longer bears solid like elastic nature and hence shear wave could not sustain. But, in low temperature, Coulomb potential energy becomes much larger than dust thermal energy and hence both fluid property (short range ordering, viscosity) and solid property (long range ordering, elasticity) coexist. For the study of such viscoelastic media, Navier-Stoke's equation of momentum of dust fluid is generalized using Maxwell's model of relaxation time. This is the time taken by any applied stress in the medium to be relaxed substantially. This parameter addresses both solid and fluid property together. For ideal fluid, relaxation time is zero but for ideal solid it becomes infinite.

In this chapter, density inhomogeneity is considered with different realistic profile e.g., sech type, parabolic type etc. and the possible effect on shear wave propagation is theoretically investigated. The plasma is considered incompressible to exclude the possible coupling with acoustic mode so that the effect of inhomogeneity on exclusive shear mode can be studied. The continuous frequency of shear wave is transformed into discrete eigen frequencies corresponding to well behaved localized eigenstates. In the last section, strongly coupled magnetized homogeneous dusty plasma is considered to study both transverse waves coming from elastic stress and magnetic stress from a generalized model. The magnetic filed lines can play the role of elastic string and support a kind of shear wave

called shear Alfvén wave. Like the magneto-sonic mode which is produced from the combined effect of plasma pressure and magnetic pressure, another mode called magneto-elastic is hereby introduced coming from the effect of elastic and magnetic stress together.

## 2.2 Generalized hydrodynamic model equations

The frequency scale of the waves and instabilities studied in this thesis is of the order  $\omega \ll kv_{te}, kv_{ti}$  where  $v_{te}$  and  $v_{ti}$  denote thermal velocities of electron and ion. For such long time scale phenomena, it is justified to assume that electrons and ions get enough time to obey the Boltzmann distribution. The momentum of dust fluid in strongly coupled dusty plasma is studied by the generalized hydrodynamic (GH) equation. This equation basically treats the fluid system which bears both viscous and elastic property together. In 1867, J C Maxwell modeled a viscoelastic medium with his thought experimental model as a series connection of a purely viscous damper and a purely elastic spring[45]. Then he simply added different strain rates for a particular external stress and shown that the stress would die out after certain relaxation time. In ideal viscous medium, any applied stress relaxes instantaneously with the flow of the fluid particles. In solid, restoring force can resist the effect of applied stress infinitely without any flow depending on the value of the stress. In visco-elastic media, stress relaxes with finite time which maintains an exponential decay in time as  $\sim \exp(-t/\tau_m)$ , where  $\tau_m$  is called Maxwell's relaxation time. This time increases with the increase of coupling parameter  $\Gamma$  [46] and these two parameters are used to quantify the solid property in strongly coupled dusty plasma. The GH equation is derived by incorporating non-local visco-elastic

operator expressing memory effect and long range ordering developed in the dust fluid. The generalized momentum equation of dust fluid is written as[47]

$$\rho \left( \frac{\partial}{\partial t} + \mathbf{v} \cdot \nabla \right) \mathbf{v} + \nabla p - n_d Z e \nabla \phi = - \int_{-\infty}^t dt' \int d\mathbf{r}' \eta(\mathbf{r} - \mathbf{r}', t - t') \mathbf{v}(\mathbf{r}', t'). \quad (2.1)$$

The symbols  $\rho$ ,  $\mathbf{v}$  and  $n_d$  represent mass density, velocity, number density of dust fluid respectively.  $Z$  denotes the no of electrons on each dust particle and  $\phi$  is the electrostatic potential. The term  $p$  denotes pressure and  $\eta$  denotes viscosity which is taken as memory dependent nonlocal operator. Now the Fourier transformation of the above equation leads to the nonlocal form in  $(\mathbf{k} - t)$  space,

$$\bar{\Gamma}(\mathbf{k}, t) = - \int_{-\infty}^t dt' \bar{\eta}(\mathbf{k}, t - t') \bar{\mathbf{v}}(\mathbf{k}, t'). \quad (2.2)$$

$\bar{\Gamma}(\mathbf{k}, t)$  represents the Fourier transformed form of the left hand side of equation(2.1) and  $\mathbf{k}$  is the wave vector. The memory dependent visco-elastic operator  $\bar{\eta}(\mathbf{k}, t - t')$  can be modeled [48, 49] as,

$$\bar{\eta}(\mathbf{k}, t - t') = \bar{\eta}(\mathbf{k}) \frac{\exp[-(t - t')/\tau_m]}{\tau_m}. \quad (2.3)$$

The equation (2.2) is re-written as,

$$\bar{\Gamma}(\mathbf{k}, t) = - \int_{-\infty}^t dt' \bar{\eta}(\mathbf{k}) \frac{\exp[-(t - t')/\tau_m]}{\tau_m} \bar{\mathbf{v}}(\mathbf{k}, t'). \quad (2.4)$$

Taking partial time derivative of equation(2.4)

$$\frac{\partial \bar{\Gamma}(\mathbf{k}, t)}{\partial t} = -\bar{\eta}(\mathbf{k}, 0) \bar{\mathbf{v}}(\mathbf{k}, t) + \int_{-\infty}^t dt' \frac{\bar{\eta}(\mathbf{k}, t - t')}{\tau_m} \bar{\mathbf{v}}(\mathbf{k}, t') \quad (2.5)$$

where we use

$$\frac{\partial \bar{\eta}(\mathbf{k}, t - t')}{\partial t} = -\frac{\bar{\eta}(\mathbf{k})}{\tau_m^2} \exp[-(t - t')/\tau_m]$$

and Leibniz's integral rule

$$\frac{\partial}{\partial t} \left( \int_{a(t)}^{b(t)} f(x, t) dx \right) = \int_{a(t)}^{b(t)} \frac{\partial f(x, t)}{\partial t} dx + f(b(t), t) \frac{\partial b(t)}{\partial t} - f(a(t), t) \frac{\partial a(t)}{\partial t}.$$

Now we multiply Eq.(2.5) by  $\tau_m$  and add with Eq.(2.2) to get

$$\left(1 + \tau_m \frac{\partial}{\partial t}\right) \bar{\Gamma}(\mathbf{k}, t) = -\bar{\eta}(\mathbf{k}) \bar{\mathbf{v}}(\mathbf{k}, t). \quad (2.6)$$

In weakly coupled limit  $\tau_m \partial/\partial t \ll 1$  the Eq. (2.6) reduces to

$$\bar{\Gamma}(\mathbf{k}, t) = -\bar{\eta}(\mathbf{k}) \bar{\mathbf{v}}(\mathbf{k}, t). \quad (2.7)$$

This equation can be transformed to standard Navier-Stokes equation by inverse Fourier transform considering

$$\bar{\eta}(\mathbf{k}) \bar{\mathbf{v}} = \eta k^2 \bar{\mathbf{v}} + (\eta/3 + \xi) \mathbf{k}(\mathbf{k} \cdot \bar{\mathbf{v}})$$

where  $\eta$  and  $\xi$  denote coefficients of shear viscosity and bulk viscosity respectively.

Applying inverse fourier transform, the equation(2.6) is transformed to[50],

$$\left(1 + \tau_m \frac{\partial}{\partial t}\right) \left[ \rho \left( \frac{\partial}{\partial t} + \mathbf{v} \cdot \nabla \right) \mathbf{v} + \nabla p - n_d Z e \nabla \phi \right] = \eta \nabla^2 \mathbf{v} + \left( \frac{\eta}{3} + \xi \right) \nabla (\nabla \cdot \mathbf{v}). \quad (2.8)$$

For  $\tau_m = 0$ , equation(2.8) reduces to the standard Navier-Stokes hydrodynamic equation. However, this form of GH momentum equation is inconsistent with Galilean invariance which should be maintained to describe non-relativistic physical phenomena. Otherwise the results and explanation of natural phenomena would differ for different inertial frame. Hence a convective term  $\tau_m \mathbf{v} \cdot \nabla$  must be added with  $\tau_m \partial/\partial t$  to get proper Galilean invariant GH momentum equation of strongly coupled charged dust fluid. The equation(2.8) is re-written in proper invariant form of generalized hydrodynamic momentum equation of dust fluid as,

$$\left[ 1 + \tau_m \left( \frac{\partial}{\partial t} + \mathbf{v} \cdot \nabla \right) \right] \left[ \rho \left( \frac{\partial}{\partial t} + \mathbf{v} \cdot \nabla \right) \mathbf{v} + \nabla p - n_d Z e \nabla \phi \right] = \eta \nabla^2 \mathbf{v} + \left( \frac{\eta}{3} + \xi \right) \nabla (\nabla \cdot \mathbf{v}). \quad (2.9)$$

Unlike dust grains, electrons and ions are weakly coupled as their thermal energy exceeds Coulomb interaction energy. The fluid equation of electron motion can be written as,

$$m_e n_e \left( \frac{\partial}{\partial t} + \mathbf{v}_e \cdot \nabla \right) \mathbf{v}_e = -\nabla p_e + n_e e \nabla \phi$$

where  $p_e$ ,  $n_e$  and  $\mathbf{v}_e$  denote respectively pressure, number density and velocity of electron fluid along with the mass  $m_e$  of each electron. Electrons may be considered as light particles for their very small mass. This causes them to respond very quickly to any net force and come to a steady state in balance of electric force and pressure gradient force and hence the inertia term on the left side of electron momentum equation can be neglected. So, the above momentum equation of electron transforms to

$$k_B T_e \nabla n_e - n_e e \nabla \phi = 0,$$

where isothermal pressure is expressed as  $P_e = n_e k_B T_e$  with Boltzmann constant  $k_B$ . In contrast to the long time response of dust grains, ions can also be treated as stationary with the force balance condition

$$k_B T_i \nabla n_i + n_i e \nabla \phi = 0.$$

These two conditions satisfy Boltzmann distributions of electrons and ions expressed as,

$$\begin{aligned} n_e &= n_{e0} \exp\left(\frac{e\phi}{k_B T_e}\right), \\ n_i &= n_{i0} \exp\left(-\frac{e\phi}{k_B T_i}\right). \end{aligned} \tag{2.10}$$

where  $\phi$  is the electrostatic potential,  $T_{i(e)}$  stand for temperature of ion (electron) fluid,  $n_{i(e)}$  is the density of ion (electron). The mass conservation of dust fluid

provides continuity equation

$$\frac{\partial \rho}{\partial t} + \nabla \cdot (\rho \mathbf{v}) = 0. \quad (2.11)$$

The electrostatic potential ( $\phi$ ) is connected with densities of different species through Poisson's equation

$$\nabla \cdot \mathbf{E} = 4\pi e [n_i - n_e - Zn_d], \quad \mathbf{E} = -\nabla \phi \quad (2.12)$$

which couples electric field fluctuation with density fluctuation. The above four equations (2.9-2.12) constitute the complete set of equations for the analysis of strongly coupled dusty plasma.

### 2.3 Existence of shear wave in dusty plasma

The linearized form of the generalized hydrodynamic momentum equation of dust fluid (2.9) can be written as,

$$\left(1 + \tau_m \frac{\partial}{\partial t}\right) \left[ \rho_0 \frac{\partial \mathbf{v}}{\partial t} + \nabla p - Zen_d \nabla \phi \right] = \eta \nabla^2 \mathbf{v}. \quad (2.13)$$

Here we assume incompressibility ( $\nabla \cdot \mathbf{v} = 0$ ) to waive any longitudinal perturbation coming from density fluctuation. No dust flow is taken in equilibrium and only small amplitude wave is considered so that nonlinear convective term has trivial effect.  $\rho_0$  denotes equilibrium homogeneous density and other variables like  $\mathbf{v}$ ,  $p$ ,  $\phi$  are the perturbation in dust fluid velocity, pressure and potential. Let us take curl of the equation (2.13) to obtain

$$\left(1 + \tau_m \frac{\partial}{\partial t}\right) \frac{\partial}{\partial t} (\nabla \times \mathbf{v}) = \frac{\eta}{\rho_0} \nabla^2 (\nabla \times \mathbf{v}). \quad (2.14)$$

For a two dimensional incompressible plasma,  $\nabla \cdot \mathbf{v} = 0$  implies the solution for the velocity as  $\mathbf{v} = \hat{e}_z \times \nabla \psi(x, y)$ , where  $\psi(x, y)$  is the velocity stream function

with  $\nabla \times \mathbf{v} = \hat{e}_z \Omega$  and vorticity  $\Omega = \nabla^2 \psi$ . Let us first consider uniform density  $\rho_0$  and investigate the above equation(2.14) in both hydrodynamic and kinetic limit.

**In hydrodynamic limit** defined as  $\tau_m \partial/\partial t \ll 1$ , z-component of the equation (2.14) is written as,

$$\frac{\partial}{\partial t} \Omega = \frac{\eta}{\rho_0} \nabla^2 \Omega \quad (2.15)$$

which resembles the diffusion equation. With the consideration of plane wave form  $\Omega \sim \exp(i\mathbf{k} \cdot \mathbf{r} - i\omega t)$ , the above diffusion equation results the dispersion relation  $\omega = -i\eta k^2/\rho_0$ . This shows that any mode will be due to viscosity in weakly coupled case.

**In kinetic limit** defined as  $\tau_m \partial/\partial t \gg 1$ , the linearized vorticity equation (2.14) reduces to

$$\frac{\partial^2 \Omega}{\partial t^2} = c_{sh}^2 \nabla^2 \Omega \quad (2.16)$$

which represent wave equation where phase velocity of shear wave is  $c_{sh}^2 = \eta/(\tau_m \rho_0)$ .  $\tau_m$  can be expressed as

$$\tau_m = \frac{4\eta m_d}{3\rho_0 T_{d0}} \frac{1}{(1 - \gamma_d \mu_d + 4u(\Gamma)/15)},$$

and using this relation, expression of the velocity of shear wave becomes,

$$c_{sh}^2 = \frac{3T_{d0}}{4m_d} \left( 1 - \gamma_d \mu_d + \frac{4}{15} u(\Gamma) \right). \quad (2.17)$$

The values of  $\mu_d$  and  $u$  can be calculated using concept of coupling parameter  $\Gamma$  from expressions,

$$\begin{aligned} \mu_d &= 1 + \frac{u(\Gamma)}{3} + \frac{\Gamma}{9} \frac{\partial u(\Gamma)}{\partial \Gamma} \\ u(\Gamma) &\approx -0.89\Gamma + 0.95\Gamma^{1/4} + 0.19\Gamma^{-1/4} - 0.81 \end{aligned} \quad (2.18)$$

where  $\gamma_d$  is the adiabatic constant,  $\mu_d$  is the compressibility and  $u$  is the excess internal energy of the system[38]. This is a purely mechanical transverse wave existing in fluid phase of strongly coupled dusty plasma. Experimentally, this has been observed in a glow discharge dusty plasma with hydrated aluminium silicate particles of micron size using as dust grains[40]. In this reference, both dust acoustic wave and shear wave have been reported to be excited simultaneously with phase velocities  $c_{da} = 4$  cm/s and  $c_{sh} = 4.2$  mm/s respectively for dust particle density  $5 \times 10^{11} m^{-3}$  and dust particle temperature 0.03 eV. The measured shear wave velocity is compared with that obtained from theoretical expression (2.17). Transverse wave has also been observed in 2D crystal phase of dusty plasma[39]. Here, 2D dust monolayer is formed in rf discharge plasma and laser beam is used to exert radiation pressure to excite shear wave.

## 2.4 Effect of inhomogeneity on shear wave in dusty plasma

Let us consider one dimensional propagation of shear wave with variation only along  $x$  such that  $\mathbf{v} = v_y(x)\hat{e}_y$  and density variation  $f(x) = \text{sech}^2(\alpha x)$  where  $\alpha$  is the inverse of the scale length of density inhomogeneity. The chosen density profile is observed in plasmas mostly controlled by diffusion process. The equation(2.13) can simply be written as,

$$\frac{d^2 v_y}{dx^2} + \gamma^2 \text{sech}^2(\alpha x) v_y = 0. \quad (2.19)$$

Since there is no density fluctuation, the pressure and electric field terms play no effect on wave propagation. The above equation (2.19) has well behaved solution

for the eigen-values

$$\gamma^2 = \frac{\omega^2}{c_{sh}^2} = n(n+1)\alpha^2 \quad (2.20)$$

where  $n = 1, 2, 3, \dots$ . For the corresponding eigenfunction one has to solve the following equation,

$$\frac{d^2 v_y}{dx^2} + n(n+1)\alpha^2 \text{sech}^2(\alpha x) v_y = 0. \quad (2.21)$$

The solution of this equation is well described in the Ref.[51]. The corresponding eigenstates for  $n = 1, 2$  can be shown as

$$\begin{aligned} v_y(x) &= v_{y0} \tanh(\alpha x), & \frac{\omega^2}{c_{sh}^2} &= 2\alpha^2 \\ v_y(x) &= v_{y0} [\text{sech}^2(\alpha x) - 2 \tanh^2(\alpha x)], & \frac{\omega^2}{c_{sh}^2} &= 6\alpha^2 \end{aligned}$$

which are localized.

## 2.5 Effect of inhomogeneity on shear wave vortex in visco-elastic fluid

In order to study mechanical shear wave vortex in two dimension, let us consider the case of a neutral inhomogeneous visco-elastic fluid where electric force term is absent. For inhomogeneous density  $\rho_0(x) = \rho_0 f(x)$  (where  $\rho_0$  is constant), perturbed velocity  $\mathbf{v} = v_x(x, y)\hat{e}_x + v_y(x, y)\hat{e}_y$  and using incompressibility condition, the z-component of the equation(2.14) takes the form

$$\frac{\partial^2}{\partial t^2} [f(x, y)\nabla^2 \psi + \nabla f \cdot \nabla \psi] = \frac{\eta}{\rho_0 \tau_m} \nabla^4 \psi, \quad (2.22)$$

where kinetic limit is considered. Taking Fourier transformation in time i.e,

$$\psi(x, y, t) = \psi(x, y) \exp(-i\omega t)$$

the equation(2.22) leads to

$$\nabla^4\psi + \gamma^2 f(x, y)\nabla^2\psi + \gamma^2\nabla f \cdot \nabla\psi = 0, \quad (2.23)$$

where  $\gamma^2 = \omega^2/c_{sh}^2$ . We need to solve the above equation to get vortex solution. But due to its complicated nature we would like to simplify this equation in the following way:

$$\nabla \cdot [\nabla(\nabla^2\psi)] + \gamma^2\nabla \cdot (f\nabla\psi) = 0.$$

This can be finally written as

$$(\nabla^2 + \gamma^2 f)\nabla\psi = \hat{e}_z \times \nabla g \quad (2.24)$$

where  $g$  is some scalar function. Up to this there is no approximation involved. For simplicity in our analysis, we shall consider the special case  $g = 0$  and write the above equation as[52],

$$(\nabla^2 + \gamma^2 f)\bar{\psi} = 0 \quad (2.25)$$

where  $\bar{\psi} = |\nabla\psi|$  and it represents magnitude of velocity of dust fluid.

**Example-I** Now, we consider  $f(x) = \text{sech}^2(\alpha x)$  and solve the equation

$$\left( \frac{\partial^2}{\partial x^2} + \frac{\partial^2}{\partial y^2} \right) \bar{\psi} + \gamma^2 \text{sech}^2(\alpha x) \bar{\psi} = 0. \quad (2.26)$$

There is no inhomogeneity in y-direction so the solution can be expressed in normal Fourier modes as  $\bar{\psi}^n(x, y) = \phi(x) \sin(n\pi\alpha y)$  to get the form

$$\frac{d^2\phi}{dx^2} + \left[ \frac{\gamma^2}{\alpha^2} \text{sech}^2(x) - n^2\pi^2 \right] \phi = 0, \quad (2.27)$$

where  $x$  is normalized by  $\alpha$ . With the transformation[53]  $\xi = \tanh x$ , this equation is reduced to

$$(1 - \xi^2)^2 \frac{d^2\phi}{d\xi^2} - 2(1 - \xi^2)\xi \frac{d\phi}{d\xi} + \left[ \frac{\gamma^2}{\alpha^2} (1 - \xi^2) - n^2\pi^2 \right] \phi = 0.$$

With the change of variable  $\phi = (1 - \xi^2)^{\lambda_n/2} \chi(\xi)$  and  $\lambda_n = n\pi$ , we get

$$(1 - \xi^2) \frac{d^2 \chi}{d\xi^2} - 2\xi(\lambda_n + 1) \frac{d\chi}{d\xi} + \left( \frac{\gamma^2}{\alpha^2} - \lambda_n - \lambda_n^2 \right) \chi(\xi). \quad (2.28)$$

This equation gives regular Gegenbauer solution only if the mode frequencies are discrete with the relation

$$\gamma_{ns}^2 = \frac{\omega^2}{c_{sh}^2} = (s + n\pi)(s + n\pi + 1)\alpha^2, \quad \text{with } s = 0, 1, 2, \dots; n = 1, 2, 3, \dots$$

For each such value of frequency, we get a corresponding shear mode eigenfunction

$$\bar{\psi}^{n,s}(x, y) = N_{ns} \sqrt{2\alpha} \frac{\sin n\pi\alpha y}{(\cosh \alpha x)^{n\pi}} G_s^{n\pi + \frac{1}{2}}(\tanh \alpha x),$$

where  $G_s^{n\pi+1/2}$  is a Gegenbauer polynomial,  $N_{ns}$  is a normalization constant. The velocity profiles and the dispersion relations for a few cases are given below

$$\begin{aligned} \bar{\psi}^{1,0} &= N_{10} \sqrt{2\alpha} \sin \pi\alpha y (\operatorname{sech} \alpha x)^\pi, & \frac{\omega^2}{c_{sh}^2} &= \pi(\pi + 1)\alpha^2 \\ \bar{\psi}^{1,1} &= N_{11} \sqrt{2\alpha} \left( \pi + \frac{1}{2} \right) \sin \pi\alpha y (\operatorname{sech} \alpha x)^\pi \tanh \alpha x, & \frac{\omega^2}{c_{sh}^2} &= (1 + \pi)(2 + \pi)\alpha^2 \\ \bar{\psi}^{1,2} &= N_{12} \sqrt{2\alpha} \left( \pi + \frac{1}{2} \right) \sin \pi\alpha y (\operatorname{sech} \alpha x)^\pi \left[ 2 \left( \pi + \frac{3}{2} \right) \tanh^2 \alpha x - 1 \right], \\ \frac{\omega^2}{c_{sh}^2} &= (2 + \pi)(3 + \pi)\alpha^2 \end{aligned} \quad (2.29)$$

where

$$N_{10}^2 = \alpha \frac{\Gamma(\pi + 1/2)}{\sqrt{\pi} \Gamma(\pi - 1/2)}, \quad N_{11}^2 = \frac{N_{10}^2}{2(\pi + 1/2)}, \quad N_{12}^2 = \frac{N_{10}^2}{2(\pi + 1/2)(\pi + 1)}.$$

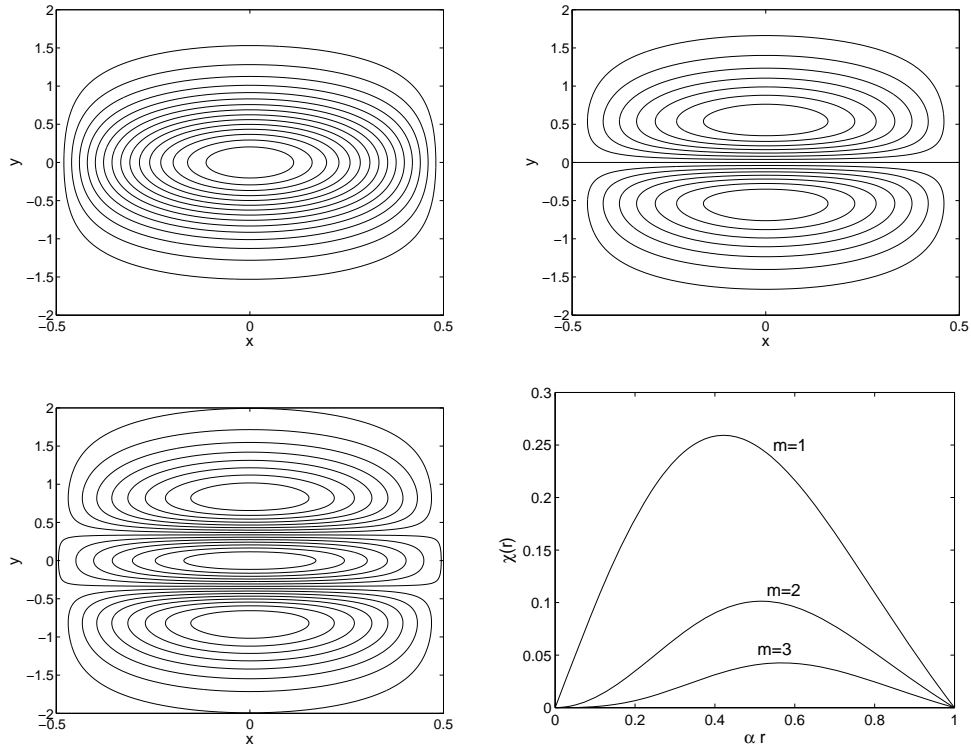


Figure 2.1: In first three graphs, monopole, dipole and tripole structures of contours of magnitude of velocity of dust fluid are plotted respectively in  $x - y$  plane as derived in the example-I. In the fourth graph, localized solutions (radial part) of  $\bar{\psi}$  are shown for different values of  $m$  as derived in example-II.

Equation(2.29) shows that for a density gradient in  $x$ , we obtain periodic solutions in  $y$ -direction, with localization in the  $x$ . The solutions corresponding to  $n = 1, s = 0, 1$  give rise to monopole and dipole vortices respectively while the solution for  $n = 1, s = 2$  represents a tripolar vortex which are plotted in Fig.(2.1).

**Example-II**, Finally, we consider a cylindrical system, with an equilibrium density profile given by  $f(r) = (1 - \alpha^2 r^2)$ . With using  $\bar{\psi} = \chi(r) \exp(im\theta)$ , the inhomogeneous shear wave equation (2.25) leads to

$$\frac{1}{r} \frac{\partial}{\partial r} \left( r \frac{\partial \chi}{\partial r} \right) - \frac{m^2}{r^2} \chi + \gamma^2 (1 - \alpha^2 r^2) \chi = 0. \quad (2.30)$$

Now we take  $\gamma r = \bar{r}$  and transform the equation to the form,

$$\bar{r}^2 \frac{d^2 \chi}{d\bar{r}^2} + \bar{r} \frac{d\chi}{d\bar{r}} - m^2 \chi + \left( \bar{r}^2 - \frac{\alpha^2 \bar{r}^4}{\gamma^2} \right) \chi = 0. \quad (2.31)$$

With the change of variable  $\chi = \bar{r}^{\pm m} \Omega$  we get

$$\bar{r}^2 \frac{d^2 \Omega}{d\bar{r}^2} + \bar{r} (\pm 2m + 1) \frac{d\Omega}{d\bar{r}} + \bar{r}^2 \left( 1 - \frac{\alpha^2 \bar{r}^2}{\gamma^2} \right) \Omega.$$

Again we transform the equation with  $\bar{r}^2 = 2\zeta$  and get the form,

$$\xi \frac{d^2 \Omega}{d\xi^2} + (1 \pm m) \frac{d\Omega}{d\xi} + \left( \frac{1}{2} - \frac{\alpha^2 \xi}{\gamma^2} \right) \Omega = 0.$$

Another transformation  $\Omega = \exp(\kappa \xi) \Gamma(\xi)$  is taken to transform the equation to the form

$$\xi \frac{d^2 \Gamma}{d\xi^2} + (1 \pm m + 2\kappa \xi) \frac{d\Gamma}{d\xi} + \left[ \kappa(1 \pm m) + \frac{1}{2} + \left( \kappa^2 - \frac{\alpha^2}{\gamma^2} \right) \xi \right] \Gamma = 0.$$

Now we consider specific case for  $\kappa^2 = \alpha^2/\gamma^2$  and take the relation  $\xi = -z/2\kappa$ .

Hence we get standard Kummer's differential equation

$$z \frac{d^2 \Gamma}{dz^2} + (d - z) \frac{d\Gamma}{dz} - az = 0, \quad (2.32)$$

with

$$d = 1 \pm m; \quad a = \frac{\kappa(1 \pm m) + \frac{1}{2}}{2\kappa}.$$

A physically well-behaved solution is obtained in the form [54]

$$\chi(r) = (\alpha r)^m e^{-\gamma \alpha r^2/2} {}_1F_1 \left( \frac{1+m}{2} - \frac{\gamma}{4\alpha}, 1+m, \gamma \alpha r^2 \right) \quad (2.33)$$

where  ${}_1F_1$  is a Kummer confluent hypergeometric function.

The physically acceptable solutions are obtained by considering that  $\chi(r)$  vanishes at  $r = 0, r\alpha = 1$ . This leads to the velocity profiles vanishing at the axis and at the boundary. These conditions give the eigenfrequencies of the shear wave. For the parabolic density profile chosen here, the radial part of eigenfunctions are shown in Fig.(2.1). The corresponding eigenfrequencies  $\omega/c_{sh}\alpha$  are given by 4.62, 6.52, 8.42 for  $m = 1, 2, 3$  respectively.

## 2.6 Shear wave in magnetized dusty plasma

Now we consider the effects of an external magnetic field  $\mathbf{B} = B_0\hat{z}$  on a strongly coupled plasma. The presence of magnetic field exerts tensile stress which causes propagation of shear Alfvén wave. The density of dust fluid gives inertia and the tension of magnetic field lines provides the restoring force to produce the wave. We would like to study the propagation of shear Alfvén wave along with the mechanical elastic wave in strongly coupled magnetized dusty plasma[55]. The characteristic wave frequency is assumed to be much smaller than the ion gyrofrequency, where dust particle dynamics is important. In such a situation the ion and electron inertial forces are much smaller than the corresponding Lorentz forces. Therefore equations of motion for the electron and ion fluids can be written as:

$$0 = -en_e(\mathbf{E} + \mathbf{v}_e \times \mathbf{B}), \quad (2.34)$$

$$0 = en_i(\mathbf{E} + \mathbf{v}_i \times \mathbf{B}), \quad (2.35)$$

where,  $n_{e,i}$  is the number density of electron and ion fluid and  $\mathbf{v}_{e,i}$  is the corresponding velocity. The electric and magnetic fields are denoted as  $\mathbf{E}$  and  $\mathbf{B}$  respectively.

The momentum equation for the dust fluid can be written

$$m_d n_d \frac{d\mathbf{v}}{dt} = -Zen_d(\mathbf{E} + \mathbf{v} \times \mathbf{B}) + \eta \nabla^2 \mathbf{v} + \left(\xi + \frac{\eta}{3}\right) \nabla(\nabla \cdot \mathbf{v}), \quad (2.36)$$

where,  $n_d$  is the number density of dust fluid,  $\mathbf{v}_d$  is the dust fluid velocity,  $Z$  is the number of negative charges on a single dust particle,  $\eta$  and  $\xi$  are the shear and bulk viscosity coefficients of dust fluid respectively. We assume cold plasma so that pressure term is neglected. The notation  $d/dt$  represents total time derivative given by

$$\frac{d\mathbf{v}}{dt} = \frac{\partial\mathbf{v}}{\partial t} + \mathbf{v} \cdot \nabla \mathbf{v}$$

where  $\mathbf{v} \cdot \nabla$  is the convective derivative. Next we shall define the mass density, center of mass fluid flow velocity and current density for the bulk fluid. First mass density is defined as  $\bar{\rho} = m_e n_e + m_i n_i + m_d n_d$ . Since  $m_e, m_i \ll m_d$ ,  $\bar{\rho} = \rho \approx m_d n_d$ . Then average fluid velocity  $\bar{\mathbf{v}} = (m_e n_e \mathbf{v}_e + m_i n_i \mathbf{v}_i + m_d n_d \mathbf{v}) / (m_d n_d) \approx \mathbf{v}$  and finally the current density is defined as  $\mathbf{J} = e(n_i \mathbf{v}_i - n_e \mathbf{v}_e - Z n_d \mathbf{v})$ . The current density  $\mathbf{J}$  related to the magnetic field  $\mathbf{B}$  through Ampere's law is given by

$$\nabla \times \mathbf{B} = \mu_0 \mathbf{J} = \mu_0 e (n_i \mathbf{v}_i - n_e \mathbf{v}_e - Z n_d \mathbf{v}). \quad (2.37)$$

By adding the equations (2.34), (2.35) and (2.36) and working in the MHD approximation for viscous dusty plasma with infinite electrical conductivity and also with the quasineutrality condition  $n_i \approx n_e + Z n_d$  we can write down the single fluid momentum equation of the bulk fluid as

$$\rho \frac{d\mathbf{v}}{dt} = \mathbf{J} \times \mathbf{B} + \eta \nabla^2 \mathbf{v} + \left( \xi + \frac{\eta}{3} \right) \nabla (\nabla \cdot \mathbf{v}). \quad (2.38)$$

Now we add equations (2.34), (2.35) and then use quasineutrality condition ( $n_i \approx n_e + Z n_d$ ) and the expression for current density to get the following form of the generalized Ohm's law

$$\mathbf{E} = -\mathbf{v} \times \mathbf{B} - \frac{\mathbf{J} \times \mathbf{B}}{Z e n_d}. \quad (2.39)$$

Taking curl of the above equation and using Faraday's law ( $\nabla \times \mathbf{E} = -\partial\mathbf{B}/\partial t$ ), the time evolution of magnetic field for the bulk dusty plasma can be obtained as,

$$\frac{\partial\mathbf{B}}{\partial t} = \nabla \times (\mathbf{v} \times \mathbf{B}) + \frac{\nabla \times (\mathbf{J} \times \mathbf{B})}{Zen_d}, \quad (2.40)$$

where the first term in the right hand side is the convective term and the second one is the Hall term.

The ratio of the Hall to the convection term can be estimated as  $\sim v_A/L\omega_{cd} \sim \delta_d/L$ , where  $\omega_{cd}(= ZeB_0/m_d)$  and  $\delta_d = v_A/\omega_{cd} = c/\omega_{pd}$  are the cyclotron frequency and skin depth of dust particle, and  $L$  and  $v_A(= B_0/\sqrt{\mu_0\rho_0})$  are the characteristic length and Alfvén velocity of the system. For waves with scale length  $L \gg \delta_d$ , the Hall term can be neglected.

Using the model described in section(2.2), we generalize the Eq.(2.38) and obtain

$$\left(1 + \tau_m \frac{d}{dt}\right) \left[\rho \frac{d\mathbf{v}}{dt} - \mathbf{J} \times \mathbf{B}\right] = \eta \nabla^2 \mathbf{v} + \left(\xi + \frac{\eta}{3}\right) \nabla(\nabla \cdot \mathbf{v}) \quad (2.41)$$

where  $\tau_m$  is the relaxation time of the medium. Equations (2.37), (2.40) and (2.41) are magnetohydrodynamic equations describing low frequency phenomena in a strongly coupled, cold magnetized dusty plasma.

### Linear Analysis:

For simplicity we have assumed that in equilibrium, plasma is homogeneous. The equilibrium is defined by the constant variables  $\rho = \rho_0$ ,  $\mathbf{v} = 0$ ,  $\mathbf{B} = B_0 \hat{z}$ . Now we perturbed the system with small amplitude perturbations in velocity, magnetic field and current density respectively defined by the symbols  $\mathbf{v}$ ,  $\mathbf{B}$  and  $\mathbf{J}$ . Linearizing equations (2.37), (2.40) and (2.41) around the equilibrium mentioned above we have

$$\nabla \times \mathbf{B} = \mu_0 \mathbf{J}, \quad (2.42)$$

$$\frac{\partial \mathbf{B}}{\partial t} = \nabla \times (\mathbf{v} \times \mathbf{B}_0), \quad (2.43)$$

$$\left(1 + \tau_m \frac{\partial}{\partial t}\right) \left[ \rho_0 \frac{\partial \mathbf{v}}{\partial t} - \mathbf{J} \times \mathbf{B}_0 \right] = \eta \nabla^2 \mathbf{v} + \left(\xi + \frac{\eta}{3}\right) \nabla(\nabla \cdot \mathbf{v}). \quad (2.44)$$

We consider that a wave is propagating making an angle  $\theta$  with unperturbed magnetic field  $\mathbf{B}_0$  i.e, wave vector  $\mathbf{k}$  and  $\mathbf{B}$  are in the same plane with wave vector  $\mathbf{k} = k_x \hat{x} + k_z \hat{z}$ . Since the above equations are linear we can Fourier transform these equations assuming the solutions for the perturbed variables are in the form  $\sim \exp[-i(\omega t - \mathbf{k} \cdot \mathbf{r})]$ . Here  $\omega$  is the frequency and  $\mathbf{k}$  is the wave vector of the mode under consideration. Substituting perturbed solutions in Eqs. (2.42) - (2.44) we find

$$\mathbf{k} \times \mathbf{B} = -i\mu_0 \mathbf{J}, \quad (2.45)$$

$$(1 - i\omega\tau_m)[-i\omega\rho_0\mathbf{v} - \mathbf{J} \times \mathbf{B}_0] = -\eta k^2 \mathbf{v} - \left(\xi + \frac{\eta}{3}\right) \mathbf{k}(\mathbf{k} \cdot \mathbf{v}), \quad (2.46)$$

$$\omega \mathbf{B} = \mathbf{B}_0(\mathbf{k} \cdot \mathbf{v}) - (\mathbf{B}_0 \cdot \mathbf{k})\mathbf{v}. \quad (2.47)$$

In kinetic limit  $\omega\tau_m \gg 1$ , for electrostatic case  $\mathbf{B} = 0$  equation (2.46) yields compressional mode with  $\mathbf{k} \cdot \mathbf{v} \neq 0$  and shear mode with  $\mathbf{k} \times \mathbf{v} \neq 0$ . The phase velocity of the shear wave and the compressional wave are found to be  $v_{sh}^2 = \eta/\tau_m\rho_0$

and  $v_c^2 = (\xi + \frac{4}{3}\eta)/\tau_m\rho_0$  as investigated before [38]. Eliminating  $\mathbf{B}$  and  $\mathbf{J}$  from above three equations (2.45)-(2.47) we obtain equation in  $\mathbf{v}$  as,

$$[\omega^2 - v_A^2 k_z^2 - c_{sh}^2 k^2] \mathbf{v} + [(c_{sh}^2 - v_c^2) \mathbf{k} - \hat{x} k_x v_A^2] (\mathbf{k} \cdot \mathbf{v}) + k_z v_A (\mathbf{v}_A \cdot \mathbf{v}) \mathbf{k} = 0. \quad (2.48)$$

To find the dispersion relation we have taken two different kinds of polarization for the velocity vector  $\mathbf{v}$ . First let us take  $\mathbf{v} = v_x \hat{x} + v_z \hat{z}$  which means the velocity vector is polarized in the  $(x-z)$  plane i.e. in the plane where the propagation vector lies. From Eq.(2.48), considering  $x$  and  $z$  components the dispersion equation in matrix form can be written as,

$$\begin{pmatrix} \omega^2 - v_A^2 k^2 - c_{sh}^2 k_z^2 - v_c^2 k_x^2 & -(v_c^2 - c_{sh}^2) k_x k_z \\ -(v_c^2 - c_{sh}^2) k_x k_z & \omega^2 - c_{sh}^2 k_x^2 - v_c^2 k_z^2 \end{pmatrix} \begin{pmatrix} v_x \\ v_z \end{pmatrix} = 0. \quad (2.49)$$

The dispersion relation can be obtained equating the determinant of the matrix to zero which is given by

$$\frac{\omega^2}{k^2} = \frac{1}{2}(v_A^2 + v_c^2 + c_{sh}^2) \pm \frac{1}{2} [v_A^4 + (v_c^2 - c_{sh}^2)^2 - 2v_A^2(v_c^2 - c_{sh}^2) \cos 2\theta]^{\frac{1}{2}} \quad (2.50)$$

where  $\cos \theta = k_z/k$ . For  $\theta = 0$ , we obtain

$$\begin{aligned} \omega^2 &= k^2(c_{sh}^2 + v_A^2) & \text{for } v_z &= 0 \\ &= k^2 v_c^2 & \text{for } v_x &= 0 \end{aligned}$$

with the two modes being transverse and longitudinal respectively. The transverse component ( $v_z = 0$ ) propagating along the magnetic field, depends on the combined effect of mechanical stress and magnetic stress.

When the direction of propagation perpendicular to the unperturbed magnetic field i.e.  $\theta = \pi/2$ , then we have

$$\begin{aligned} \omega^2 &= k^2(v_c^2 + v_A^2) & \text{for } v_z &= 0 \\ &= k^2 c_{sh}^2 & \text{for } v_x &= 0 \end{aligned}$$

The transverse component ( $v_x = 0$ ) propagating perpendicular to the magnetic field is a purely mechanical shear mode independent of magnetic field since the Lorentz force vanishes in this case. The longitudinal component ( $v_z = 0$ ) depends on the magnetic pressure as well as pressure due to viscous force. In the general case when the propagation is oblique with respect to the magnetic field we get mixed modes that are partially transverse and partially longitudinal type with the polarization in the plane generated by the magnetic field and the propagation direction.

Next, we consider the velocity perturbation perpendicular to the direction of propagation vector i.e.  $\mathbf{v} = v_y \hat{y}$ . From Eq.(2.48) we have

$$(\omega^2 - v_A^2 k_z^2 - c_{sh}^2 k^2) v_y = 0.$$

For  $v_y \neq 0$ , a transverse mode propagates in the  $x - z$  plane with phase velocity

$$v_p = \frac{\omega}{k} = \sqrt{(v_A^2 \cos^2 \theta + c_{sh}^2)}$$

When  $\theta = 0$  i.e, when the transverse shear wave is propagating along the unperturbed magnetic field ( $\mathbf{B}_0$ ), the phase velocity becomes

$$v_p = \frac{\omega}{k} = \sqrt{(v_A^2 + c_{sh}^2)} \quad (2.51)$$

In the absence of magnetic field, equation (2.51) reduces to the dispersion relation for a purely elastic mode obtained in Ref.[38]. In the weakly coupled limit, the above mode reduces to the well known shear Alfvén wave. In analogy with the magnetosonic mode [56] which is longitudinal compressional wave propagating perpendicular to the magnetic field in presence of finite temperature, this mode propagating in a magnetized elastic fluid can be termed as ‘magnetoelastic mode’ which propagates along the magnetic field and transverse in nature.

## 2.7 Summary

Strong coupling between dust particles give rise to long range correlation in the system. This introduces elastic nature in strongly coupled dusty plasma. These property enables the system to support transverse shear wave. Here, a theoretical study is reported to show existence of shear wave and also its discrete nature under density inhomogeneity. This inhomogeneity forms localized shear modes with discrete set of eigen frequencies in contrast to the freely propagating wave with continuous dispersion relation  $\omega = kc_{sh}$  in uniform dusty plasma. Different type of profiles (e.g, sech profile, parabolic profile) are analyzed in this study. In magnetized strongly coupled dusty plasma, a transverse shear mode called magnetoelastic mode is analytically predicted. Here two different shear modes, shear Alfvén wave and mechanical shear wave are said to be superposed. It is well known that magnetosonic mode originates from coupled effect of magnetic pressure and plasma pressure. In the present study, combined effect of magnetic stress and elastic stress is responsible for the generation of magnetoelastic wave.



# Chapter 3

## Instability of ‘shear mode’ in presence of velocity shear

### 3.1 Introduction

Strong electrostatic coupling between dust particles due to their huge negative charge generates some solid property. This enables the propagation of mechanical shear mode in fluid phase of dusty plasma. The stability of such shear wave in inhomogeneous plasma is currently being studied in both theory and experiments. Recently, shear wave is shown to be unstable in presence of charge and size distribution of dust grains[57]. In this chapter, shear wave is shown to be unstable in presence of equilibrium linear velocity shear. The shear rate dependent viscosity does the mechanism to extract energy from shear flow to drive the instability. This dependance of viscosity on shear rate is known as non-Newtonian behaviour. In their recent experiment with dust shear flow, Ivlev et. al.[33] have shown first time the signature of such non-Newtonian behaviour in complex plasma. The experiment has been done with gas induced shear flow for different discharge currents and also by applying laser beams of different power. This has enabled measurement of the shear viscosity and confirmation of the non-Newtonian property over

a considerable wide range of shear rate. It has been demonstrated that for low shear rate viscosity remains constant like Newtonian fluid. Then as shear rate being increased, viscosity decreases which is known as shear thinning property. After certain critical shear rate viscosity again increases with increase of shear rate showing shear thickening behaviour. In another experimental analysis using laser beam, Gavrikov et al. have also reported[34] this phenomenon in a dusty plasma liquid. In this context, we should also mention of the simulation works which have predicted the signature of non-Newtonian property in Youkawa liquids [58, 59].

Linear stress strain relationship of Newtonian viscous stress is no longer valid here. Instead nonlinear stress strain relation should be taken with proper modeling of the functional dependence of viscosity on velocity shear rate. In our analysis, we are concerned over shear thinning regime and adopt power law as used in the Ref.[33] for analysis. The choice of appropriate model is different for different physical system and fitting of experimental data provides correct power law exponent. It is particularly useful because of the exact solutions which can be obtained for this model. Although it is very popular model but it can not be used for the limit of zero shear rate. In this limit( $|\dot{\gamma}| \rightarrow 0$ ), power law represents either infinite viscosity or zero viscosity which is unphysical. To remove such inconsistencies, many other models are studied of which Carreau-Bird model is an well known substitute[60]. In our analysis, only shear thinning region safely away from zero shear rate is considered so that use of power law doesn't make any inconsistency.

### 3.2 Model of non-Newtonian viscous stress

The viscous stress tensor of non-Newtonian plasma is expressed as[61],

$$\sigma_{ij} = \eta(|\gamma|) \left[ \left( \frac{\partial v_i}{\partial x_j} + \frac{\partial v_j}{\partial x_i} \right) - \frac{2}{3} \delta_{ij} (\nabla \cdot \mathbf{v}) \right], \quad \delta_{ij} = 1 \text{ for } i = j$$

$$= 0 \text{ for } i \neq j. \quad (3.1)$$

where  $\eta(|\gamma|)$  is the non-Newtonian viscosity coefficient which depends on the scalar invariant quantity  $|\gamma|$  made from the rate of strain tensor

$$\gamma_{ij} = \left( \frac{\partial v_i}{\partial x_j} + \frac{\partial v_j}{\partial x_i} \right).$$

Here  $i, j$  varies as  $x, y$  in the  $(x - y)$  plane and  $\sigma$  and  $\gamma$  can be written as  $2 \times 2$  matrix like as,

$$\sigma = \begin{pmatrix} \sigma_{xx} & \sigma_{xy} \\ \sigma_{yx} & \sigma_{yy} \end{pmatrix}, \quad \gamma = \begin{pmatrix} \gamma_{xx} & \gamma_{xy} \\ \gamma_{yx} & \gamma_{yy} \end{pmatrix}$$

and few components are

$$\sigma_{xx} = 2\eta(|\gamma|) \left( \frac{\partial v_x}{\partial x} - \frac{1}{3} \nabla \cdot \mathbf{v} \right), \quad \sigma_{yx} = \eta(|\gamma|) \left( \frac{\partial v_y}{\partial x} + \frac{\partial v_x}{\partial y} \right)$$

$$\gamma_{yy} = 2 \frac{\partial v_y}{\partial y}, \quad \gamma_{xy} = \left( \frac{\partial v_x}{\partial y} + \frac{\partial v_y}{\partial x} \right).$$

Viscous coefficient  $\eta$  is a scalar quantity but it is to depend on tensor  $\gamma$ . According to tensor algebra, it should depend on scalar invariant quantity of  $\gamma$ . In  $2 \times 2$  tensor, two invariant quantity can be formed by taking trace of  $\gamma$  and  $\gamma^2$ . These invariants are scalar quantity and independent of the choice of co-ordinate system to which the components of tensor  $\gamma$  are referred[35].

These two invariants are known as,

$$I = \sum_i \gamma_{ii} \quad \text{and} \quad II = \sum_i \sum_j \gamma_{ij} \gamma_{ji}, \quad (3.2)$$

where  $i, j$  varies as  $x, y$ . For incompressible medium,

$$I = \gamma_{xx} + \gamma_{yy} = 2 \left( \frac{\partial v_x}{\partial x} + \frac{\partial v_y}{\partial y} \right) = 2(\nabla \cdot \mathbf{v}) = 0.$$

Finally  $|\gamma|$  is modeled as

$$|\gamma| = \sqrt{II/2} = \sqrt{(\gamma_{xx}^2 + \gamma_{yy}^2 + 2\gamma_{xy}\gamma_{yx})/2}. \quad (3.3)$$

Now, we need to model the correct functional dependence of  $\eta$  on  $|\gamma|$ . In the literature of non-Newtonian fluid, there exist many models applicable for different physical systems. The common idea of all model is that for very small shear rate it should go to Newtonian limit i.e, constant viscosity. In asymptotic limit, for large shear rate it shows power law behaviour.

### 3.3 Basic equations and equilibrium

In kinetic limit  $\tau_m \partial/\partial t \gg 1$ , the generalized momentum equation of dust fluid (2.9) with non-Newtonian stress can be written as,

$$\tau_m \left( \frac{\partial}{\partial t} + \mathbf{v} \cdot \nabla \right) \left[ \rho \left( \frac{\partial}{\partial t} + \mathbf{v} \cdot \nabla \right) \mathbf{v} + \nabla p - n_d Z e \nabla \phi \right] = \frac{\partial \sigma_{ij}}{\partial x_j}. \quad (3.4)$$

For incompressible plasma

$$\sigma_{ij} = \eta(|\gamma|) \left( \frac{\partial v_i}{\partial x_j} + \frac{\partial v_j}{\partial x_i} \right).$$

We assume, that the equilibrium velocity is directed along  $y$  direction and has variation in  $x$ , i.e.  $\mathbf{v}_0 = v_{0y}(x)\hat{e}_y$ . The left hand side of equation(3.4) will not contribute in steady state equilibrium since time variation is zero in steady state and for shear flow  $v_{0y}(x)$  convective derivative also becomes zero.

Hence, the equilibrium is described by the equation

$$\frac{d}{dx} \left[ \eta(|\gamma|) \frac{dv_{0y}}{dx} \right] = 0, \quad (3.5)$$

where in equilibrium  $|\gamma| = dv_{0y}/dx$ . The functional form of dependence of viscosity( $\eta$ ) on shear rate( $\gamma$ ) for modeling shear thinning region is considered as[62],

$$\eta(|\gamma|) = \bar{\eta} \left[ \frac{|\gamma|}{\bar{\gamma}} \right]^{-\frac{2\delta}{1+\delta}}, \quad (3.6)$$

here,  $\delta$  is a positive exponent and  $\bar{\eta}$  and  $\bar{\gamma}$  are constants having the dimension of viscosity and shear rate. If we define  $2\delta/(1+\delta) = \alpha$ , then the parameter  $\alpha$  is a positive non-zero constant. In this model, one can't go to the limit ( $|\gamma| \rightarrow 0$ ) as viscosity diverges unphysically. In equilibrium, using this model (3.6) in equation (3.5), we have found that  $dv_{0y}/dx$  is constant and hence we can write the equilibrium velocity as  $v_{0y}(x) = v'_0 x$ , where  $v'_0$  is equilibrium shear rate.

### 3.4 Linear equations and eigenvalue analysis

Let us consider shear wave propagation in presence of equilibrium linear velocity shear. We assume small amplitude wave so that linear analysis can be used neglecting the 2nd and higher order terms. Let us first do linearization of the non-Newtonian viscous force term (R.H.S. of the equation(3.4)). The linearized form of the rate of strain tensor  $\gamma$  takes the form

$$\gamma \equiv \begin{pmatrix} 2\frac{\partial v_x}{\partial x} & \epsilon_0 + \epsilon_1 \\ \epsilon_0 + \epsilon_1 & 2\frac{\partial v_y}{\partial y} \end{pmatrix}$$

here

$$\epsilon_0 = \frac{dv_{0y}}{dx}; \quad \epsilon_1 = \frac{\partial v_x}{\partial y} + \frac{\partial v_y}{\partial x}.$$

The term  $|\gamma|$  can be expressed in linearized form using equation(3.3)

$$|\gamma| = \sqrt{2 \left( \frac{\partial v_x}{\partial x} \right)^2 + 2 \left( \frac{\partial v_y}{\partial y} \right)^2 + (\epsilon_0 + \epsilon_1)^2}.$$

For linear analysis, quadratic shear rate fluctuation terms are neglected and the form is simplified to

$$|\gamma| = \epsilon_0 \sqrt{1 + 2 \frac{\epsilon_1}{\epsilon_0}}.$$

For  $\epsilon_1 \ll \epsilon_0$ , the square root can be expanded binomially as,

$$|\gamma| = \epsilon_0 + \epsilon_1.$$

Now, viscosity  $\eta(|\gamma|)$  can be expanded in Taylor series form as,

$$\eta(\epsilon_0 + \epsilon_1) \simeq \eta(\epsilon_0) + \frac{d\eta}{d\epsilon_0} \epsilon_1 = \eta_0 + \eta'_0 \epsilon_1 \quad (3.7)$$

where  $\eta'_0$  is the gradient of viscosity with unperturbed velocity shear rate  $v'_{0y}$ . The  $x$ -component of viscous force in linearized form,

$$\begin{aligned} \frac{\partial \sigma_{xx}}{\partial x} + \frac{\partial \sigma_{xy}}{\partial y} &= \frac{\partial}{\partial x} \left[ (\eta_0 + \eta'_0 \epsilon_1) 2 \frac{\partial v_x}{\partial x} \right] + \frac{\partial}{\partial y} [(\eta_0 + \eta'_0 \epsilon_1)(\epsilon_0 + \epsilon_1)], \\ &= \eta_0 \nabla^2 v_x + \eta'_0 v'_{0y} \frac{\partial}{\partial y} \left( \frac{\partial v_x}{\partial y} + \frac{\partial v_y}{\partial x} \right) + 2\eta'_0 v''_{0y} \frac{\partial v_x}{\partial x}. \end{aligned}$$

Like as, the  $y$ -component of viscous force in linearized form,

$$\frac{\partial \sigma_{yy}}{\partial y} + \frac{\partial \sigma_{yx}}{\partial x} = \eta_0 \nabla^2 v_y + \left\{ 2\eta'_0 v''_{0y} + \eta''_0 v''_{0y} v'_{0y} + \eta'_0 v'_{0y} \frac{\partial}{\partial x} \right\} \left( \frac{\partial v_x}{\partial y} + \frac{\partial v_y}{\partial x} \right),$$

where  $v'_{0y}$  and  $v''_{0y}$  denote 1st and 2nd order derivative of velocity with  $x$ .

The linearized components of dust momentum equation(3.4) can be written as,

$$\begin{aligned} \left( \frac{\partial}{\partial t} + v_{0y} \frac{\partial}{\partial y} \right) \left[ \frac{\partial v_y}{\partial t} + v_{0y} \frac{\partial v_y}{\partial y} + v_x \frac{dv_{0y}}{dx} - n_d Z e \frac{\partial \phi}{\partial y} + \frac{\partial p}{\partial y} \right] \\ = \frac{\eta_0}{\tau_m \rho_0} \nabla^2 v_y + \frac{\eta'_0 v'_{0y}}{\tau_m \rho_0} \frac{\partial}{\partial x} \left( \frac{\partial v_x}{\partial y} + \frac{\partial v_y}{\partial x} \right), \quad (3.8) \end{aligned}$$

and

$$\begin{aligned} & \left( \frac{\partial}{\partial t} + v_{0y} \frac{\partial}{\partial y} \right) \left[ \frac{\partial v_x}{\partial t} + v_{0y} \frac{\partial v_x}{\partial y} - n_d Z e \frac{\partial \phi}{\partial x} + \frac{\partial p}{\partial x} \right] \\ & = \frac{\eta_0}{\tau_m \rho_0} \nabla^2 v_x + \frac{\eta'_0 v'_{0y}}{\tau_m \rho_0} \frac{\partial}{\partial y} \left( \frac{\partial v_x}{\partial y} + \frac{\partial v_y}{\partial x} \right), \end{aligned} \quad (3.9)$$

where  $v''_{0y}$  is zero for linear velocity shear. In many existing articles[63, 49], studies have been done with a model which is not Galilean invariant. In those work, the term  $\tau_m v_{0y} \partial/\partial y$  is neglected for the sake of mathematical convenience. But in recent nonlinear study, the important role of the galilean invariant model have been discussed[64, 65]. In this section, the analytical calculation and results of our earlier study[62] are shown first and then a non-modal analysis with proper Galilean invariant equation(3.8-3.9) are also discussed.

**Case-I** the term  $\tau_m v_{0y} \partial/\partial y$  is not taken and mathematical analysis is done to form Weber equation. Incompressibility assumption is taken which leads to the velocity  $\mathbf{v} = \hat{e}_z \times \nabla \psi$ . Subtracting y-derivative of equation(3.9) from x-derivative of equation(3.8) we get,

$$\frac{\partial}{\partial t} \left[ \frac{\partial}{\partial t} + v'_0 x \frac{\partial}{\partial y} \right] \nabla_{\perp}^2 v_x = c_{sh}^2 \nabla_{\perp}^4 v_x + \left( \frac{\eta'_0 v'_0}{\tau_m \rho_0} \right) \left( \frac{\partial^2}{\partial x^2} - \frac{\partial^2}{\partial y^2} \right)^2 v_x, \quad (3.10)$$

where  $\nabla_{\perp}^2 = \partial^2/\partial x^2 + \partial^2/\partial y^2$  and  $v_x = -\partial\psi/\partial y$ . We note here that if the velocity shear is absent in Eqs. (3.10), we get back the shear mode dispersion relation  $\omega^2 = (k_x^2 + k_y^2)c_{sh}^2$ . We assume the solution of the form  $v_x = \bar{v}(x) \exp(ik_y y - i\omega t)$ , where  $k_y$  is the wave vector in  $y$  direction and  $\omega$  is the frequency of the mode. Fourier mode is taken only in  $y$  direction since inhomogeneity is present in the  $x$ -direction through velocity shear.

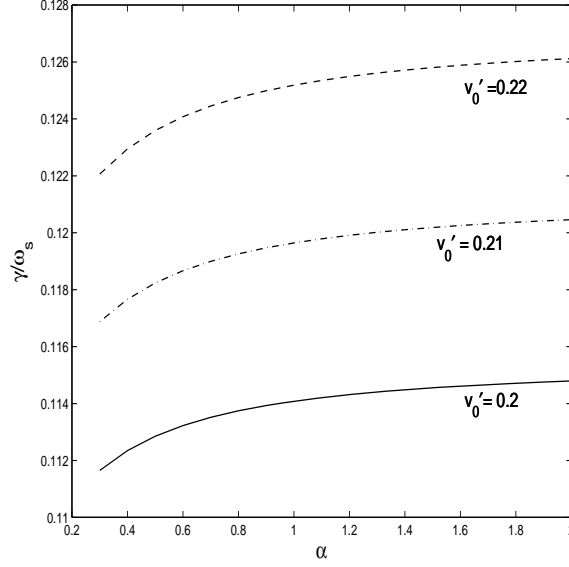


Figure 3.1: Normalized growth rate  $\gamma/\omega_s$  as a function of  $\alpha = |\eta'_0 v'_0 / \eta_0|$ , shows the growth rate of shear mode for different velocity shear rate  $v'_0$ .

The linear equation(3.10) reduces to

$$\begin{aligned} \frac{\omega_s^2}{k_y^2} \left( 1 + \frac{\eta'_0 v'_0}{\eta_0} \right) \frac{d^4 \bar{v}}{dx^4} + \left[ \omega^2 - \omega k_y v'_0 x - 2\omega_s^2 \left( 1 - \frac{\eta'_0 v'_0}{\eta_0} \right) \right] \frac{d^2 \bar{v}}{dx^2} \\ + \left[ k_y^2 \omega_s^2 \left( 1 + \frac{\eta'_0 v'_0}{\eta_0} \right) - k_y^2 (\omega^2 - \omega k_y v'_0 x) \right] \bar{v} = 0, \end{aligned} \quad (3.11)$$

where  $\omega_s^2 = k_y^2 \eta_0 / \rho_0 \tau_m$ . Here we are looking for long radial( $x$ ) scale solution for the differential equation and therefore the fourth order derivative is subdominant compared with the second. The desired eigenvalue equation can be written as

$$\frac{d^2 \bar{v}}{dx^2} - k_y^2 \left[ \frac{\omega^2 - \omega_s^2 (1 - \alpha) - \omega k_y v'_0 x}{\omega^2 - 2\omega_s^2 (1 + \alpha) - \omega k_y v'_0 x} \right] \bar{v} = 0. \quad (3.12)$$

For the condition  $\omega k_y v'_0 / [\omega^2 - 2\omega_s^2 (1 + \alpha)] \ll 1$ , which implies that, when the shear rate is small compared to the frequency of the mode, the above equation can be written in terms of the well known Weber equation which is given by

$$\frac{d^2 \bar{v}}{d\xi^2} - (\xi^2 - K) \bar{v} = 0 \quad (3.13)$$

where

$$\xi = \left[ k_y^2 \beta_2^2 \left( \frac{\beta_2 - \beta_1}{\beta_1} \right) \right]^{1/4} \left( x + \frac{1}{2\beta_2} \right), \quad K = -\frac{k_y}{4} \left( \frac{1}{\beta_2} + \frac{3}{\beta_1} \right) \sqrt{\frac{\beta_1}{\beta_2 - \beta_1}}.$$

and

$$\beta_1 = \frac{k_y v_0' \omega}{\omega^2 - \omega_s^2 (1 - \alpha)}, \quad \beta_2 = \frac{k_y v_0' \omega}{\omega^2 - 2\omega_s^2 (1 + \alpha)}.$$

The solution of Eq. (3.13) for the lowest order eigenmode is given by

$$\bar{v} \sim \exp \left[ -\frac{1}{2} k_y \beta_2 \sqrt{\left( \frac{\beta_2 - \beta_1}{\beta_1} \right) \left( x + \frac{1}{2\beta_2} \right)^2} \right] \quad (3.14)$$

representing the existence of an unstable eigenmode. The condition for bounded solution is  $Re(\beta_2[(\beta_2/\beta_1) - 1]^{1/2}) > 0$ . The behaviour of the eigenfunction  $\bar{v}$  at  $x \rightarrow \pm\infty$  is bounded and the typical mode width  $\Delta \sim \left[ \frac{1}{k_y \beta_2} \sqrt{\frac{\beta_1}{\beta_2 - \beta_1}} \right]^{1/2}$ . The corresponding dispersion relation is given by

$$\omega^2 - \frac{\omega_s^2}{4} (5 - \alpha) = -v_0' \omega \omega_s \sqrt{\frac{1 + 3\alpha}{\omega^2 - 2\omega_s^2 (1 + \alpha)}}, \quad (3.15)$$

where  $\alpha = -\eta_0' v_0' / \eta_0 > 1$  and  $\omega_s^2 = k_y^2 \eta_0 / \rho_0 \tau_m$ . In presence of velocity shear and velocity shear induced viscosity gradient we have solved Eq. (3.15) and found that for  $\alpha < 2$  there is one unstable root for real  $\omega > 0$ . The growth rate for the instability for the given range of  $\alpha$  can be seen in the figure 3.1. The curves in the figure shows that the growth rate increases with increase of shear thinning parameter  $\alpha$  and velocity shear rate( $v_0'$ ). The shear mode becomes more unstable for stronger velocity shear.

**Case-II**, now proper Galilean invariant equations (3.8-3.9) are solved using non-modal analysis. With taking the term  $\tau_m v_{0y} \partial / \partial y$  and subtracting y-derivative of equation(3.9) from x-derivative of equation(3.8) we get,

$$\begin{aligned} \left[ \frac{\partial}{\partial t} + v'_0 x \frac{\partial}{\partial y} \right]^2 \nabla^2 v_x + v'_0 \frac{\partial}{\partial y} \left[ \left( \frac{\partial}{\partial t} + v'_0 x \frac{\partial}{\partial y} \right) \frac{\partial v_x}{\partial x} + v'_0 \frac{\partial v_x}{\partial y} \right] \\ = c_{sh}^2 \nabla^4 v_x + \frac{\eta'_0 v'_0}{\tau_m \rho} \left( \frac{\partial^2}{\partial x^2} - \frac{\partial^2}{\partial y^2} \right)^2 v_x \end{aligned} \quad (3.16)$$

We consider a moving frame where temporal problem can be solved by solving differential equation in time. For this purpose we use a spatially-inhomogeneous Galilean transformation

$$\xi = y - v'_0 x t; \quad \tau = t$$

Hence, we get the transformation of the partial derivatives as

$$\frac{\partial}{\partial x} = -v'_0 t \frac{\partial}{\partial \xi}, \quad \frac{\partial}{\partial y} = \frac{\partial}{\partial \xi}, \quad \frac{\partial}{\partial t} = -v'_0 x \frac{\partial}{\partial \xi} + \frac{\partial}{\partial \tau}$$

and the laplacian  $\nabla^2 = (1 + v_0'^2 \tau^2) \frac{\partial^2}{\partial \xi^2}$ . With these transformation relations, the equation(3.16) reduces to

$$\frac{d^2 v_x}{d\tau^2} - \frac{v_0'^2 \tau}{1 + v_0'^2 \tau^2} \frac{d v_x}{d\tau} + \left[ c_{sh}^2 (1 + v_0'^2 \tau^2) k_\xi^2 + \frac{2v_0'^2}{1 + v_0'^2 \tau^2} - \alpha k_\xi^2 c_{sh}^2 \frac{(1 - v_0'^2 \tau^2)^2}{(1 + v_0'^2 \tau^2)} \right] v_x = 0, \quad (3.17)$$

where inhomogeneity manifests in transformed time( $\tau$ ) and velocity is taken of the form  $v_x = v_x(\tau) \exp(-ik_\xi \xi)$ . In absence of velocity shear this equation leads to pure shear wave represented by

$$\frac{d^2 v_x}{dt^2} + c_{sh}^2 k_y^2 v_x = 0 \quad (3.18)$$

This time evolution equation(3.17) is solved by runge-kutta time integration method. The initial conditions are taken  $v_x = 1$  and  $dv_x/d\tau = 1$ . The 2nd

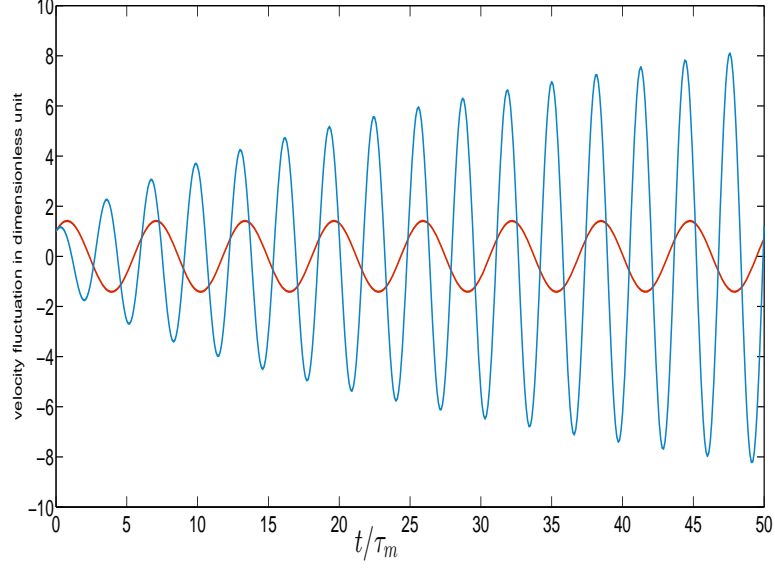


Figure 3.2: The red line curve represents sinusoidal shear wave and the blue line curve represents amplified shear wave in presence of velocity shear rate  $v'_0 = 1.2$ ,  $\alpha = 1.0$ . The velocity of dust fluid is normalized by  $v'_0 L$  where  $L$  is the length of plasma system. The amplitude increases monotonically with time.

order equation in time is decoupled in two first order equations in time as

$$\begin{aligned} \frac{dv_x}{d\tau} &= \tilde{v}_x \\ \frac{d\tilde{v}_x}{d\tau} - \frac{v_0'^2 \tau}{1 + v_0'^2 \tau^2} \tilde{v}_x + c_{sh}^2 (1 + v_0'^2 \tau^2) k_\xi^2 v_x + \frac{2v_0'^2 v_x}{1 + v_0'^2 \tau^2} - \alpha k_\xi^2 c_{sh}^2 \frac{(1 - v_0'^2 \tau^2)^2}{(1 + v_0'^2 \tau^2)} v_x &= 0. \end{aligned} \quad (3.19)$$

In Fig.(3.2), pure oscillation shown in red line is the solution of the equation in absence of velocity shear. In presence of velocity shear the solution is shown in blue line curve. It is clear that the amplitude of the shear wave monotonically increases with time. This confirms the instability of shear wave in presence of velocity shear.

### 3.5 Summary

The transverse mechanical shear wave is shown to become unstable due to shear flow. The linear velocity shear supplies the necessary energy to drive the instability. The non-Newtonian property plays the key role enabling the coupling between velocity fluctuation and equilibrium flow. The variation in the velocity is responsible for viscosity modulation, which provides feedback to the velocity through the momentum equation. For positive feedback of the velocity, an instability is triggered. This novel low-frequency instability disappears when viscosity is uniform and we are left with a shear wave. The growth rate of instability increases with increase of velocity shear rate. This interesting mechanism of instability needs experimental verification which has not been done yet.

# Chapter 4

## Kelvin-Helmholtz instability of dust shear flow in strong coupling

### 4.1 Introduction

Kelvin-Helmholtz (KH) instability is a well observed phenomena in nature which causes energy transfer from mean flow to low frequency long wavelength fluctuation in parallel shear flows. This instability occurs at the interface of two adjacent fluids of different densities under relative motion. A well known example is the case of wind blowing over water surface where instability causes water waves. There are other familiar examples like ocean wave, patterns in the relative motion of cloud layers, surface waves in Saturn's band. This instability also plays an important role in astrophysical plasma involving sheared plasma flow in solar wind, polar cusps, dynamic structure of cometary tails[66]. In 1871, Kelvin[67] had given a theoretical model to study such instability in ocean waves and later Helmholtz[68] applied this theory to billow clouds. In 1880, Rayleigh[69, 70] with his famous inflection point theorem established the idea that the KH instability can also occur in a single fluid for velocity shear which has an inflection point (2nd derivative of velocity vanishes) at some space point. Three years later, Reynolds[71] made

a series of laboratory experiment with laminar pipe flow and demonstrated KH instability and its transition to turbulent layer. Since then the study of linear and nonlinear KH instability has been an evergreen topic of research in oceanography, fluid mechanics, astrophysical plasma, laboratory plasma etc.

In plasma, existence of multi-species charged fluids like electron fluid, ion fluid, neutral fluid and the possible relative motion between them makes it a rich media for KH instability. In fully ionized plasma, D'Angelo[72] with inhomogeneous streaming flow of ions had formulated the condition of KH instability which was later verified in different experiments[73, 74] in thermally ionised cesium plasma (Q machine). For plasma flow perpendicular to field lines, magnetic field has no effect on the instability and it behaves as the instability in neutral fluid. But, if the plasma flow is along the magnetic field, then the condition for instability is that the total velocity jump should exceed twice the Alfvén speed[75]. In kinetic theory, it has been shown that the KH instability is strongly damped when ion temperature is comparable to or larger than electron temperature[76].

In dusty plasma, the effect of dust charge fluctuation on the instability of ion flow has been studied with static dust grains[77] and later with dust flow also[78]. The effect of negatively charged dust grains on the Kelvin-Helmholtz instability of inhomogeneous ion flow is recently studied experimentally in a magnetized cesium plasma with static dust particles[79]. In this chapter, instability of unmagnetized dust shear flow is studied observing the effect of strong coupling between dust particles. Unbounded free shear layer of dust fluid is considered where the shear layer under observation is far away from physical boundary. Both the cases of zero shear width and finite shear width are considered for the investigation of the KH

instability. Zero shear width correspond to vortex sheet modeled by step profile. For finite shear width standard hyperbolic tangent profile is analyzed numerically.

## 4.2 Basic equations with linearized form

The generalized hydrodynamic model is utilized here to study the effects of strong coupling between dust particles on the Kelvin-Helmholtz instability driven by dust shear flow. The temporal scale of this fundamental instability is long enough so that the electrons and ions are assumed to follow Boltzmann's distribution. Incompressible dusty plasma is considered so that density fluctuation is absent. Hence, no part of energy is lost in exciting longitudinal compressible waves and the most unstable situation can be achieved. The spatial scale of the instability is much larger than plasma Debye length so that the density of dust fluid is assumed homogeneous. The equilibrium dust flow is taken along  $y$ -direction with variation in  $x$  so that  $\mathbf{v}_0 = v_{0y}(x)\hat{e}_y$ . The total dust flow is the sum of equilibrium flow and a small perturbation in  $x$ - $y$  plane:

$$\mathbf{v}(x, y, t) = v_x(x, y, t)\hat{e}_x + [v_{0y}(x) + v_y(x, y, t)]\hat{e}_y.$$

We linearize the Eq. (2.9) around equilibrium flow  $v_{0y}$ , and write scalar components as

$$\left\{ 1 + \tau_m \left( \frac{\partial}{\partial t} + v_{0y} \frac{\partial}{\partial y} \right) \right\} \left[ \left( \frac{\partial}{\partial t} + v_{0y} \frac{\partial}{\partial y} \right) v_x + \frac{1}{\rho_0} \frac{\partial p}{\partial x} - \frac{eZ}{m_d} \frac{\partial \phi}{\partial x} \right] = \nu \nabla^2 v_x, \quad (4.1)$$

$$\left\{ 1 + \tau_m \left( \frac{\partial}{\partial t} + v_{0y} \frac{\partial}{\partial y} \right) \right\} \left[ \left( \frac{\partial}{\partial t} + v_{0y} \frac{\partial}{\partial y} \right) v_y + v_x \frac{dv_{0y}}{dx} + \frac{1}{\rho_0} \frac{\partial p}{\partial y} - \frac{eZ}{m_d} \frac{\partial \phi}{\partial y} \right] = \nu \nabla^2 v_y, \quad (4.2)$$

where kinematic viscosity coefficient  $\nu = \eta/\rho_0$ . Differentiating equation(4.1) with respect to  $y$ , and equation(4.2) with respect to  $x$ , and taking a difference we obtain

$$\begin{aligned} & \left\{ 1 + \tau_m \left( \frac{\partial}{\partial t} + v_{0y} \frac{\partial}{\partial y} \right) \right\} \left[ \left( \frac{\partial}{\partial t} + v_{0y} \frac{\partial}{\partial y} \right) \left( \frac{\partial v_x}{\partial y} - \frac{\partial v_y}{\partial x} \right) - v_{0y}'' v_x \right] \\ - \tau_m v_{0y}' \frac{\partial}{\partial y} & \left[ \left( \frac{\partial}{\partial t} + v_{0y} \frac{\partial}{\partial y} \right) v_y + v_{0y}' v_x + \frac{1}{\rho_0} \frac{\partial p}{\partial y} - \frac{Ze}{m_d} \frac{\partial \phi}{\partial y} \right] = \nu \nabla^2 \left( \frac{\partial v_x}{\partial y} - \frac{\partial v_y}{\partial x} \right) \end{aligned} \quad (4.3)$$

where  $Z$  is the number of electrons on each dust grain and  $v_{0y}'$  and  $v_{0y}''$  are respectively 1st and 2nd derivative of velocity with  $x$ . In electrostatic limit, electric field fluctuation only couples with the density fluctuation of charge particles which are mathematically connected through Poisson's equation. In incompressibility limit, no density fluctuation occurs and hence both the pressure and the electric field perturbation terms in equation (4.3) will vanish. The assumption of incompressibility condition ( $\nabla \cdot \mathbf{v} = 0$ ) permits to define a stream function  $\psi$  such that

$$v_x = -\frac{\partial \psi}{\partial y}, \quad v_y = \frac{\partial \psi}{\partial x}.$$

Hence the equation(4.3) can be written as,

$$\begin{aligned} & \left\{ 1 + \tau_m \left( \frac{\partial}{\partial t} + v_{0y} \frac{\partial}{\partial y} \right) \right\} \left[ \left( \frac{\partial}{\partial t} + v_{0y} \frac{\partial}{\partial y} \right) \nabla^2 \psi - v_{0y}'' \frac{\partial \psi}{\partial y} \right] \\ & + \tau_m v_{0y}' \frac{\partial}{\partial y} \left[ \left( \frac{\partial}{\partial t} + v_{0y} \frac{\partial}{\partial y} \right) \frac{\partial \psi}{\partial x} - v_{0y}' \frac{\partial \psi}{\partial y} \right] = \nu \nabla^4 \psi. \end{aligned} \quad (4.4)$$

The physical system is linear and inhomogeneous in  $x$ , so any arbitrary disturbance may be decomposed into normal modes as

$$\psi(x, y, t) = \varphi(x) e^{i(k_y y - \omega t)},$$

where  $\omega = k_y c$ , and  $c$  is the phase velocity of the wave. In homogeneous  $y$ -direction, fourier mode (plane waveform) is used. Using this normal mode form,

equation(4.4) can be written in a dimensionless form as,

$$(D^2 - k_y^2)^2 \varphi(x) = ik_y R [\{1 + ik_y \tau_m (v_{0y} - c)\} \{(v_{0y} - c) (D^2 - k_y^2) - v_{0y}''\} + ik_y \tau_m v_{0y}' \{(v_{0y} - c) D - v_{0y}'\}] \varphi(x) \quad (4.5)$$

where,  $D$  denotes  $d/dx$ , Reynolds number  $R = V_0 L \rho_0 / \eta$ ,  $L$  is equilibrium shear length scale and  $V_0$  is the maximum value of equilibrium velocity. Here, we have used normalization scheme as:  $x \rightarrow x/L$ ,  $t \rightarrow tV_0/L$ . This equation may be called as generalized hydrodynamic Orr-Sommerfeld equation since it describes the instability of dust shear flow in the presence of viscosity and elasticity in the medium[80]. In the limit  $\tau_m = 0$ , this equation leads to the celebrated Orr-Sommerfeld equation[81, 82]

$$(D^2 - k_y^2)^2 \varphi(x) = ik_y R [(v_{0y} - c) (D^2 - k_y^2) - v_{0y}'] \varphi(x) \quad (4.6)$$

which examines the behavior of small disturbances in the parallel flow of an incompressible viscous fluid.

### 4.3 Local approximation

For small wavelength of perturbation compared to inhomogeneity scale length of equilibrium shear ( $k_x L \gg 1$ ), the equilibrium velocity can be treated as constant parameters ( $x$  independent) in local limit and normal Fourier mode analysis is applicable to both  $x$  and  $y$  direction. Here,  $v_{0y}$  and  $v_{0y}'$  are taken as constant parameters and  $v_{0y}'' = 0$ . In weakly coupled limit ( $\tau_m \rightarrow 0$ ), local dispersion relation of Orr-Sommerfeld equation becomes  $\omega = -ik_y^2 \eta$ . So, local dispersion could not predict any instability. In strongly coupled limit ( $\tau_m \partial/\partial t \gg 1$ ), the local dispersion

could be written as,

$$\omega^2 + \frac{ik_x k_y v'_{0y}}{k_x^2 + k_y^2} \omega + \frac{k_y^2 v_{0y}'^2}{k_x^2 + k_y^2} - \nu \frac{k_x^2 + k_y^2}{\tau_m} = 0 \quad (4.7)$$

where  $\omega$  represents Doppler shifted frequency  $\omega - k_y v_{0y}$ . In absence of equilibrium velocity, local dispersion relation gives  $\omega = k c_{sh}$  which represents transverse shear wave with phase velocity  $c_{sh} = \sqrt{\eta/\tau_m \rho_0}$ . Roots of the equation (4.7) indicates instability of shear mode in presence of velocity shear for the condition  $v_{0y}'^2 > 4\nu k_x^2/5\tau_m$  in the limit  $k_x \gg k_y$ .

## 4.4 Non-local Eigenvalue Analysis

In this section, no restriction on the perturbation scale is taken and hence equilibrium velocity can no longer be considered as independent of  $x$ . Here, long wavelength (small  $k$ ) is of special interest. Instead of choosing plane waveform in  $x$ -direction, one has to solve ordinary differential equation in  $x$ . The standard hyperbolic tangent profile is chosen as a realistic shear layer. The generalized hydrodynamic Orr-Sommerfeld equation with this profile is difficult to solve analytically. We have studied this problem numerically using matrix eigenvalue technique. Before showing numerical results, an analytical solution is outlined with step profile which is chosen as approximate form of tanh profile.

### 4.4.1 Using step profile

The mathematical form of this type of velocity profile looks like

$$v_{0y}(x) = x/|x|; \quad -\infty \leq x \leq \infty, \quad (4.8)$$

This is known as vortex sheet where tangential component of velocity is discontinuous across the vortex sheet, but normal component of the flow velocity is

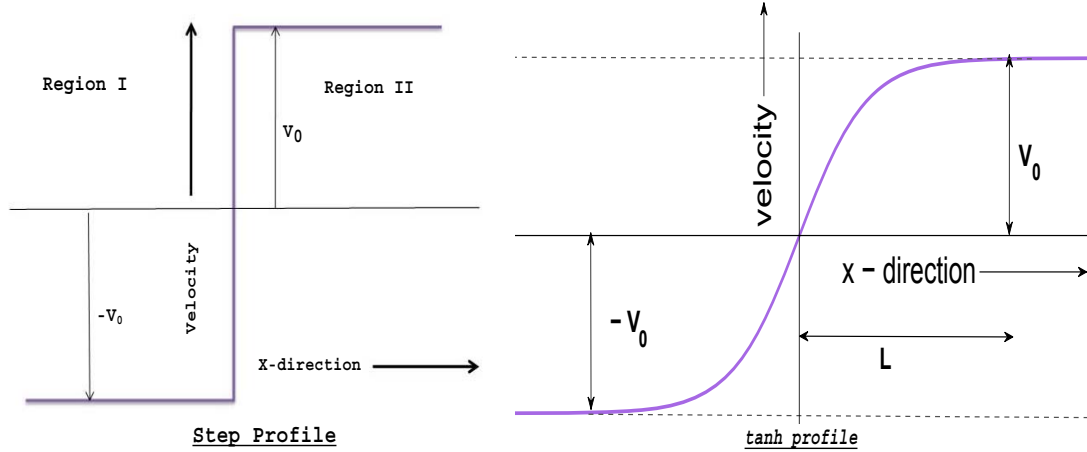


Figure 4.1: Graphical representation of step profile (left figure) and tanh profile (right figure) is shown. Both of these are vortex sheet with step profile of zero thickness and tanh profile of finite thickness.

continuous. In zero shear thickness limit, hyperbolic tangent profile becomes similar to step profile. This profile shows that at  $x = 0$ ,  $v_{0y}$  has a sudden finite jump (from  $-1$  to  $1$ ) but, in the regions  $x > 0$  and  $x < 0$ , the velocity remains constant ( $\pm 1$ ). Only at  $x = 0$ , both first and second derivatives of velocity exist. In 1961, Drazin used such step profile and solved analytically to predict the instability of Orr-Sommerfeld equation[83]. Here, we have used the same mathematical tools to solve the GH Orr-Sommerfeld equation. For the regions  $x < 0$  (velocity value  $-1$ ) and  $x > 0$  (velocity value  $+1$ ) and excluding the point  $x = 0$ , the Generalized Hydrodynamic Orr-Sommerfeld equation (4.5) reduces to

$$(D^2 - k_y^2)^2 \varphi = ik_y R \{1 + ik_y \tau_m (\mp 1 - c)\} (\mp 1 - c) (D^2 - k_y^2) \varphi. \quad (4.9)$$

Note here that  $v'_{0y}$  and  $v''_{0y}$  do not appear in the above equation. But, the effect of sudden jump in the velocity profile at  $x = 0$  would appear through the matching condition (boundary condition at  $x = 0$ ). The most general solution of equation

(4.9) satisfying the boundary condition at infinity is of the form

$$\begin{aligned}\varphi &= Ae^{-k_y x} + Be^{-\beta_1 x} \quad (x > 0) \\ &Ce^{k_y x} + De^{\beta_2 x} \quad (x < 0)\end{aligned}\quad (4.10)$$

where

$$\begin{aligned}\beta_1 &= [k_y^2 - ik_y R(c-1) \{1 - i\tau_m k_y (c-1)\}]^{1/2}, \\ \beta_2 &= [k_y^2 - ik_y R(c+1) \{1 - i\tau_m k_y (c+1)\}]^{1/2}.\end{aligned}$$

So, we get solutions of equation (4.5) in  $x$  excluding the jump point  $x = 0$ . The solutions on both sides ( $x > 0$  and  $x < 0$ ) will be matched through proper matching conditions which are derived now. The equation (4.5) is integrated in the region  $-\epsilon$  to  $\epsilon$  with the limit  $\epsilon \rightarrow 0$ .

$$\begin{aligned}\left[ \frac{d^3 \varphi}{dx^3} - 2k_y^2 \frac{d\varphi}{dx} - ik_y R(v_{0y} - c) \frac{d\varphi}{dx} + ik_y R v_0' \varphi + \beta (v_{0y} - c)^2 \frac{d\varphi}{dx} - \frac{\beta}{2} \frac{d}{dx} (v_{0y} - c)^2 \varphi \right]_{-\epsilon}^{\epsilon} \\ = -k_y^4 \int_{-\epsilon}^{\epsilon} \varphi dx - ik_y^3 R \int_{-\epsilon}^{\epsilon} (v_{0y} - c) \varphi dx + \beta k_y^2 \int_{-\epsilon}^{\epsilon} (v_{0y} - c)^2 \varphi dx\end{aligned}$$

The integrations on the RHS would vanish for continuous  $\varphi$ . Two successive integration of the Eq. (4.5) yields

$$\left[ \frac{d^2 \varphi}{dx^2} + ik_y R(v_{0y} - c) \varphi - \frac{\beta}{2} (v_{0y} - c)^2 \varphi \right]_{-\epsilon}^{\epsilon} = 0 \quad (4.11)$$

Three successive integration of the Eq.(4.5) would prove that first derivative of  $\varphi$  is continuous for continuous stream function  $\varphi$ . After some algebraic steps, the matching conditions can be formulated as

$$\begin{aligned}[\varphi] &= 0, \\ [D\varphi] &= 0, \\ \left[ (D^2 + \beta^2) \varphi + \frac{R\tau_m k_y^2}{2} (v_{0y} - c)^2 \varphi \right] &= 0, \\ [(D^2 - \beta^2) D\varphi] &= 0,\end{aligned}\quad (4.12)$$

where

$$\beta = [k_y^2 - ik_y R(c - v_{0y}) \{1 - i\tau_m k_y (c - v_{0y})\}]^{1/2}.$$

Third bracket indicates the jump of the variable inside from  $-\epsilon$  to  $\epsilon$  in the limit  $\epsilon \rightarrow 0$ . The first two relations represent that jumps of the function  $\varphi$  and its 1st derivative are zero i.e, they are continuous at  $x = 0$ . But the last two relations indicate finite jumps or discontinuities of 2nd and 3rd derivative of  $\varphi$ . This matching conditions at  $x = 0$ , gives four linear algebraic conditions in  $A, B, C$  and  $D$  which are the four constants in Eq.(4.10). A non zero solution for these set of equations exists if and only if their discriminant is zero and the eigenvalue relation is

$$\begin{vmatrix} 1 & 1 & 1 & 1 \\ -k_y & -\beta_1 & k_y & \beta_2 \\ k_y^2 + \beta_1^2 + \Delta(1 - c)^2 & 2\beta_1^2 + \Delta(1 - c)^2 & k_y^2 + \beta_2^2 + \Delta(1 + c)^2 & 2\beta_2^2 + \Delta(1 + c)^2 \\ -k_y^3 + k_y\beta_1^2 & 0 & k_y^3 - k_y\beta_2^2 & 0 \end{vmatrix} = 0$$

A straightforward algebra result to the eigenvalue condition

$$k_y^2 + \beta_1^2 + \beta_2^2 - \beta_1\beta_2 + k_y(\beta_1 + \beta_2) = 2\Delta \left( \frac{\beta_1 - \beta_2}{\beta_1 + \beta_2} \right), \quad (4.13)$$

where  $2\Delta = R\tau_m c k_y^2$ .

Figure (4.2) shows a plot of growth rate vs. wave number for various values of  $\tau_m$ . For  $\tau_m = 0$ , the dotted curve shows the result in a weakly coupled limit. This figure clearly indicates that increase of relaxation time enhances the instability. The effect of strong coupling on the KH instability manifests through  $\tau_m$  which increases with the coupling between dust grains. The dispersion of the instability changes with different values of  $\tau_m$ . In weakly coupled limit, growth rate increases through parabolic function with wave number  $k_y$  but large  $\tau_m$  shows linear increase of growth rate with  $k_y$ .

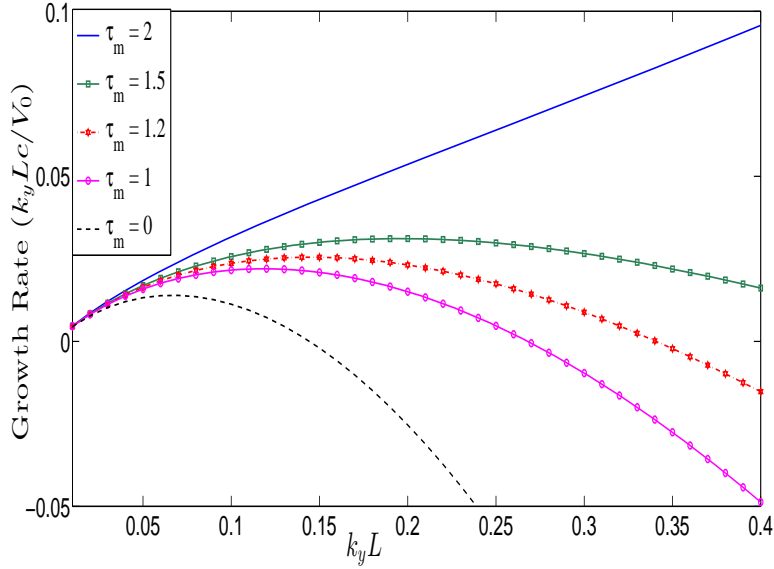


Figure 4.2: Growth rate (positive imaginary part of eigenvalue) is plotted against wavenumber ( $k_y$ ) for step profile with Reynolds Number  $R = 1$  and different values of  $\tau_m$  enlisted in the legend. Increase of relaxation time enhances the growth rate and also changes the dispersion.

#### 4.4.2 Shear layer of finite width

As a step profile is not a realistic one, a similar shear flow profile like standard tanh type which is widely used in both experimental and theoretical studies[84, 85] is taken. The expression of such a profile is given by

$$v_{0y}(x) = V_0 \tanh(x/L) \quad (4.14)$$

where  $L$  is the half-width of the velocity shear and  $\bar{v}_0$  is the magnitude of velocity far away from shear region. In the limit of zero shear layer width ( $L \rightarrow 0$ ), tanh profile reduces to step profile. Using the expression of  $v_{0y}$  from equation(4.14), the equation (4.5) is written in simplified form as,

$$[A_0 - \omega A_1 - \omega^2 A_2] \varphi = 0, \quad (4.15)$$

where  $A_i$ 's are the operators on  $\varphi$  and  $\omega = k_y c$  ( $c$  is the phase velocity). The expressions of different A operators are defined below as

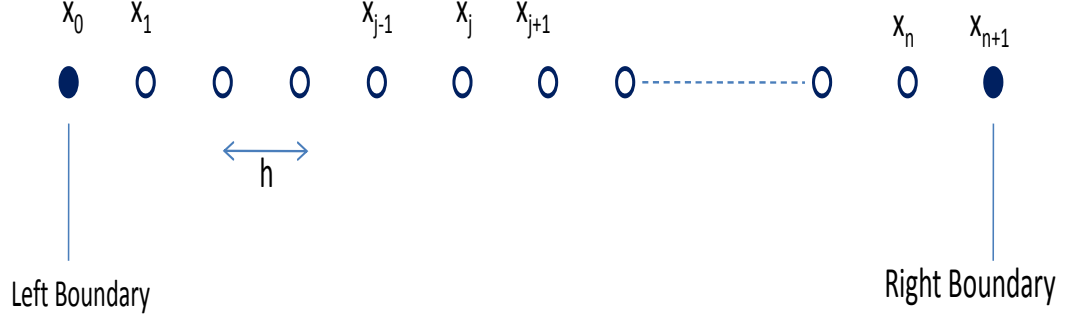


Figure 4.3: Discretization of x-space where white dots are inner and filled dots represent boundary points

$$\begin{aligned}
 A_0 &= D^4 - 2k_y^2 D^2 + k_y^4 + iRk_y v_{0y}'' (1 + ik_y \tau_m v_{0y}) - iRk_y v_{0y} (1 + ik_y \tau_m v_{0y}) (D^2 - k_y^2) \\
 &\quad + Rk_y^2 \tau_m v_{0y}' (v_{0y} D - v_{0y}') \\
 A_1 &= -iR(1 + 2ik_y \tau_m v_{0y}) (D^2 - k_y^2) + k_y R \tau_m v_{0y}' D - kR \tau_m v_{0y}'' \\
 A_2 &= -R \tau_m (D^2 - k_y^2)
 \end{aligned}$$

To solve the differential equation(4.15), We have done matrix eigenvalue analysis using **eig** subroutine in MATLAB[86]. The differential operators mentioned above is transformed into matrix form with proper discretization of space and spacial derivatives with central difference scheme. One dimensional space along  $x$  is considered to be made of  $n + 2$  no equally spaced discrete points so that continuous independent variable  $x$  becomes a set of discrete points  $\{x_j\}$  for  $j = 0 \cdots n + 1$  with  $h$  being the spacing between two neighboring points as depicted in the figure[4.3]. Also the continuous dependent variable  $\varphi$  is changed to a set of discrete values  $\{\varphi_j\}$  at different discrete points  $x_j$ 's.

Following central difference scheme is used here for the purpose of discretization

$$\begin{aligned}\frac{d^4\varphi}{dx^4} &= \frac{\varphi_{j+2} - 4\varphi_{j+1} + 6\varphi_j - 4\varphi_{j-1} + \varphi_{j-2}}{h^4} \\ \frac{d^2\varphi}{dx^2} &= \frac{\varphi_{j+1} - 2\varphi_j + \varphi_{j-1}}{h^2} \\ \frac{d\varphi}{dx} &= \frac{\varphi_{j+1} - \varphi_{j-1}}{2h}\end{aligned}$$

and the applied boundary conditions are

$$\varphi = 0, \quad \frac{d\varphi}{dx} = 0, \quad \text{at} \quad x = x_0, x_{n+1}.$$

In matrix representation  $x$  and  $\varphi$  can be represented as column matrix.

$$\varphi \rightarrow \begin{pmatrix} \varphi_1 \\ \varphi_2 \\ \varphi_3 \\ \cdot \\ \cdot \\ \cdot \\ \cdot \\ \varphi_{n-2} \\ \varphi_{n-1} \\ \varphi_n \end{pmatrix}_{n \times 1}; \quad x \rightarrow \begin{pmatrix} x_1 \\ x_2 \\ x_3 \\ \cdot \\ \cdot \\ \cdot \\ \cdot \\ x_{n-2} \\ x_{n-1} \\ x_n \end{pmatrix}_{n \times 1}$$

where the boundary points ( $x_0$  and  $x_{n+1}$ ) are not taken since  $\varphi$ 's are zero there.

Different differential operators can be written as square matrix form as,

$$D^4 \rightarrow \frac{1}{h^4} \begin{pmatrix} 7 & -4 & 1 & 0 & 0 & \dots & 0 & 0 & 0 & 0 \\ -4 & 6 & -4 & 1 & 0 & \dots & 0 & 0 & 0 & 0 \\ 1 & -4 & 6 & -4 & 1 & \dots & 0 & 0 & 0 & 0 \\ & & & & & \cdot & & & & \\ & & & & & & \cdot & & & \\ & & & & & & & \cdot & & \\ & & & & & & & & \cdot & \\ & & & & & & & & & \cdot \\ 0 & 0 & 0 & \dots & 0 & 1 & -4 & 6 & -4 & 1 \\ 0 & 0 & 0 & \dots & 0 & 0 & 1 & -4 & 6 & -4 \\ 0 & 0 & 0 & \dots & 0 & 0 & 0 & 1 & -4 & 7 \end{pmatrix}_{n \times n}$$

$$D^2 \rightarrow \frac{1}{h^2} \begin{pmatrix} -2 & 1 & 0 & 0 & 0 & \dots & 0 & 0 & 0 & 0 \\ 1 & -2 & 1 & 0 & 0 & \dots & 0 & 0 & 0 & 0 \\ 0 & 1 & -2 & 1 & 0 & \dots & 0 & 0 & 0 & 0 \\ & & & & & \cdot & & & & \\ & & & & & & \cdot & & & \\ & & & & & & & \cdot & & \\ & & & & & & & & \cdot & \\ & & & & & & & & & \cdot \\ 0 & 0 & 0 & \dots & 0 & 0 & 1 & -2 & 1 & 0 \\ 0 & 0 & 0 & \dots & 0 & 0 & 0 & 1 & -2 & 1 \\ 0 & 0 & 0 & \dots & 0 & 0 & 0 & 0 & 1 & -2 \end{pmatrix}_{n \times n}$$

$$D \rightarrow \frac{1}{2h} \begin{pmatrix} 0 & 1 & 0 & 0 & 0 & \dots & 0 & 0 & 0 & 0 \\ -1 & 0 & 1 & 0 & 0 & \dots & 0 & 0 & 0 & 0 \\ 0 & -1 & 0 & 1 & 0 & \dots & 0 & 0 & 0 & 0 \\ & & & & & \cdot & & & & \\ & & & & & & \cdot & & & \\ & & & & & & & \cdot & & \\ & & & & & & & & \cdot & \\ & & & & & & & & & \cdot \\ 0 & 0 & 0 & \dots & 0 & 0 & -1 & 0 & 1 & 0 \\ 0 & 0 & 0 & \dots & 0 & 0 & 0 & -1 & 0 & 1 \\ 0 & 0 & 0 & \dots & 0 & 0 & 0 & 0 & -1 & 0 \end{pmatrix}_{n \times n}$$

$v_{0y}$ ,  $v'_{0y}$  and  $v''_{0y}$  are all diagonal matrix of dimension  $n \times n$  like

$$v_{0y} = \begin{pmatrix} v_{0y}[1] & 0 & 0 & 0 & \dots & 0 & 0 & 0 \\ 0 & v_{0y}[2] & 0 & 0 & \dots & 0 & 0 & 0 \\ 0 & 0 & v_{0y}[3] & 0 & \dots & 0 & 0 & 0 \\ & & & & \cdot & & & \\ & & & & & \cdot & & \\ & & & & & & \cdot & \\ & & & & & & & \cdot \\ & & & & & & & & \cdot & \\ 0 & 0 & 0 & 0 & \dots & v_{0y}[n-2] & 0 & 0 \\ 0 & 0 & 0 & 0 & \dots & 0 & v_{0y}[n-1] & 0 \\ 0 & 0 & 0 & 0 & \dots & 0 & 0 & v_{0y}[n] \end{pmatrix}_{n \times n}$$

The equation(4.15) now becomes a polynomial (2nd order in  $\omega$ ) matrix eigenvalue problem. This can be changed into simple eigenvalue problem using the dummy variable  $\chi = \omega\varphi$ .

Hence, the new eigenvalue problem is

$$\begin{pmatrix} A_0 & Z \\ Z & I \end{pmatrix} \begin{pmatrix} \varphi \\ \chi \end{pmatrix} = \omega \begin{pmatrix} A_1 & A_2 \\ I & Z \end{pmatrix} \begin{pmatrix} \varphi \\ \chi \end{pmatrix},$$

where  $I$  is identity matrix and  $Z$  is a null matrix of order  $n \times n$ . This trick

simplifies original polynomial eigenvalue problem into a simple and well known matrix eigenvalue problem as

$$R\bar{\varphi} = \omega S\bar{\varphi}$$

where

$$R = \begin{pmatrix} A_0 & Z \\ Z & I \end{pmatrix}; \quad S = \begin{pmatrix} A_1 & A_2 \\ I & Z \end{pmatrix}; \quad \bar{\varphi} = \begin{pmatrix} \varphi \\ \chi \end{pmatrix}.$$

Now, we can use eig subroutine to solve the eigenvalue equation. We have cal-

culated the imaginary part of eigenvalues  $\omega$ , the positive value of which indicates the growth rate of the KH mode. First we should validate our code with respect to existing results. In weakly coupled limit ( $\tau_m \ll 1$ ), equation(4.5) reduces to the well known Orr-Sommerfeld equation which has been thoroughly studied in the last century.

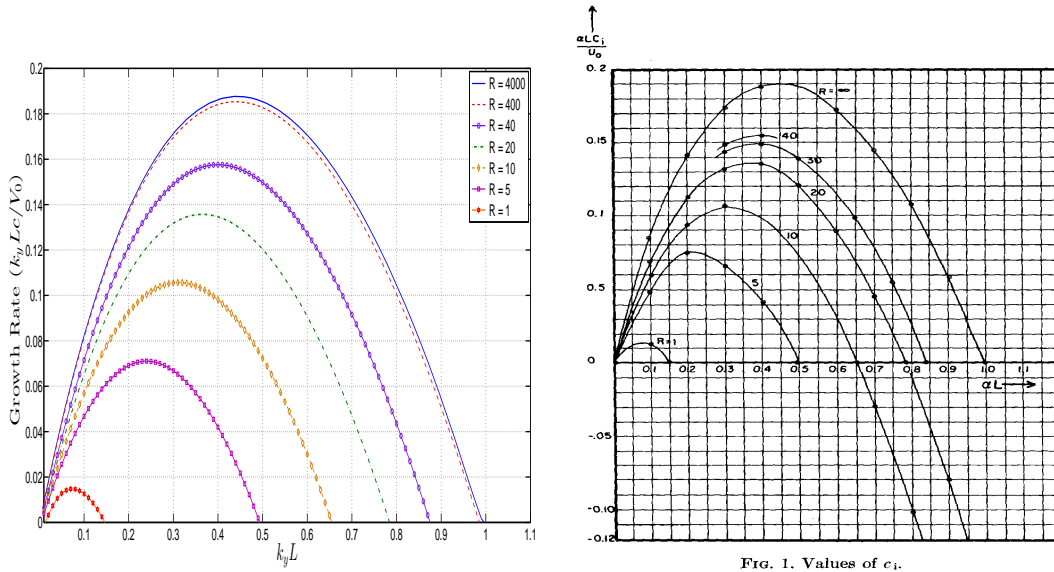
FIG. 1. Values of  $c_1$ .

Figure 4.4: The similarity of two figures provides the validity of eigenvalue analysis code developed in this thesis. The left figure represents the result from this code and the right figure is taken from the Ref.[85]. Growth rate( $k_y c$ ) is calculated in unit of  $V_0/L$  and wavenumber( $k_y$ ) in unit of  $1/L$ . Viscous stabilization is clearly seen for small  $R$  and large growth rate proceeds towards inviscid limit ( $R \rightarrow \infty$ ).

In figure (4.4.2), we have plotted the growth rate against wave number for different values of Reynolds number  $R$  and compare with the results of Fig.(1) in Ref.[85]. The code also shows that instability of *tanh* velocity profile increases as viscosity decreases and for very large value of Reynolds number  $R$ , the result resemble to those obtained in the inviscid limit. Now, we investigate the growth rate of KH instability for different values of viscosity and relaxation time. The fact is that unstable mode has no real part i.e., it lies on the imaginary axis in the complex plane. In figure (4.4), eigenvalues in the complex plane have been plotted for  $R = 1, 10$  and  $\tau_m = 1$  and the corresponding localized eigenfunctions are also shown. In figures (4.6)-(4.7), growth rate vs. wave number curves are drawn for different values of  $\tau_m$  and  $R$ . The Generalized Hydrodynamic model is becoming

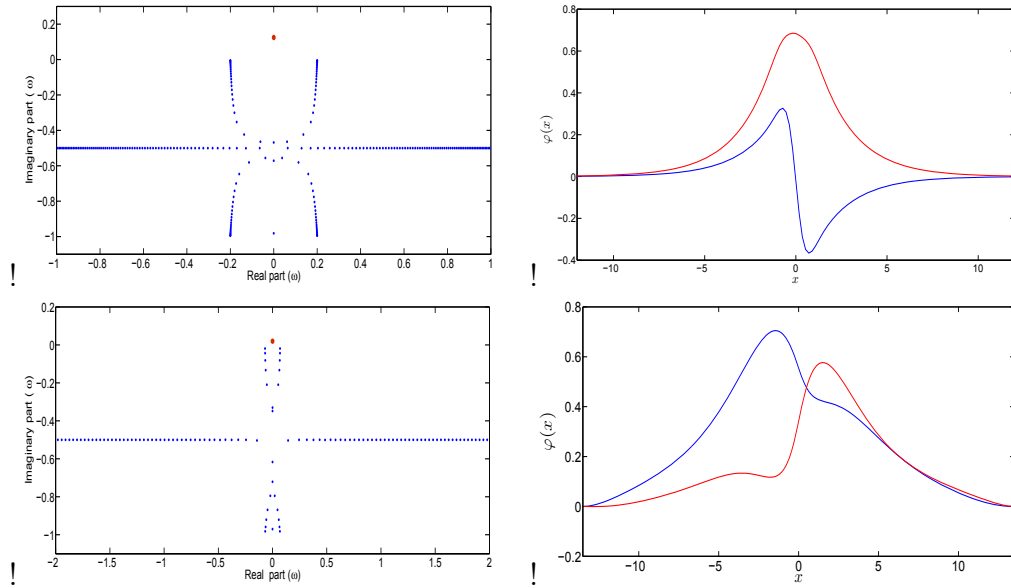


Figure 4.5: Eigenvalues are shown in complex plane in the left two figures - the upper figure for  $\tau_m = 1$  and  $R = 10$  and the lower one for  $\tau_m = 1$  and  $R = 1$ . Red (big) dot represents the only unstable mode which is purely imaginary. Corresponding eigenfunctions of the unstable mode are shown in the right two figures. Blue line represents the real part of eigenfunction and the red one represents the imaginary part.

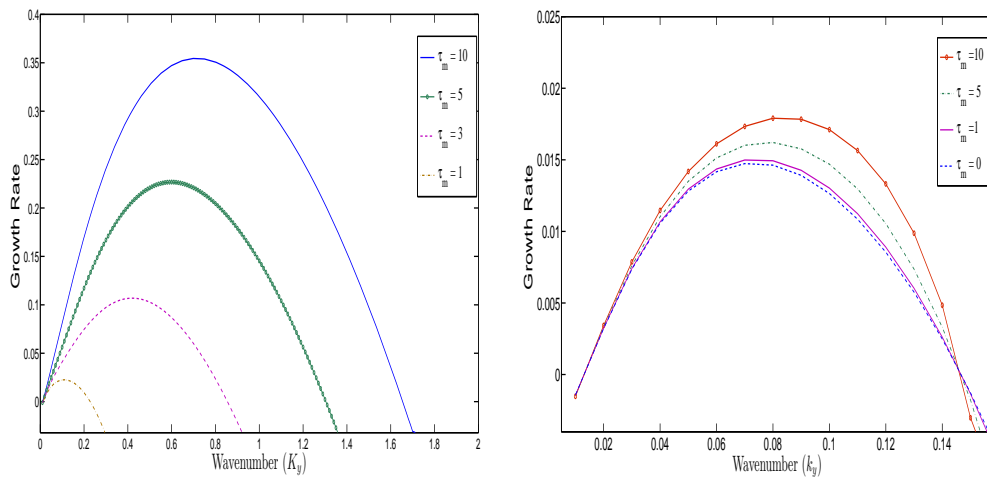


Figure 4.6: Growth rate vs. wavenumber curves are shown for different values  $\tau_m$  and  $R = 1$  for two different cases – left one with taking  $\tau_m(\mathbf{v} \cdot \nabla)$  term in GH model and right one without that term.

$\tau_m$	Max Growth rate with convective term	Max Growth rate without convective term
0.0	0.01474	0.01474
1.0	0.02256	0.01499
2.0	0.07569	0.01520
3.0	0.1069	0.01575
5.0	0.2267	0.01621
8.0	0.3197	0.01690
10.0	0.3545	0.0179

Table 4.1: Comparison of growth rates for Galilean invariant and non-invariant GH model for  $R = 1$

an inevitable tool to study the effect of strong coupling between dust particles on different waves and instabilities in a dusty plasma. In many cases, proper model was not taken into consideration. For the study of Kelvin-Helmholtz instability where equilibrium shear flow plays an important role, it is necessary to consider a proper Galilean invariant GH model.

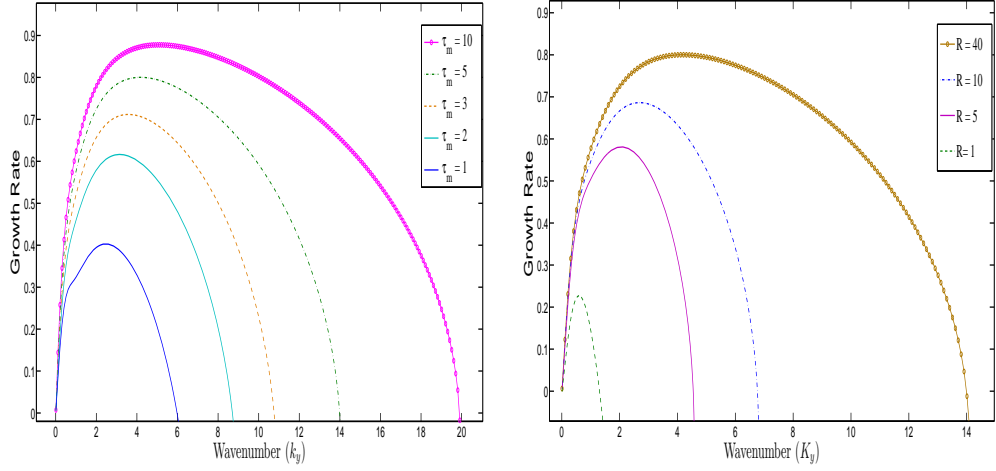


Figure 4.7: In left figure, growth rate vs.  $k_y$  is plotted for  $R = 40$  and different  $\tau_m$ . Right figure shows growth rate variation with  $k_y$  for  $\tau_m = 5$  but different Reynolds numbers.

The growth rate of unstable mode is plotted against wave number in fig. (4.6) for  $R = 1$  in both cases of including or excluding the term  $\tau_m (\mathbf{v} \cdot \nabla)$ . These two figures clearly indicate that the proper Galilean invariant form of the GH model makes a drastic change in growth rate using *tanh* type velocity profiles. A comparison of growth rates is given in tabular form for different  $\tau_m$  values(4.1). It is also observed that the limiting value of  $k_y$  beyond which instability vanishes also changes for different values of relaxation time  $\tau_m$ . In figure (4.8), contour plot is being shown in 2D plane of Reynolds number and wavenumber which clearly shows that unstable region in this parameter space increases with the effect of elasticity.

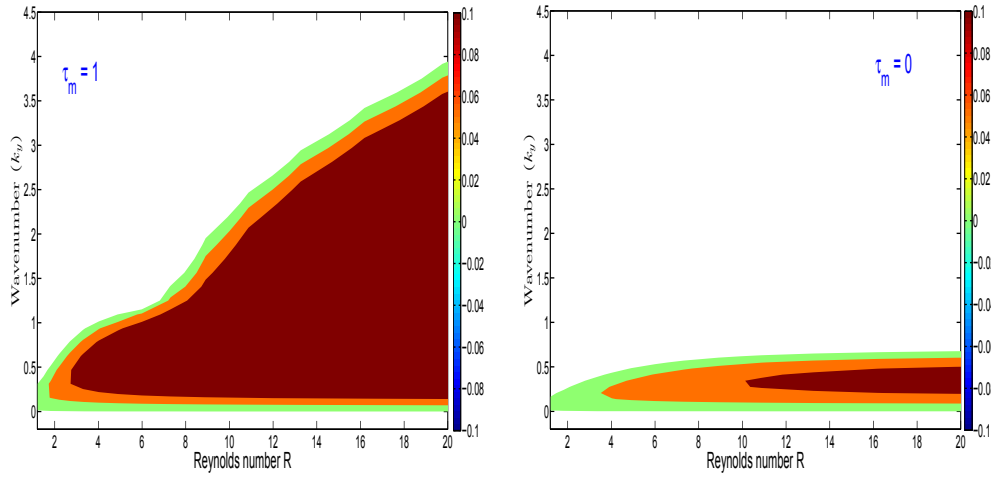


Figure 4.8: Growth rate of KH instability is plotted in 2D plane of  $k_y$  and  $R$  for both  $\tau_m = 0$  and  $\tau_m = 1$  which shows rapid increase of unstable region in presence of strong coupling. Colorbar indicates the values of growth rate in different color regions.

## 4.5 Summary

Viscosity being a dissipative effect, acts against instability. It arises between different shear layers in fluid and transforms available energy into heat which conducts away. Thus free energy is lost and growth rate diminishes accordingly. In Fig.(4.4), growth rate of instability is shown to be decreasing with increase of Reynolds' number( $R$ ) which is inverse of viscosity. For large value of  $R$ , it approaches to inviscid limit. However, elasticity which has energy storing property could enhance the instability. It opposes the dissipation of shear flow energy and supplies to the instability. This basic idea is reflected in all the graphs regarding the growth rate. Here, growth rate increases with increase of relaxation time  $\tau_m$  which manifests the elastic property coming from strong coupling. The equation(4.5) is derived using Galilean invariant form of generalized hydrodynamic momentum equation of dust fluid. One should keep in mind that every equation representing the dynamics of

physical system must be independent of inertial frames. In Fig.(4.6), a comparison is shown between the results which are obtained both from proper invariant model and improper non-invariant model. The table (4.1) shows the difference of data for growth rate. So, a substantial change in growth rate and dispersion of the unstable KH mode demands proper Galilean invariant form of generalized hydrodynamic equation to be used. In the absence of the convective term, bunching of the curves is observed with the growth rate vanishing at a particular wave number independent of  $\tau_m$ . However, the inclusion of the convective term( $\tau_m \mathbf{v} \cdot \nabla$ ) in the GH operator causes a wide dispersion for the growth rate curves obtained for different values of  $\tau_m$ . Since the shear profile is antisymmetric with respect to its inflection point( $x = 0$ ), frequency of the unstable mode[87] becomes imaginary complex number (real part vanishes) as shown in the figure (4.5).



# Chapter 5

## Stabilization of Kelvin-Helmholtz instability in non-Newtonian dusty plasma

### 5.1 Introduction

In this chapter, Kelvin-Helmholtz instability of bounded dust shear flow has been studied with the effect of non-Newtonian property of dusty plasma. In non-Newtonian dusty plasma, coefficient of viscosity is not merely a constant like Newtonian fluid but, it varies with velocity shear rate. Here, both shear thinning and thickening regimes are considered for the study of KH instability with the experimentally verified model discussed in the Ref.[33].

In the previous chapter, Kelvin-Helmholtz instability has been discussed for unbounded dust shear flow which have inflectional points. Here, parabolic type bounded flow without any inflectional point is considered. For such flow in inviscid case, the perturbation cannot extract energy from the basic shear flow and it behaves as stable flow. But onset of viscosity enable it for drawing energy and hence viscosity could play the mechanism to destabilize such flow[88]. Since shear thinning and thickening property depends oppositely on the values of shear rate,

so it is expected that these properties may have the opposite effect on the KH instability of inhomogeneous parabolic type flow. Motivated by these ideas, we have studied the effect of the velocity shear rate dependent viscosity on the growth rates and its dispersion by using the standard matrix eigenvalue technique.

## 5.2 Physical system and basic equations

In discharge plasma, the dust particles forming dust cloud levitate vertically (z-direction) in presence of external vertical electric field which balances the gravity effect on dust particles. A bounded equilibrium flow is generated along the axis of the cylindrical vessel (y-direction) with variation in the perpendicular x-direction. In our analysis, we consider the flow region ( $-L < x < L$ ) with the maximum flow speed in the middle of the discharge tube ( $x = 0$ ) and it vanishes along the boundary. In Newtonian fluid, such bounded flow is seen as parabolic and small wavy disturbance could be unstable which leads to the well known KH instability. Due to the non-Newtonian property of the dusty plasma, the unperturbed flow would deviate from the parabolic shape.

Weakly coupled unmagnetized dusty plasma is completely described by the three basic equations (the continuity equation obeying the mass conservation, the Navier-Stoke's equation showing the momentum balance and Poisson's equation which connects the potential fluctuation with the density variation) which are the following:

$$\frac{\partial n_d}{\partial t} + \nabla \cdot (n_d \mathbf{v}) = 0, \quad (5.1)$$

$$\rho \left( \frac{\partial}{\partial t} + \mathbf{v} \cdot \nabla \right) \mathbf{v} - n_d e Z \nabla \phi + c_d^2 \nabla \rho = \frac{\partial \sigma_{ij}}{\partial x_j}, \quad (5.2)$$

$$\nabla \cdot \mathbf{E} = -4\pi e (n_e + Z n_d - n_i), \quad (5.3)$$

where  $c_d = \sqrt{T_d \mu_d \gamma_d / m_d}$ ,  $T_d$  is the temperature dust particle due to random thermal motion,  $\mu_d$  and  $\gamma_d$  are respectively compressibility factor and adiabatic index [38],  $m$  is mass of dust particle. The electric field is denoted as  $\mathbf{E}$ ,  $n_d$  is defined as number density of dust particles where mass density  $\rho = n_d m_d$ ,  $\mathbf{v}$  is the velocity of dust fluid and  $Z$  denotes number of electronic charge on dust particle. The non-Newtonian viscous stress tensor is written as given in the sec.(3.2),

$$\sigma_{ij} = \eta(|\gamma|) \left[ \left( \frac{\partial v_i}{\partial x_j} + \frac{\partial v_j}{\partial x_i} \right) - \frac{2}{3} \delta_{ij} (\nabla \cdot \mathbf{v}) \right], \quad \delta_{ij} = 1 \text{ for } i = j$$

$$= 0 \text{ for } i \neq j.$$

where  $\eta(|\gamma|)$  is the non-Newtonian viscosity coefficient which depends on the magnitude of the rate of strain tensor  $\gamma$ . For the study of low frequency instabilities ( $\omega \ll kv_{te}, kv_{ti}$ , where  $v_{te}, v_{ti}$  are thermal velocities of electrons and ions respectively) electron and ion dynamics are considered to obey the Boltzmann relations,

$$n_e = n_{e0} \exp(e\phi/T_e), \quad n_i = n_{i0} \exp(-e\phi/T_i),$$

where  $T_e$  and  $T_i$  represents electron and ion thermal temperature measured in the Boltzmann unit,  $n_{e0}$  and  $n_{i0}$  are density of electron and ion fluid at zero potential.

### 5.3 Steady state and bounded flow profile

In equilibrium, the density and temperature are assumed to be constant and a constant electric field ( $E_0$ ) is directed along the y-direction. Dust particles are drifted along the y-direction with inhomogeneity in the  $x$ -direction (perpendicular to the electric field). For homogeneous dust particle density, the continuity equation(5.1) supports any form shear flow  $v_{0y}(x)$ . From equation(5.2), the y-component of the

equilibrium momentum equation can be written as

$$\frac{d}{dx} [\eta_0(\gamma_0)\gamma_0] = eZn_{d0}E_0, \quad (5.4)$$

where  $|\gamma| = \gamma_0 = dv_{0y}/dx$ . In the above equation subscript ‘0’ indicates equilibrium quantities. Non-Newtonian viscosity has specific functional dependence on equilibrium shear flow rate and for analytical purpose proper mathematical model is required in this context. In case of complex plasma, the experimentally verified model for the kinematic viscosity  $\nu(\gamma_0)$  with shear rate  $\gamma_0$ , given in Ref.[33] can be written as

$$\nu(\gamma_0) = \frac{2(1 + \epsilon)}{\sqrt{1 + 4\gamma_0^2 - 4\epsilon\gamma_0^4 + 1 - 2\epsilon\gamma_0^2}} \bar{\nu}, \quad (5.5)$$

where  $\bar{\nu}$  is the value of Newtonian viscosity,  $\gamma_0$  is equilibrium velocity shear rate which is normalized by  $(\beta v_{T_0}^2/\bar{\nu})^{1/2}$ . Here  $\beta$  is the friction rate,  $v_{T_0}^2$  is the thermal velocity. The other parameter  $\epsilon$  which characterizes the non-Newtonian property is given as  $\epsilon = (\mathcal{A}/\mathcal{B})(T_0/T_m)^{\alpha+\tau}$  and  $\alpha = \tau = 1$ . Here,  $T_0$  is the temperature at zero shear rate and  $T_m$  is the melting temperature and  $\mathcal{A}, \mathcal{B}$  are weak function of density as given in the above mentioned reference. In the limit  $\gamma, \epsilon \rightarrow 0$ , the model converges to the Newtonian viscosity limit  $\nu \rightarrow \bar{\nu}$ . In experiment[33], gas-induced flow is used to generate equilibrium shear flow of dust particles. To take into account this experimental condition we have included another space dependent term  $Ax^2$  in right hand side of Eq.(5.4) with equilibrium force  $F_0(x) = Ax^2 + eZn_{d0}E_0$  where  $A$  is the gas drag coefficient.

For the Newtonian viscosity, the solution of the Eq.(5.4) gives a parabolic velocity profile i.e.  $v_{0y}(x) = \bar{v}(1 - (x/L)^2)$ ,  $L$  is the half width of shear layer. In our analysis, the equilibrium equation is solved with the non-Newtonian viscosity model(5.5) for the equilibrium force term  $F_0(x)$  using values of different parameters

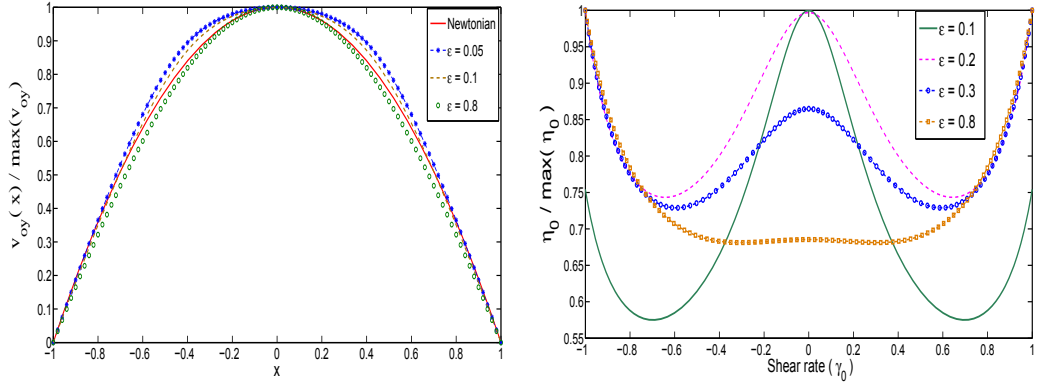


Figure 5.1: In the left figure, equilibrium flow profiles of dust grains are plotted for different  $\epsilon$ . The solid red line curve shows the same for the Newtonian limit ( $\epsilon, \gamma \rightarrow 0$ ). In the right figure, non-Newtonian viscosity is plotted against unperturbed velocity shear rate. For  $\epsilon = 0.1$ , shear thinning property exists then as  $\epsilon$  increases, the property changes from shear thinning to shear thickening and for  $\epsilon = 0.8$ , shear thinning property almost ceases.

from respective experimental paper. Here, `fzero` function of MATLAB is used for solving equation(5.4) to calculate numerically values of  $\gamma_0$  for each discrete points of space variable  $x$  in the range  $[-1 : 1]$ . Then the array of values of  $\gamma_0$  is integrated to get equilibrium velocity profile keeping in mind the boundary conditions  $v_{0y} = 0$  for  $x = \pm 1$  and  $dv_{0y}/dx|_{x=0} = 0$ . With the numerical values of  $\gamma_0$ , non-Newtonian viscosity could be calculated from the model(5.5). In the figure(5.1), both velocity and corresponding viscosity has been plotted for different values of  $\epsilon$ . In non-Newtonian regime, flow profiles deviates from the parabolic flow in Newtonian limit. Viscosity is plotted against the shear rate for different values of  $\epsilon$  which clearly shows that the fluid property changes from shear thinning to shear thickening with increasing  $\epsilon$ .

## 5.4 Linearized form of basic equations

We carry out linear stability analysis for the small amplitude wave so that the higher order terms in perturbation can be ignored for the assumption  $|v_x|, |v_y| \ll |v_{0y}|$  where  $v_x$  and  $v_y$  are the components of the small disturbance in dust flow. The total flow is the sum of the equilibrium flow and a small perturbation in flow:

$$\mathbf{v}(x, y, t) = [v_{0y}(x) + v_y(x, y, t)]\hat{e}_y + v_x(x, y, t)\hat{e}_x.$$

x, y components of the linearized dimensionless momentum equation of the dust fluid are respectively given by,

$$\begin{aligned} \left(\frac{\partial}{\partial t} + v_{0y}\frac{\partial}{\partial y}\right)v_x - \frac{\partial\phi}{\partial x} + c_d^2\frac{\partial n_d}{\partial x} &= \eta_0\nabla^2v_x + \left(\frac{\eta_0}{3}\frac{\partial}{\partial x} - \frac{2}{3}\eta_0'v_{0y}''\right)(\nabla\cdot\mathbf{v}) \\ &+ \eta_0'v_{0y}'\frac{\partial}{\partial y}\left(\frac{\partial v_x}{\partial y} + \frac{\partial v_y}{\partial x}\right) + 2\eta_0'v_{0y}''\frac{\partial v_x}{\partial x} \end{aligned} \quad (5.6)$$

and

$$\begin{aligned} \left(\frac{\partial}{\partial t} + v_{0y}\frac{\partial}{\partial y}\right)v_y + v_x\frac{dv_{0y}}{dx} - \frac{\partial\phi}{\partial y} + c_d^2\frac{\partial n_d}{\partial y} &= \eta_0\nabla^2v_y + \frac{\eta_0}{3}\frac{\partial}{\partial y}(\nabla\cdot\mathbf{v}) \\ &+ \left\{2\eta_0'v_{0y}'' + \eta_0''v_{0y}''v_{0y}' + \eta_0'v_{0y}'\frac{\partial}{\partial x}\right\}\left(\frac{\partial v_x}{\partial y} + \frac{\partial v_y}{\partial x}\right) \end{aligned} \quad (5.7)$$

Space and time are normalized by the Debye length  $\lambda_D = \sqrt{T_i/4\pi Z n_{d0}e^2}$  and dust plasma frequency  $\omega_{pd} = \sqrt{4\pi n_{d0}Z^2e^2/m_d}$  respectively. Electron, ion and dust particle densities are normalized by  $n_{d0}$  and the electrostatic potential  $\phi$  by  $T_i/e$  ( $\phi \equiv e\phi/T_i$ ) where  $\eta_0$  is normalized by  $\omega_{pd}\lambda_D^2m_dn_{d0}$ . The  $\eta_0'$  and  $\eta_0''$  denotes the single and double derivative of  $\eta_0$  with respect to  $v_{0y}'$  and  $v_{0y}'' = dv_{0y}'/dx$ . The linear continuity equation in normalized variables can be written as,

$$\left(\frac{\partial}{\partial t} + v_{0y}\frac{\partial}{\partial y}\right)n_d + \frac{\partial v_x}{\partial x} + \frac{\partial v_y}{\partial y} = 0. \quad (5.8)$$

For small potential fluctuations ( $\phi \ll 1$ ), the normalized Boltzmann relations can be expressed as,

$$n_e = \frac{n_{eo}}{n_{d0}} \left( 1 + \phi \frac{T_i}{T_e} \right), \quad n_i = \frac{n_{io}}{n_{d0}} (1 - \phi).$$

The linearized dimensionless Poisson's equation is written as,

$$\nabla^2 \phi = n_d + \alpha \phi, \quad (5.9)$$

where  $\alpha = (n_{e0}T_i + n_{i0}T_e) / (n_{d0}ZT_e)$ .

## 5.5 Eigenvalue analysis

It is not possible to carry out Fourier analysis along the direction of inhomogeneity. Thus the perturbed variables  $v_x$ ,  $v_y$ ,  $\phi$  and  $n$  is taken as  $\phi(x, y, t) = \phi(x)e^{i(k_y y - \omega t)}$ . So the linearized equations (5.6-5.9) can be expressed as four normalized ordinary differential equation in  $y$  by the following equations:

$$k_y v_{0y}(x)n_d + k_y v_y - i \frac{dv_x}{dx} = \omega n_d, \quad (5.10)$$

$$n_d + \left( \alpha - \frac{d^2}{dx^2} + k_y^2 \right) \phi = 0, \quad (5.11)$$

$$\begin{aligned} & -i c_d^2 \frac{dn_d}{dx} + i \frac{d\phi}{dx} + \left[ k_y v_{0y} + i \eta_0 \left( \frac{d^2}{dx^2} - k_y^2 \right) - i \eta'_0 v'_{0y} k_y^2 + 2i \eta'_0 v''_{0y} \frac{d}{dx} \right. \\ & \left. + i \left( \frac{\eta_0}{3} \frac{d}{dx} - \frac{2}{3} \eta'_0 v''_{0y} \right) \frac{d}{dx} \right] v_x + \left[ -\eta'_0 v'_{0y} \frac{d}{dx} - \left( \frac{\eta_0}{3} \frac{d}{dx} - \frac{2}{3} \eta'_0 v''_{0y} \right) \right] k_y v_y = \omega v_x, \end{aligned} \quad (5.12)$$

$$\begin{aligned} & k_y c_d^2 n_d - k_y \phi + \left[ -i \frac{v'_{0y}}{k_y} - \left( 2\eta'_0 v''_{0y} + \eta''_0 v''_{0y} v'_{0y} + \eta'_0 v'_{0y} \frac{d}{dx} \right) - \frac{\eta_0}{3} \frac{d}{dx} \right] k v_x + \\ & \left[ k_y v_{0y} + i \eta_0 \left( \frac{d^2}{dx^2} - k_y^2 \right) - \frac{i}{3} k_y^2 \eta_0 + i \left( 2\eta'_0 v''_{0y} + \eta''_0 v''_{0y} v'_{0y} + \eta'_0 v'_{0y} \frac{d}{dx} \right) \frac{d}{dx} \right] v_y = \omega v_y, \end{aligned} \quad (5.13)$$

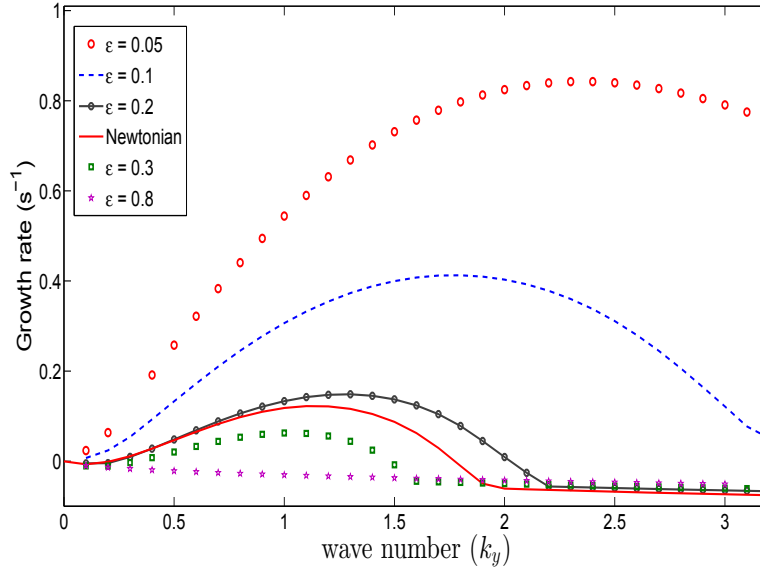


Figure 5.2: Growth rate of instability is plotted against wave number for different values of parameter  $\epsilon$  in incompressible limit. The solid red line curve shows that for Newtonian limit. For  $\epsilon = 0.2$ , the growth rate is close to that of Newtonian limit.

We have solved these four coupled linear eigenvalue equations and investigated the growth rate of the KH instability with the variation of different parameters like Mach number ( $M = |v_{0y}|/c_d$ ), non-Newtonian parameter ( $\epsilon$ ) and wave number ( $k_y$ ). We have carried out the matrix eigenvalue analysis using the standard eigenvalue subroutine (eig) in MATLAB. Each equation (5.10-5.13) is first discretized in matrix form as given in section (4.4.2). Following central difference scheme has been used for the purpose of discretization

$$\frac{d^2\phi}{dx^2} = \frac{\phi_{j+1} - 2\phi_j + \phi_{j-1}}{h^2},$$

$$\frac{d\phi}{dx} = \frac{\phi_{j+1} - \phi_{j-1}}{2h},$$

where  $h$  is the grid spacing.

The discretized equations would take the form,

$$A_1 n_d + Z\phi + C_1 v_x + D_1 v_y = \omega I n_d$$

$$A_2 n_d + B_2 \phi + Z v_x + Z v_y = \omega Z \phi$$

$$A_3 n_d + B_3 \phi + C_3 v_x + D_3 v_y = \omega I v_x$$

$$A_4 n_d + B_4 \phi + C_4 v_x + D_4 v_y = \omega I v_y$$

where  $A_i, B_i, C_i, D_i$  are different matrix operators of dimension  $(n \times n)$  and  $n_d$ ,  $\phi, v_x, v_y$  are column matrices of dimension  $n$  with  $Z$  and  $I$  are respectively null matrix and identity matrix of order  $(n \times n)$ . Now a single eigenvalue equation can be formed as

$$P\Theta = \omega R\Theta$$

and

$$P \rightarrow \begin{pmatrix} A_1 & Z & C_1 & D_1 \\ A_2 & B_2 & Z & Z \\ A_3 & B_3 & C_3 & D_3 \\ A_4 & B_4 & C_4 & D_4 \end{pmatrix}_{4n \times 4n} ; \quad R \rightarrow \begin{pmatrix} I & Z & Z & Z \\ Z & Z & Z & Z \\ Z & Z & I & Z \\ Z & Z & Z & I \end{pmatrix}_{4n \times 4n} ; \quad \Theta \rightarrow \begin{pmatrix} n_d \\ \phi \\ v_x \\ v_y \end{pmatrix}_{4n \times 1}$$

First we investigate the incompressible limit ( $c_d \gg |v_{0y}|$ ) where the density and the potential fluctuations are negligibly small so that equation(5.11) becomes trivial and continuity equation(5.10) reduces to  $k_y v_y - i d v_x / dx = 0$ . In figure (5.2), the growth rate is shown plotted against the wave number( $k_y$ ) for different values of  $\epsilon$ . The solid red line curve indicates the Newtonian regime and the other curves are for values of  $\epsilon = 0.05, 0.1, 0.2, 0.3$  and  $0.8$ . The kinematic viscosity in Newtonian limit is considered as  $1.538 \times 10^{-4} m^2/s$ . Different values of  $\epsilon$  incorporates different functional dependance of viscosity with flow shear rate. In figure(5.1), we have shown how viscosity coefficient changes its property from shear

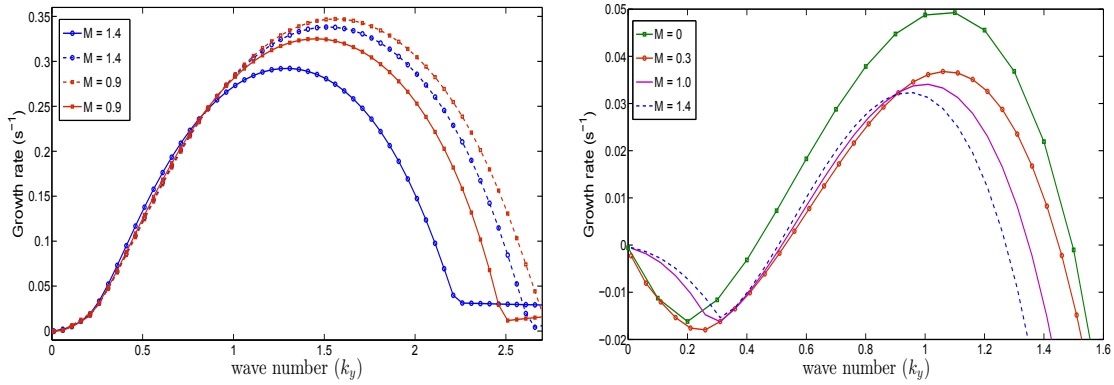


Figure 5.3: In the left figure, two sets of curves are shown for two different Mach number ( $M$ ) including and excluding dispersion term in Poisson's equation for  $\epsilon = 0.1$ . In each set of curves, dotted line represents the curve without dispersion effect and the solid line with dispersion term. In the right one, compressibility is introduced by increasing the Mach number and it indicates that the growth rate diminishes as compressibility strengthens in the medium for  $\epsilon = 0.3$ . Here,  $M = 0$  curves shows incompressible limit for comparison.

thinning to shear thickening one with increase of plasma temperature  $T_0$ . As the value of  $\epsilon$  is increased to 0.3, growth rate diminishes below that of the Newtonian case and the shear thickening property overpowers the effect of shear thinning. Hence, we can summarize that the shear thinning property enhances the instability but on the contrary, the shear thickening property has stabilizing role on the KH instability. For  $\epsilon = 0.8$ , shear thickening effect stabilizes the medium. Here, variation of viscosity with shear rate plays the stabilizing role on the KH instability. Now, we include the effects of compressibility in our system to study the role of density fluctuation on the instability. Figure(5.3) shows that the growth rate decreases as we increase the Mach number i.e., compressibility weakens the instability. Inclusion of compressibility effect enables dissipation of some energy to drive longitudinal waves. For small mach no, compressibility effect is too weak to stabilize but here, shear thickening property could play the role. In plasma,

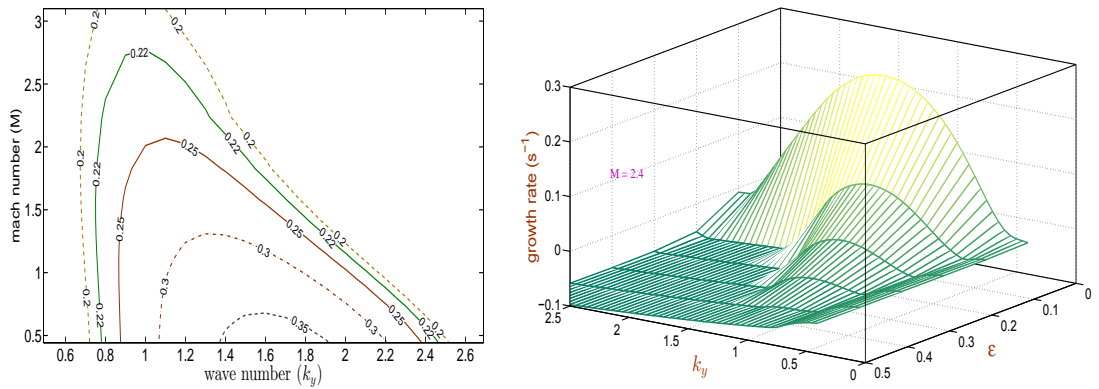


Figure 5.4: The left figure shows contour plot of growth rate in the plane of mach number ( $M$ ) and wave number for  $\epsilon = 0.1$ . In the right figure surface plot of growth rate is drawn on the parametric space of  $\epsilon$  and  $k_y$  for mach no.  $M = 2.4$ .

quasi-neutrality is a widely accepted approximation for wavelengths larger than Debye length ( $\lambda_D$ ) where the dispersion term of poisson's equation has negligible contribution. In figure(5.3), for two different values of  $M = 1.4, 0.9$  growth rate is plotted with and without considering the dispersion term in Poisson's equation. The dispersion is much prominent for higher compressibility ( $M = 1.4$ ). So, in the regime of higher mach number quasi-neutrality is not a correct approximation. In figure (5.4), contour plot of growth rate is drawn in 2D plane of wave number and Mach number and it is seen that as growth rate decreases from 0.3 to 0.21, the unstable region spans. A surface plot of the growth rate vs wave number and  $\epsilon$  is shown for  $M = 2.4$ . The flat area addresses the stability region on the ( $\epsilon - k_y$ ) plane and the hill area indicates unstable portion. For higher temperature (large values of  $\epsilon$ ), the unstable region shrinks and flat area widens which depicts the stabilizing effect of shear thickening property.

## 5.6 Summary

The numerical results have revealed opposite effect of shear thinning and shear thickening property on the Kelvin Helmholtz instability of inhomogeneous bounded dust flow. Shear thinning effect is more favorable for the instability. But thickening property diminishes and hence it acts against the instability and stabilizes the medium. So the study of the growth rate of KH instability could characterize the non-Newtonian property of dusty plasma. Incompressible limit shows the maximum growth of instability and as one include finite density fluctuation (compressibility), a part of energy available for the instability is exhausted for the longitudinal fluctuation in the system and thus instability weakens by some percentage. Viscosity has dissipative effect but also it has the nature of diffusing momentum of fluid. In bounded flow strong velocity shear exists in boundary layers which is diffused inwards by viscosity which leads to instability[82].

# Chapter 6

## Nonlinear shear wave and recurrence

### 6.1 Introduction

In this chapter, transverse shear wave of large amplitude is addressed for which the linear assumption will no longer be valid. Linear equations are quite easy to solve than finding the evolution of nonlinear terms. However, every physical system usually goes to nonlinear stage as the amplitude of small fluctuation increases with time. Hence, one has to solve the dynamical equations giving special attention to the nonlinear terms. In strongly coupled non-Newtonian dusty plasma, nonlinear effect arises both from convective nonlinear term (the term  $\mathbf{v} \cdot \nabla$  in the momentum equation of motion of dust fluid) and non-Newtonian stress tensor through the dependence of viscosity coefficient on the velocity shear rate tensor.

In one spatial dimension the convective nonlinearity plays no role in the propagation of ‘shear wave’. The effective nonlinear contribution comes from non-Newtonian stress tensor. Using well known Carreau-Bird non-Newtonian model[60, 89], the nonlinear shear wave equation in one spatial dimension is formed. We solve this equation numerically in which the time evolution is studied using a standard

software of nonlinear wave study[41]. As an initial solution, a simple sine wave is used. As time goes on nonlinear term dominates and different higher harmonics generate. But after certain recurrence time, all the higher harmonics disappear and the total energy gets back to the initial sinusoidal mode. Hence the initial sine wave is reached again. This result has resemblance with the cubic nonlinear solution of famous Fermi-Pasta-Ulam (FPU) problem[42].

## 6.2 Nonlinear shear wave equation

In the study of nonlinear shear wave equation, we consider unmagnetized homogeneous strongly coupled non-Newtonian dusty plasma. Since the shear wave originates due to vorticity fluctuations the density fluctuations may be ignored in order to avoid coupling of shear wave with longitudinal dust-acoustic wave. In such situation, continuity equation(2.11) turns out to be an incompressibility condition  $\nabla \cdot \mathbf{v} = 0$ . The generalized hydrodynamic momentum equation of dust fluid(2.9) is rewritten as

$$\left\{ 1 + \tau_m \left( \frac{\partial}{\partial t} + \mathbf{v} \cdot \nabla \right) \right\} \left[ \rho \left( \frac{\partial}{\partial t} + \mathbf{v} \cdot \nabla \right) \mathbf{v} - n_d Z e \nabla \phi + \nabla p \right] = \frac{\partial \sigma_{ij}}{\partial x_j} \quad (6.1)$$

where  $i, j$  varies from  $x$  to  $y$  and the components of viscous force are respectively

$$F_x = \frac{\partial \sigma_{xx}}{\partial x} + \frac{\partial \sigma_{xy}}{\partial y}, \quad F_y = \frac{\partial \sigma_{yy}}{\partial y} + \frac{\partial \sigma_{yx}}{\partial x}.$$

As discussed in the section(3.10), non-Newtonian stress in incompressible limit is taken as,

$$\sigma_{ij} = \eta(|\gamma|) \left( \frac{\partial v_i}{\partial x_j} + \frac{\partial v_j}{\partial x_i} \right)$$

where  $|\gamma| = \sqrt{II/2}$  and scalar invariant of strain tensor[61]

$$II = 4 \left( \frac{\partial v_x}{\partial x} \right)^2 + 4 \left( \frac{\partial v_y}{\partial y} \right)^2 + 2 \left( \frac{\partial v_x}{\partial y} + \frac{\partial v_y}{\partial x} \right)^2.$$

In electrostatic limit, electric field fluctuation only comes from density fluctuation of electron, ion and dust particles through poisson's equation. Hence, incompressibility assumption denies any electric field fluctuation and so explicit electron and ion dynamics are not taken into account. In strongly coupled limit, temperature fluctuation of dust fluid is trivial and correspondingly thermal pressure can be taken as constant in time and space. With these assumptions taken, we can drop the force terms coming from pressure and electric field. In strongly coupled limit  $\tau_m \partial/\partial t \gg 1$ , the Eq.(6.1) is reduced to the form,

$$\tau_m \left( \frac{\partial}{\partial t} + \mathbf{v} \cdot \nabla \right) \left[ \rho \left( \frac{\partial}{\partial t} + \mathbf{v} \cdot \nabla \right) \mathbf{v} \right] = \frac{\partial \sigma_{ij}}{\partial x_j} \quad (6.2)$$

Since the motion is considered incompressible,  $\rho$  remains constant in space and time and the velocity is the only dynamical variable. To study only transverse shear wave, we assume velocity fluctuation  $\mathbf{v} = v_y(x, t)\hat{e}_y$  i.e, velocity directs along  $y$ -direction and it varies in perpendicular  $x$ -direction. Hence we are considering wave for which dust particle motion is perpendicular to wave propagation. In this situation, the usual convective nonlinearity in fluid equation would not survive as  $\mathbf{v} \cdot \nabla \mathbf{v} = \mathbf{0}$  but the effective nonlinearity would come from non-Newtonian viscous force. In this case, only one component  $\sigma_{yx}$  exists which is expressed as(see section 3.2),

$$\sigma_{yx} = \eta (|\gamma|) \frac{\partial v_y}{\partial x} \quad \text{and} \quad |\gamma| = \frac{\partial v_y}{\partial x}.$$

To proceed further one needs to know the functional form of viscosity. For this study, we consider well known Carreau-Bird viscosity model[35] which is mathematically expressed as

$$\eta = \eta_0 \left[ 1 + \left( \frac{c_{sh}}{L} |\gamma| \right)^2 \right]^{(n-1)/2}. \quad (6.3)$$

This model is feasible in solving analytically and it has advantage over power law model as it produces Newtonian viscosity( $\eta_0$ ) in the limit  $|\gamma| \rightarrow 0$ . The model describes shear thinning behaviour for  $n < 1$  and shear thickening behaviour for  $n > 1$ . Using this expression, equation (6.2) is simplified as

$$\frac{\partial^2 v}{\partial t^2} = \frac{\partial}{\partial x} \left[ \eta(|\gamma|) \frac{\partial v}{\partial x} \right] \quad (6.4)$$

To write the above equation we have used normalization as follows:  $v \rightarrow v_y/c_{sh}$ ,  $\eta \rightarrow \eta/\eta_0$ ,  $x \rightarrow x/L$ ,  $t \rightarrow tc_{sh}/L$  where,  $\eta_0, L$ , are some arbitrary viscosity and length,  $c_{sh} = \sqrt{\eta_0/\rho\tau_m}$ .

For small values of  $c_{sh}/L$ , this model(6.3) can be written in dimension less form

$$\eta(|\gamma|) = 1 + \alpha|\gamma|^2.$$

where  $\alpha = (n - 1)/2$  and  $n$  is the power law exponent. The parameter  $\alpha$  is used as a measure of non-Newtonian effect and modeled as  $|\alpha| < 1$ . For negative (positive)  $\alpha$  the fluid behaves like a shear thinning (thickening) medium. Substituting this model into equation (6.4), we obtain

$$\frac{\partial^2 v}{\partial t^2} = \frac{\partial^2 v}{\partial x^2} + \alpha \frac{\partial}{\partial x} \left( \frac{\partial v}{\partial x} \right)^3 \quad (6.5)$$

This is a nonlinear wave equation where the last term in right hand side illustrates cubic nonlinearity[90]. In absence of non-Newtonian effect i.e.  $\alpha = 0$  we get back the linear shear wave equation (normalized form).

### 6.3 Numerical solution

In this section, we show the result of time evolution of this nonlinear equation (6.5) numerically. Then we discuss the numerical result with possible mathematical interpretation and show the difference between analytical and numerical results. The equation is discretized in space with grid spacing  $h$  and the space discretized equation is given by

$$\frac{\partial^2 v}{\partial t^2} = \frac{1}{h^2} (v_{j+1} - 2v_j + v_{j-1}) + \frac{\alpha}{h^4} [(v_{j+1} - v_j)^3 - (v_j - v_{j-1})^3] \quad (6.6)$$

where central difference scheme of 2nd order is used and  $j = 0, 1, 2 \dots N + 1$  with  $v_0$  and  $v_{N+1}$  as two boundary points.

Next, we use mean value finite discretization in time

$$\frac{\partial^2 v}{\partial t^2} = \frac{v_j^{k+1} - 2v_j^k + v_j^{k-1}}{(\delta t)^2}.$$

The final discretized equation in both space and time takes the form,

$$v_j^{k+1} = 2v_j^k - v_j^{k-1} + \beta^2 (v_{j+1}^k - 2v_j^k + v_{j-1}^k) + \gamma [(v_{j+1}^k - v_j^k)^3 - (v_j^k - v_{j-1}^k)^3] \quad (6.7)$$

where  $\beta = (\delta t/h)^2$  and  $\gamma = \alpha\beta/h^2$ . In order to ensure the numerical stability, one should follow the condition  $\beta^2 \leq 1$  which is known as CFL condition in numerical analysis[91]. This has to be maintained with the adjustment of  $\delta t$  and  $h$  otherwise one would get incorrect result.

Here we have used standard software CAPOW to solve the equation(6.7) and see time evolution of shear wave in presence of nonlinearity[41]. We have used in the numerical investigation  $\delta t = 0.03$ ,  $h = 0.04$ ,  $\gamma \approx 351.5\alpha$  with  $\alpha = 0.1$ . So, the CFL condition is adjusted as  $\beta^2 = (\delta t)^2/(h)^2 = 0.56 < 1$ .

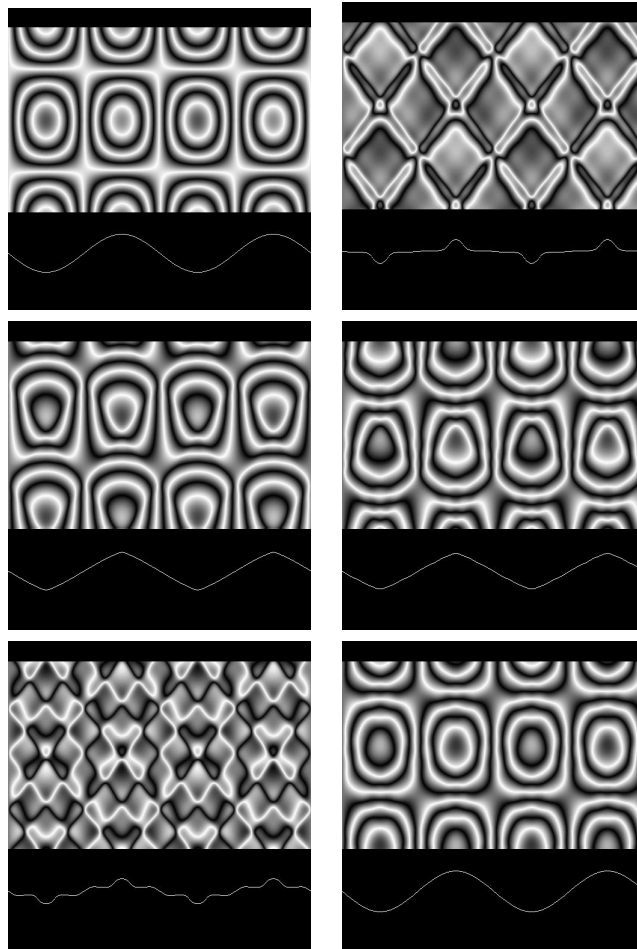


Figure 6.1: Time evolution of the shear wave structure for  $\alpha = 0.1$  for different time (time increasing column wise) with initial and final state almost identical. X-axis represents space and y-axis represents time slots

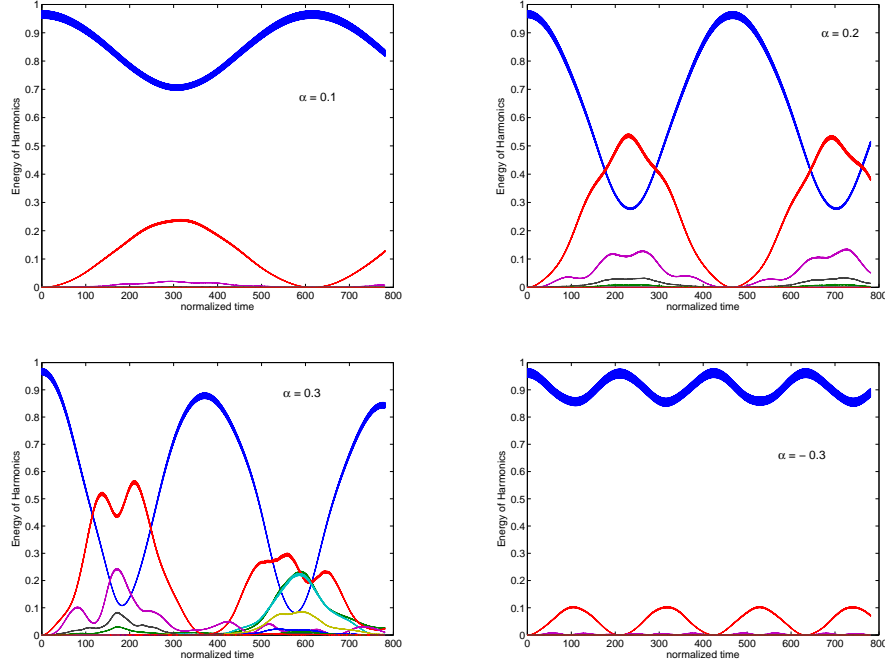


Figure 6.2: Energy of different harmonics is plotted against normalized time for different values of nonlinearity  $\alpha$ . Blue line shows energy of fundamental harmonic and other red, brown, yellow etc show for different higher harmonics. Hence, energy sharing to higher harmonics is greater for  $\alpha = 0.3$  than that of 0.1 and 0.2. Also recurrence is faster for larger values of  $\alpha$ . Fourth graph is for shear thinning medium.

Initially (at  $t=0$ ), we perturb the system with a pure sine wave and keep observing its changes in time. As time goes on, the amplitude of the wave form diminishes and the periodicity of the wave changes with time. After few time steps (see figure 6.1), wave is seen to change into a periodic triangular wave. Then it again gets back to initial sine wave with almost same intensity. With an appropriate scaling  $t \rightarrow ht$  and  $v \rightarrow (hv\sqrt{1/3\alpha})$  equation(6.6) can be written as,

$$v_{tt} = (v_{j+1} - 2v_j + v_{j-1}) + \frac{1}{3} [(v_{j+1} - v_j)^3 - (v_j - v_{j-1})^3] \quad (6.8)$$

Let us express amplitudes of velocity fluctuations in normal modes decomposition

form as

$$v_j(t) = \left(\frac{2}{N+1}\right)^{1/2} \sum_{i=1}^N a_i(t) \sin\left(\frac{ij\pi}{N+1}\right), \quad (j = 1, 2 \dots N)$$

and the equation(6.8) excluding nonlinear terms takes the form

$$\sum_i \ddot{a}_i(t) \sin\left(\frac{ij\pi}{N+1}\right) + 2 \sum_i a_i(t) \sin\left(\frac{ij\pi}{N+1}\right) \left[1 - \cos\left(\frac{i\pi}{N+1}\right)\right] = 0$$

which reduces to

$$\ddot{a}_i + \omega_i^2 a_i = 0; \quad \omega_i^2 = 4 \sin^2\left(\frac{i\pi}{2(N+1)}\right).$$

Here the contribution to potential energy from nonlinear term is not taken. This only leads to few percentage error in total energy calculation for weak nonlinearity (small  $\alpha$ ). This is clearly seen in energy curves for different values of  $\alpha$ . So the individual mode oscillates independently like a simple harmonic oscillator with frequency  $\omega_i$  and the modal energy takes the form

$$E_i = \frac{1}{2} (\dot{a}_i^2 + \omega_i^2 a_i^2).$$

The equation(6.8) is numerically solved using ordinary differential equation solver ODE45 in Matlab[86]. The energy variation with time of first few modes are graphically shown in fig.(6.2). Nonlinearity excites higher harmonics in the system and initial energy of fundamental mode is distributed through different harmonics. The interesting feature is that after a large number of time steps, all the high frequency modes start to disappear and initial energy of the system accumulates in the fundamental mode (initial sinusoidal perturbation as shown in Fig (6.1). Therefore nonlinearity redistributes energy of the wave in different harmonics and they interact themselves and finally come back to its initial state. This feature

of the solution reminds us the famous Fermi-Pasta-Ulam (FPU) problem in a completely different physical situation. Numerical analysis has also been carried out for shear thinning medium i.e when  $\alpha$  is negative e.g,  $\alpha = -0.3$ . But, for this medium, energy sharing is negligible compared to that for shear thickening media and thus this branch is not continued further. It is shown that the solutions of Eq.(6.5) retrace the initial condition and maintain its periodicity in spite of the strong nonlinearity present in the equation.

## 6.4 Analytical approach

The mathematical analysis of nonlinear hyperbolic differential equation leads to an unphysical singular solution[92, 93]. It has been shown that the solution blows out after certain breaking time. This is due to a lack of presence of any dispersion factor in the nonlinear equation so that nonlinear growth could not be balanced. This contradicts with the numerical solution which projects stable and recurring solution. This is probably because discretization invokes the required effects of dispersive corrections. Such effect leads to periodic recurrent solutions that arise due to a balance between the discretization induced dispersion and nonlinearity present in the equation. So in continuous equation one has to include a term which measure the discreteness of the system. This has resemblance with famous FPU (Fermi-Pasta-Ulam) paradox. In 1955, Enrico Fermi , J. Pasta And S. Ulam had decided to made a computer simulation to see ergodicity and equipartition of energy among different harmonics in irreversible statistical system. They consider a finite chain of coupled oscillators with weak nonlinear coupling considering quadratic and cubic term in interacting force term. They failed to see any equipartition but rather

observed nonlinear recurrence of initial disturbance. Later Zabusky in his famous paper(1965) explained this recurrence with synchronizing these results with the birth of solitons[43]. Let us give a possible explanation transforming the discrete equation(6.8) to the continuum limit keeping higher space derivatives in the Taylor series expansion of the velocity function. In continuum limit,  $v_{j+1}$  and  $v_{j-1}$  can be expanded in Taylor series form

$$v_{j+1} = v(x+h) = v(x) + hv'(x) + \frac{h^2}{2}v''(x) + \frac{h^3}{6}v'''(x) + \frac{h^4}{24}v^{iv}(x) + O(h^5)$$

$$v_{j-1} = v(x-h) = v(x) - hv'(x) + \frac{h^2}{2}v''(x) - \frac{h^3}{6}v'''(x) + \frac{h^4}{24}v^{iv}(x) - O(h^5)$$

Using these expansion we can evaluate

$$v_{j+1} - 2v_j + v_{j-1} = h^2v''(x) + \frac{h^4}{12}v^{iv}(x) + O(h^6)$$

and

$$(v_{j+1} - v_j)^3 - (v_j - v_{j-1})^3 = 3h^4v'^2v'' + O(h^6)$$

Neglecting 6th and higher order terms, the equation (6.8) reduces to

$$v_{tt} = h^2v'' + \frac{h^4}{12}v^{iv} + h^4v'^2v'' + O(h^6) \quad (6.9)$$

Now we make a transformation  $\xi = x - ht, \tau = h^3t/12$  and use field variable

$$\phi = -\frac{v_t}{2h} + \frac{1}{2} \int_0^{v_x} (1 - h^2\eta^2)^{1/2} d\eta$$

to obtain

$$v_{tt} = h^2 \left( 2\frac{\partial\phi}{\partial\xi} - \frac{\partial v_x}{\partial\xi} \right) + \frac{h^4}{2} \left( v_x^2 \frac{\partial v_x}{\partial\xi} - \frac{1}{6} \frac{\partial\phi}{\partial\tau} + \frac{1}{12} \frac{\partial v_x}{\partial\tau} \right) + O(h^6). \quad (6.10)$$

Let us equate expression of  $v_{tt}$  from equation(6.9) and Eq.(6.10) and then compare same order terms to get

$$h^2 \frac{\partial^2 v}{\partial x^2} = 2h^2 \frac{\partial\phi}{\partial\xi} - h^2 \frac{\partial v_x}{\partial\xi}$$

and

$$v_{xxxx}h^4 + 6v_x^2v_{xx}h^4 + \phi_\tau h^4 = 0.$$

From  $h^2$  order term we get  $\phi = v_x$  and substituting this relation in  $h^4$  order term we obtain

$$\phi_\tau + 6\phi^2\phi_\xi + \phi_{\xi\xi\xi} = 0. \quad (6.11)$$

This is well known modified Korteweg-deVries equation (mKdV) where nonlinearity is balanced by diffusion term to form solitary wave structure. The general solution of this equation[44] can be expressed in the form of jacobian elliptical function  $[cn(\xi, q)]$  which represents periodic solution stationary in the frame  $\xi - U\tau$ . This type of waves are known as cnoidal waves and  $q$  is called cnoidal parameter which measures the relative importance of nonlinearity to dispersion. In the linear limit ( $q \rightarrow 0$ ) the solution shows small amplitude sinusoidal wave ( $cn\xi \rightarrow \cos\xi$ ) and in the solitary wave limit( $q \rightarrow 1$ ), it represents solitary wave solution (sech type)[94]. The numerical solution of mKdV equation would show formation of solitons, their elastic collisions and finally recurrence as shown in Ref.[43]. This may be the case why we observe recurring solution in the numerical investigation of nonlinear shear wave equation.

## 6.5 Summary

Every nonlinear system which could support soliton like structure, shows FPU recurrence. This interesting nonlinear phenomena is observed in many branches of physics like magnetic films[95], ion accoustic solitons in plasma[96]. Here, we have reported possible existence of such recurrence in complex plasma. The usual convective nonlinearity has no role but the effect comes from newly discovered non-Newtonian property in dusty plasma. Here we report nonlinear dust shear wave which might be an interesting research topic in future. For the shear thickening medium nonlinear shear waves redistribute their energy and finally come back to the initial state while for a shear thinning medium energy distribution is negligibly small. Therefore the propagation of transverse shear waves is an important technique for characterization of strongly coupled Yukawa fluids. The dependence of the time period of recurrence of periodic solutions on the nonlinearity parameter can enable the characterization of non-Newtonian properties.

# Chapter 7

## Conclusion of results and future scope

### 7.1 Summary

The interesting topics what are covered in this doctoral thesis are listed as:

- Existence of solid like elastic property in dusty plasma fluid in strong coupling.
- Propagation of mechanical transverse shear wave in inhomogeneous dusty plasma.
- Viscosity gradient driven instability of shear wave in presence of velocity shear.
- Strong coupling effect on the Kelvin-Helmholtz instability of unbounded dust shear flow.
- Non-Newtonian stabilization of Kelvin-Helmholtz instability of bounded inhomogeneous dust flow.
- FPU recurrence and soliton formation in nonlinear shear wave.

A brief summary of the results and discussions of the studies made in this thesis on these topics are drawn here.

At low temperature, potential energy of highly charged dust particle ( $\sim 10^4 e$ ) becomes stronger than average thermal energy which leads to strong coupling between massive dust grains. This is characterized by coupling parameter( $\Gamma$ ) which is the ratio of potential energy to kinetic energy. Large values of  $\Gamma$  introduces some solid like property (long range correlation, elasticity) even in the fluid phase of plasma. The inherent fluid property also persists leading to a new visco-elastic phase. Hence both viscosity and elasticity are on equal footing. This type of property is first modeled by Maxwell who gave idea of relaxation time( $\tau_m$ ). The relaxation time increases with the increase of coupling parameter. In my thesis, different low frequency waves and instabilities are studied in such visco-elastic dusty plasma. For this study, we have used the generalized hydrodynamic equation derived in the section(2.2) as in the Ref.[38]. Changing values of  $\tau_m$ , both weakly coupled and strongly coupled limit have been investigated.

In this phase, mechanical shear wave could propagate in plasma similar to the transverse elastic wave in solid or s-wave during earthquake. This is a low frequency wave( $\sim$  few Hz) and the phase velocity( $\sim mm/s$ ) is much smaller than dust acoustic speed( $\sim cm/s$ ). Experimentally this shear wave is found to be coupled with dust acoustic wave. We have studied properties of shear wave in presence of both density inhomogeneity and inhomogeneous dust flow. The propagating shear wave becomes modulated under the effect of density inhomogeneity. In the section(2.5), different types density profiles like sech and parabolic are analyzed and proper eigen states with discrete frequency of shear wave are shown.

Shear wave is shown to be unstable in presence of linear velocity shear where gradient of viscosity plays the mechanism to trigger the instability. In dusty plasma viscosity does not remain constant for large shear rate. Instead it varies with velocity shear rate which is experimentally verified recently. This is well known as non-Newtonian property since linear stress strain relation of Newton stress tensor is no longer valid. Proper model of functional dependence of viscosity has to be chosen. Here we consider power law model to investigate the shear thinning region where viscosity decreases with increase of shear rate. Analytical approximation shows the formation of Weber equation which is solved for certain eigenvalue condition for well behaved solution. The Fig.(3.1) shows the increase of growth rate with velocity shear rate. A non-model analysis is also done with Galilean invariant model.

Strong coupling between dust particles introduces elastic property which is manifested through relaxation time( $\tau_m$ ). Elasticity becomes dominant over viscous property for  $\tau_m \gg 1$ . In strongly coupled fluid regime, Kelvin-Helmholtz instability of dust shear flow is investigated. Due to energy storing property, elasticity could capture more kinetic energy from mean flow and thus enhances growth rate of instability. Different plots of growth rate against wavenumber( $k_y$ ) for different values of  $\tau_m$  in chapter(4), confirms this physical fact. Other way viscosity being dissipative in nature decreases the growth rate. In our study, proper galilean invariant form of generalized hydrodynamic momentum equation is taken instead of existing study with non-invariant model. The growth rate and dispersion with proper invariant equation differs from the result of improper non invariant model. The comparison of the results are shown in the Fig.(4.6) and in the table(4.1).

The possible application of this study is that the measure of growth rate of KH instability could help to characterize the elastic property of dusty plasma.

Non-Newtonian property of complex plasma has active role on the Kelvin-Helmholtz instability of dust shear flow. A linear stability analysis is done in Chapter(5) with matrix eigenvalue analysis using MATLAB. Here, proper experimentally verified non-Newtonian model is adopted from ref[33]. The parameter  $\epsilon$  is scanned to change from shear thinning to thickening behavior. The results of both compressible and incompressible limit are shown in chapter(6). The growth in incompressible limit is larger since compressibility introduces longitudinal modes which draws some available energy. It has been shown graphically that shear thinning behavior could enhance the growth rate whereas shear thickening behavior stabilizes the instability. This study might be helpful for characterization of non-Newtonian property of dusty plasma.

Non-Newtonian property leads to nonlinear shear wave. This nonlinearity causes recurrence behaviour similar to famous FPU recurrence in lattice. In chapter(6), mathematical formation of nonlinear shear wave equation is shown and time evolution of such equation is done numerically. The initial sine wave is seen to transform through different periodic structure with generation of different higher harmonics. After recurrence time higher harmonics disappear and the initial form of sine wave is reached again. The time evolution of modal energy of first few harmonics is shown in Fig.(6.2). It is clearly shown that after certain recurrence time initial energy gets back to initial sine wave and other harmonics dies out. This property is known as recurrence. This property ensures that non-Newtonian

complex media could support shear wave solitons that is explicitly shown in chapter(6).

## 7.2 Future directions

- Kelvin-Helmholtz instability is studied in linearized form with the assumption of small amplitude fluctuation. With the onset of instability, amplitude starts to increase and after certain time it could enter into nonlinear phase. Here, nonlinear terms contribute and linear analysis fails. So, one should study nonlinear KH instability of dust shear flow as well. If it is done in non-Newtonian phase, it would be more interesting as two different type of nonlinearity acts together. One would come from usual convective term and other one from non-Newtonian stress tensor. In this thesis, only one dimensional propagation of nonlinear shear wave is investigated where usual convective nonlinearity plays no role. So, study of nonlinear shear wave with two dimensional propagation should be done where both convective nonlinearity and non-Newtonian nonlinearity works together.
- We have formulated two dimensional vortex equation[65] for the study of evolution of vortex in strongly coupled dusty plasma. We are trying to solve the vortex equation derived and expecting results soon. In weakly coupled plasma, numerical study using pseudo-spectral method had shown that different initial state transforms to Lamb dipole vortex which is time stationary state[97]. So, it would also be interesting to carry out such numerical study in complex plasma in order to gain more physical insight in this direction.
- The coupling between transverse shear wave and longitudinal dust acoustic

wave is an challenging research topic. In recent article, coupling has been shown to be made due to variation in charge and size of dust grains. Another interesting way of coupling would be through velocity shear effect. We are developing a theory and hope to see interesting results in near future.

- Kelvin-Helmholtz instability in strongly coupled non-Newtonian dusty plasma would be interesting to study where both the effect of elasticity and viscosity gradient effect are included. It is reported in this thesis that elasticity enhances the instability but shear thickening property stabilizes it. Here, these effects are investigated differently.
- Charge fluctuation is an important physical aspect in dusty plasma research. So it would be necessary to investigate the effect of charge fluctuation on Kelvin-Helmholtz instability in detail in strongly coupled non-Newtonian dusty plasma.
- Kelvin-Helmholtz instability is well studied in different experiments regarding neutral fluid or weakly coupled electron-ion plasma. So, experimental verification of the results made in my thesis is most welcome and naturally it is in my plan for future research work.

# Bibliography

- [1] Chen, F. F. *Introduction to Plasma Physics and Controlled Fusion, 2nd edition*. Srpinger, New York, (1984).
- [2] Goree, J. *Plasma Sources Sci. Technol.* **3**, 400 (1994).
- [3] Morfill, G. E. and Ivlev, A. V. *Rev. Mod. Phys.* **81**, 1353 (2009).
- [4] Merlino, R. L. and Goree, J. A. *Phys. Today* **57(7)**, 32 (2004).
- [5] Nosenko, V. and Goree, J. *Phys. Rev. Lett.* **93**, 155004 (2004).
- [6] Chan, C. L., Lai, Y. J., Woon, W. Y., Chu, H. Y., and Lin, I. *Plasma Phys. Control. Fusion* **47**, A273 (2005).
- [7] Alfvén, H. *On The Origin of The Solar System*. Clarendon Press, Oxford, (1954).
- [8] Spitzer, L. *Physical Processes in the Interstellar Medium*. John Wiley and Sons, New York, (1978).
- [9] Krishan, V. *Astrophysical Plasmas and Fluids*. Kluwer Academic, Dordrecht, (1999).
- [10] Watson, W. D. and Salpeter, E. E. *Astro. Phys. J.* **174**, 321 (1972).

- [11] Goertz, C. K. *Rev. Geophys.* **27**, 271 (1989).
- [12] Northrop, T. G. *Phys. Scripta* **45**, 475 (1992).
- [13] Horanyi, M., Houppis, H. L. F., and Mendis, D. A. *Astrophys. Space Sci.* **144**, 215 (1988).
- [14] Morfill, G. E., Grün, E., and Johnson, T. V. *Planet Space Sci* **28**, 1087 (1980).
- [15] Robinson, P. and Coakley, P. *IEEE Trans. Elec. Insul.* **27**, 944 (1992).
- [16] Whipple, E. C. *Rep. Prog. Phys.* **44**, 1197 (1981).
- [17] Selwyn, G. S., Sing, J., and Bennett, R. S. *J. Vac. Sci. Technol.* **A7**, 2758 (1989).
- [18] Bouchoule, A. *Dusty Plasmas: Physics, Chemistry and Technological Impacts in Plasma Processing*, pp. 305-396. Wiley, Chichester, (1999).
- [19] Sharpe, J. P., Petti, D. A., and Bartels, H. W. *Fusion Eng. Des.* **63**, 153 (2002).
- [20] Winter, J. *Phys. Plasmas* **7**, 3862 (2000).
- [21] Ikeji, H. *Phys. Fluids* **29**, 1764 (1986).
- [22] Thomas, H., Morfill, G. E., Demmel, V., Goree, J., Feuerbacher, B., and Möhlmann, D. *Phys. Rev. Lett.* **73**, 652 (1994).
- [23] Chu, J. H. and Lin, I. *Phys. Rev. Lett.* **72**, 4009 (1994).
- [24] Hayashi, Y. and Tachibana, K. *Jpn. J. Appl. Phys.* **33**, L804 (1994).

- [25] Melzer, A., Trottenberg, T., and Piel, A. *Phys. Lett. A* **191**, 301 (1994).
- [26] Tsytovich, V. N., Morfill, G. E., Vladimirov, S. V., and Thomas, H. M. *Elementary Physics of Complex Plasmas*. Springer, Berlin Heidelberg, (2008).
- [27] Pieranski, P. *Contemp. Phys.* **24**, 25 (1983).
- [28] Fortov, V., Ivlev, A., Khrapak, S., Khrapak, A., and Morfill, G. *Phys. Reports* **421**, 1 (2005).
- [29] Tsytovich, V. N., Morfill, G. E., Vladimirov, S. V., and Thomas, H. M. *Elementary Physics of Complex Plasmas, Lect. Notes Phys. 731*. Springer, Berlin Heidelberg, (2008).
- [30] Piel, A. and Melzer, A. *Plasma Phys. Control. Fusion* **44**, R1 (2002).
- [31] Konopka, U., Morfill, G. E., and Ratke, L. *Phys. Rev. Lett.* **84**, 891 (2000).
- [32] Ichimaru, S. *Rev. Mod. Phys.* **54**, 1017 (1982).
- [33] Ivlev, A. V., Steinberg, V., Kompaneets, R., Höfner, H., Sidorenko, I., and Morfill, G. E. *Phys. Rev. Lett.* **98**, 145003 (2007).
- [34] Gavrikov, A. V., Goranskaya, D. N., Ivanov, A. S., Petrov, O. F., Timirkhanov, R. A., Vorona, N. A., and Fortov, V. E. *J. Plasma Physics* **76**, 579 (2010).
- [35] Bird, R. B., Armstrong, R. C., and Hassager, O. *Dynamics of polymeric liquids Vol. 1*. Wiley, New York, (1987).
- [36] White, E. E. B., Chellamuthu, M., and Rothstein, J. P. *Rheol Acta* **49**, 119 (2010).

- [37] Thurston, G. *Biophys. J.* **12**, 1205 (1972).
- [38] Kaw, P. and Sen, A. *Phys. Plasmas* **5**, 3552 (1998).
- [39] Nunomura, S., Samsonov, D., and Goree, J. *Phys. Rev. Lett.* **84**, 5141 (2000).
- [40] Pramanik, J., Prasad, G., Sen, A., and Kaw, P. K. *Phys. Rev. Lett.* **88**, 175001 (2002).
- [41] Rucker *et. al.*, R. <http://www.cs.sjsu.edu/faculty/rucker/capow/download.html>  
**CAPOW**, free download (2007).
- [42] Fermi, E., Pasta, J., and Ulam, S. *Studies of Nonlinear Problems Los Alamos Report*, LA-1940 (1955).
- [43] Zabusky, N. J. and Kruskal, M. D. *Phys. rev. Lett.* **15**, 240 (1965).
- [44] Driscoll, C. F. and O'Neil, T. M. *Phys. Rev. Lett.* **37**, 69 (1976).
- [45] Frenkel, Y. *Kinetic Theory of Liquids*. Clarendon, Oxford, (1946).
- [46] Feng, Y., Goree, J., and Liu, B. *Phys. Rev. E* **82**, 036403 (2010).
- [47] Berkovsky, M. A. *Phys. Scripta* **51**, 769 (1995).
- [48] Murillo, M. S. *Phys. Rev. Lett.* **85**, 2514 (2000).
- [49] Veerasha, B. M., Tiwary, S. K., Sen, A., Kaw, P. K., and Das, A. *Phys. Rev. E.* **81**, 036407 (2010).
- [50] Kaw, P. K. *Phys. Plasmas* **8**, 1870 (2001).
- [51] Lekner, J. *Am. J. Phys.* **75**, 1151 (2007).

- [52] Janaki, M. S., Banerjee, D., and Chakrabarti, N. *Phys. Plasmas*. **18**, 092114 (2011).
- [53] Makowski, A. J. *Ann. Phys.* **324**, 2465 (2009).
- [54] Abramowitz, M. and Stegun, I. A. *Handbook of Mathematical Functions*. Dover Publications, INC., New York, (1972).
- [55] Banerjee, D., Janaki, M. S., and Chakrabarti, N. *Phys. Plasmas* **17**, 113708 (2010).
- [56] Bittencourt, J. A. *Fundamentals of Plasma Physics*. Springer, New York, (2004).
- [57] Mishra, A., Sen, P. K., and Sen, A. *Phys. Plasmas* **7**, 3188 (2000).
- [58] Donkó, Z., Goree, J., Hartmann, P., and Kutasi, K. *Phys. Rev. Lett.* **96**, 145003 (2006).
- [59] Hartmann, P., Sándor, M. C., Kovács, A., and Donkó, Z. *Phys. Rev. E*. **84**, 016404 (2011).
- [60] Bird, R. B. *Annu. Rev. Fluid Mech.* **8**, 13 (1976).
- [61] Mitsoulis, E. and Hatzikiriakos, S. G. *J. Non-Newtonian Fluid Mech.* **157**, 26–33 (2009).
- [62] Banerjee, D., Janaki, M. S., Chakrabarti, N., and Chaudhuri, M. *New J. Phys.* **12**, 123031 (2010).
- [63] Ashwin, J. and Ganesh, R. *Phys. Plasmas* **17**, 103706 (2010).

- [64] Ghosh, S., Gupta, M. R., Chakrabarti, N., and Chadhuri, M. *Phys. Rev. E* **83**, 066406 (2011).
- [65] Janaki, M. S. and Chakrabarti, N. *Phys. Plasmas* **17**, 053704 (2010).
- [66] Parker, E. N. *Interplanetary Dynamical Processes*. Interscience, New York, (1963).
- [67] Kelvin, L. *Phil. Mag.* **42**, 362 (1871).
- [68] von Helmholtz, H. *Ann. Phys.* **41**, 641 (1890).
- [69] Rayleigh, L. *Proc. London Math. soc.* **11**, 57 (1880).
- [70] Rayleigh, L. *Scientific Papers, vol. I, 474-87*. Cambridge University Press, Cambridge, (1899).
- [71] Reynolds, O. *Phil. Trans. Roy. Soc.* **174**, 935 (1883).
- [72] D'angelo, N. *Phys. Fluids* **8**, 1748 (1965).
- [73] D'Angelo, N. and Goeler, S. V. *Phys. Fluids* **9**, 309 (1966).
- [74] Willig, J., Merlino, R. L., and D'Angelo, N. *Phys. Lett. A* **236**, 223 (1997).
- [75] Chandrasekhar, S. *Hydrodynamic and Hydromagnetic Stability*. Oxford University Press, New York, (1961).
- [76] Ganguli, G. *Phys. Plasmas.* **4**, 1544 (1997).
- [77] D'Angelo, N. and Song, B. *Planet Space Sci.* **38**, 1577 (1990).
- [78] Li, L., Zhong-Yuan, L., and Zhen-Xing, L. *Phys. Plasmas.* **7**, 424 (2000).

- [79] Luo, Q. Z., D'Angelo, N., and Merlino, R. L. *Phys. Plasmas* **8**, 31 (2001).
- [80] Banerjee, D., Janaki, M. S., and Chakrabarti, N. *Phys. Rev. E* **85**, 066408 (2012).
- [81] Orszag, S. A. *J. Fluid Mech.* **50**, 689 (1971).
- [82] Drazin, P. G. and Reid, W. H. *Hydrodynamic Stability*. Cambridge University Press, Cambridge, (1981).
- [83] Drazin, P. *J. Fluid Mech.* **10**, 571 (1961).
- [84] Freymuth, P. *J. Fluid Mech.* **25**, 683 (1966).
- [85] Betchov, R. and Szewczyk, A. *Phys. Fluids* **6**, 1391 (1963).
- [86] MATLAB. <http://www.mathworks.com/>.
- [87] Tatsumi, T. and Gotoh, K. *J. Fluid Mech.* **7**, 433 (1959).
- [88] Kundu, P. K. and Cohen, I. M. *Fluid Mechanics, Second Edition*. ACADEMIC PRESS, New York, (1990).
- [89] Carreau, P. J. *Trans. Soc. Rheol.* **16**, 99 (1972).
- [90] Banerjee, D., Janaki, M. S., Chakrabarti, N., and Chaudhuri, M. *Phys. Plasmas*. **19**, 062301 (2012).
- [91] Courant, R., Friedrichs, K., and Lewy, H. *Mathematische Annalen* **100**, 32 (1928).
- [92] Zabusky, N. J. *J. Math Phys.* **3**, 1028 (1962).

- [93] Lax, P. D. *J. Math Phys.* **5**, 611 (1964).
- [94] Whitham, G. B. *Linear and Nonlinear Waves*. Wiley-Interscience, New York, (1974).
- [95] Wu, M. and Patton, C. E. *Phys. Rev. Lett.* **98**, 047202 (2007).
- [96] Ikeji, H. *Phys. Fluids* **16**, 1668 (1973).
- [97] Nielson, A. H. and Rasmussen, J. J. *Phys. Fluids* **9**, 982 (1997).